Hes·so VALAIS WALLIS
Haute Ecole d'Ingénierie
Hochschule für Ingenieurwissenschaften

Hes·so

Degree Programme
Life Technologies

Major Analytical Chemistry

Bachelor's thesis
Diploma 2023

Grkljanov Blazhe

Synthesis and characterization of autonomous molecular motors

Professor
Prof. Dr. Andreas Peer

Expert
Prof. Dr. Max von Delius

Submission date of the report
16.10.2023

HES-SO Valais

SYND	ETE	TEVI
X	X	X

Données du travail de diplôme
Aufgabenstellung der Bachelorarbeit

FO 1.2.02.07.EB
che/31/05/2021

Filière / Studiengang **TEVI**	Année académique / *Studienjahr* **2022-23**	No TB / *Nr. BA* **CA/2023/42**
Mandant / *Auftraggeber* ☐ HES—SO Valais ☐ Industrie X Etablissement partenaire *Partnerinstitution*	Etudiant / *Student* **Grkljanov Blazhe** Professeur / *Dozent* **Peer Andreas**	Lieu d'exécution / *Ausführungsort* X Etablissement partenaire *Partnerinstitution :* *Universität Ulm, Prof, Max von Delius*
Travail confidentiel / *vertrauliche Arbeit* ☐ oui / ja X non / nein	Expert / *Experte (données complètes)* **Prof. Max von Delius**	

Titre / *Titel:*

Synthesis and Characterization of autonomous molecular motors / Synthese und Charakterisierung von autonomen molekularen Motoren / Synthèse et caractérisation de moteurs moléculaires autonomes

Description / *Beschreibung*

Die Arbeit wird sich mit der Synthese und Charakterisierung von autonomen molekularen Motoren befassen, die durch diese dissipativen Reaktionszyklen betrieben werden sollen. Die Zielmoleküle bestehen aus einer Stator- (blau) und einer Rotoreinheit (rot), die über eine Einfachbindung verbunden sind. Um eine Richtungsvorspannung zu erzeugen, werden chirale Kraftstoffe (z.B. Carbodiimide) und Katalysatoren (z.B. Pyridine oder Imidazole) eingesetzt und auch synthetisiert.

Objectifs / *Ziele*

— Synthesis of a motor library
— Synthesis of a chiral catalyst and chiral fuels
— LC-method development of atropisomers and kinetic analysis

Signature ou visa / *Unterschrift oder Visum*

Responsable de l'orientation / *Leiter der Vertiefungsrichtung:*

.....

[1] Etudiant / Student:

.....

Délais / *Termine*

Attribution du thème / *Ausgabe des Auftrags:*
01.05.2023

Fin des travaux de diplôme dans les laboratoires de l'école / Ende der Diplomarbeiten in den Labors der Schule:
01.09.2023

Remise du rapport final / *Abgabe des Schlussberichts:*
16.10.2023

Expositions / *Ausstellungen der Diplomarbeiten:*
N/A

Défense orale / *Mündliche Verfechtung:*
Entre **30.10.2023 et 10.11.2023**

[1] *Par sa signature, l'étudiant-e s'engage à respecter strictement la directive DI.1.2.02.07 liée au travail de diplôme.*
Durch seine Unterschrift verpflichtet sich der/die Student/in, sich an die Richtlinie DI.1.2.02.07 der Diplomarbeit zu halten.

Rapport reçu le / *Schlussbericht erhalten am* ..... Visa du secrétariat / *Visum des Sekretariats* .....

Hes·so VALAIS WALLIS

Haute Ecole d'Ingénierie
Hochschule für Ingenieurwissenschaften

Synthèse et caractérisation des moteurs moléculaires autonomes

Diplômant/e Grkljanov Blazhe

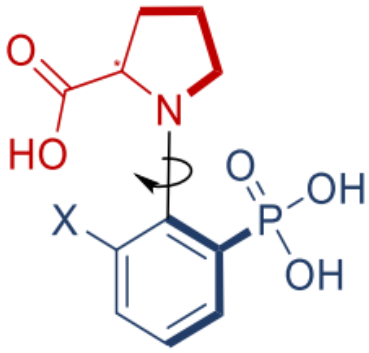

Objectif du projet

Evaluer la possibilité d'atteindre un état stable hors équilibre à partir des phosphonates d'acyl puis explorer ce système avec des moteurs moléculaires à base de phosphonate. La synthèse de ces moteurs constitue également un objectif essentiel du projet.

Méthodes | Expériences | Résultats

Tout d'abord un état stable hors équilibre à partir des phosphonates d'acyl a été mis en place et évalué afin qu'il puisse être appliquer dans l'analyse cinétique d'un moteur moléculaire à base de phosphonate. Des méthodes analytiques ont été également développé qui permettent de suivre ce système à base de phosphonates d'acyl.

Pour la synthèse des moteurs moléculaires, plusieurs strategies ont été explorées : couplage d'Ulmann qui s'est avérée sans succès, couplage d'Ulmann intramoléculaire qui a été également sans succès, et la dernière qui consistait à essayer le couplage aromatique nucléophilie suivi par la réaction de Sandmeyer pour essayer d'insérer le groupe phosphonate dans la position ortho de la partie stator du moteur, cette stratégie également n'a pas pu donner le résultat souhaité.

Une perspective de recherche future dans la synthèse du composé moteur implique une exploration plus approfondie de la réaction de Sandmeyer pour l'insertion du groupe phosphonate. En outre, il serait avantageux de développer une méthode analytique utilisant la chromatographie liquide avec une colonne chirale, ce qui faciliterait l'étude de la cinétique du composé moteur.

Travail de diplôme
| édition 2023 |

Filière
Technologies du vivant

Domaine d'application
Chimie analytique

Professeur responsable
Andreas Peer
andreas.peer@hevs.ch

Partenaire
Prof. Dr. Max von Delius,
Institut de Chimie Organique 1,
Université d'Ulm, 89073 Ulm,
Allemagne

max.vondelius@uni-ulm.de

Hes·so VALAIS WALLIS

Haute Ecole d'Ingénierie
Hochschule für Ingenieurwissenschaften

Synthese und Charakterisierung von autonomen molekularen Motoren

Diplomand/in Grkljanov Blazhe

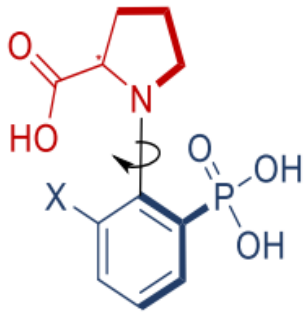

Ziel des Projekts

Bewertung der Möglichkeit, mit Acylphosphonaten einen stabilen Nichtgleichgewichtszustand zu erreichen, und anschließende Erforschung dieses Systems mit molekularen Motoren auf Phosphonatbasis. Die Synthese dieser Motoren ist ebenfalls ein wesentliches Ziel des Projekts.

Methoden | Experimente | Resultate

Zunächst wurde ein stabiler Nichtgleichgewichtszustand von Acylphosphonaten entwickelt und evaluiert, der für die kinetische Analyse eines molekularen Phosphonatmotors verwendet werden kann. Außerdem wurden analytische Methoden entwickelt, die es ermöglichen, das Acylphosphonat-System zu verfolgen.

Für die Synthese der molekularen Motoren wurden mehrere Strategien untersucht: die Ulmann-Kupplung, die sich als erfolglos erwies, die intramolekulare Ulmann-Kupplung, die ebenfalls erfolglos war, und die letzte Strategie, die darin bestand, die nukleophile aromatische Kupplung gefolgt von der Sandmeyer-Reaktion zu versuchen, um die Phosphonatgruppe in die ortho-Position des Statorteils des Motors einzufügen.

Eine Perspektive für die zukünftige Forschung bei der Synthese der Motorverbindung beinhaltet die weitere Erforschung der Sandmeyer-Reaktion zur Insertion der Phosphonatgruppe. Darüber hinaus wäre es von Vorteil, eine analytische Methode zu entwickeln, die Flüssigchromatographie mit einer chiralen Säule verwendet, was die Untersuchung der Kinetik der Motorverbindung erleichtern würde.

Diplomarbeit
| 2023 |

Studiengang
Life Technologies

Anwendungsbereich
Analytische Chemie

Verantwortliche/r Dozent/in
Andreas Peer
andreas.peer@hevs.ch

Partner
Prof. Dr. Max von Delius,
Institut für Organische Chemie
1, Universität Ulm, 89073 Ulm,
Deutschland

max.vondelius@uni-ulm.de

universität ulm

Hes·so VALAIS WALLIS

Integration of sustainability [21]

Even though this research project may appear theoretical, and its immediate real-world applications are yet to be realized, it still can be connected to some of the sustainable development goals that have to be reached by 2030.

This research into innovative chemical processes and the synthesis of motor compounds can contribute to advancements in industry and infrastructure. With the possible application of this project, it could enhance new sustainable industrial practices and promote innovation. This aligns with goal 9 – “Industry, Innovation and Infrastructure”.

Furthermore, If the energy that produced by these motor compounds can be harnessed and coupled with mechanical work this may contribute to goal 7 which is affordable and clean energy.

Potential nanotechnology application in medicine using these motor compounds could have positive health implications, contributing to goal 3 – “Good health and well-being”.

While the connection might be indirect, research that promotes innovation, knowledge sharing, and responsible production can contribute to building strong institutions and supporting peaceful societies. This can be linked to goal 16 which is peace, justice, and strong institutions.

In conclusion, the research project of this thesis holds the promise to a more sustainable and equitable world. By addressing the challenges of today’s society, this project, even though its immediate practical applications are yet to be realized, is a little step toward achieving the “Sustainable Development Goals” by 2030.

Table of Contents

List of Abbreviations

ACN	Acetonitrile
APCI	Atmospheric Pressure Chemical Ionization
ATP	Adenosine tri phosphate
CuI	Cupper Iodide
d (NMR)	Doublet
DCM	Dichloromethane
DMA	Dimethylacetamide
DMAP	4-Dimethylaminopyridine
DMF	Dimethylformamide
DMSO	Dimethyl sulfoxide
DoE	Doing of experiments
EDC	1-Ethyl-3-(3-dimethylaminopropyl) carbodiimide
EDU	1-ethyl-3-(3-dimethylamino) urea
Equiv.	Equivalent
ESI	Electron Spray Ionization
Et. al.	Et alias (and others)
EtOAc	Ethyl acetate
EtOH	Ethanol
HPLC	High Performance Liquid Chromatography
HPLC-MS	High Performance Liquid Chromatography – Mass Spectrometry
HPLC-UV	High Performance Liquid Chromatography – Ultraviolet
HRMS	High Resolution Mass Spectrometry
ISTD	Internal standard
m (NMR)	Multiplet
MES	2-(N-morpholino) ethane sulfonic acid
MOPS	3-(N-Morpholino) propane sulfonic acid
NA	Not available
NESS	Non-equilibrium steady states
NMR	Nuclear magnetic resonance
PEG	Polyethylene glycol
ppm	Parts per million
PPTS	Pyridinium p-toluenesulfonate
r.t.	Room temperature
s (NMR)	Singulet
t (NMR)	Triplet
TEA	Triethylamine
temp.	Temperature
TFA	Trifluoroacetic acid
THF	Tetrahydrofuran
TLC	Thin-Layer Chromatography

TMP	Trimethyl phosphate
TMS	Tetramethylsilane
TOF	Time-of-flight (analyzer)

1. Introduction

1.1 Motor proteins in biology

Motor proteins serve as exemplary molecular machines, translating chemical energy into mechanical work. They are a class of proteins that are found in biological systems and are responsible for generating mechanical work powered by chemical cycles such as hydrolysis of ATP.[1] Kinesin was the first motor protein in biology to be extensively studied. Its primary function is to move cargo along intracellular microtubule as depicted on **Figure 1**.[2] This movement is driven by the energy released during the hydrolysis of ATP into ADP and inorganic phosphate (Pi).[3]

Nearly all the movements and forces in cells are generated by the actions of these motor proteins. They are also critical for a wide range of cellular processes, each family has distinct characteristics and functions, but together they ensure the proper functioning and dynamics of eukaryotic cells.[3]

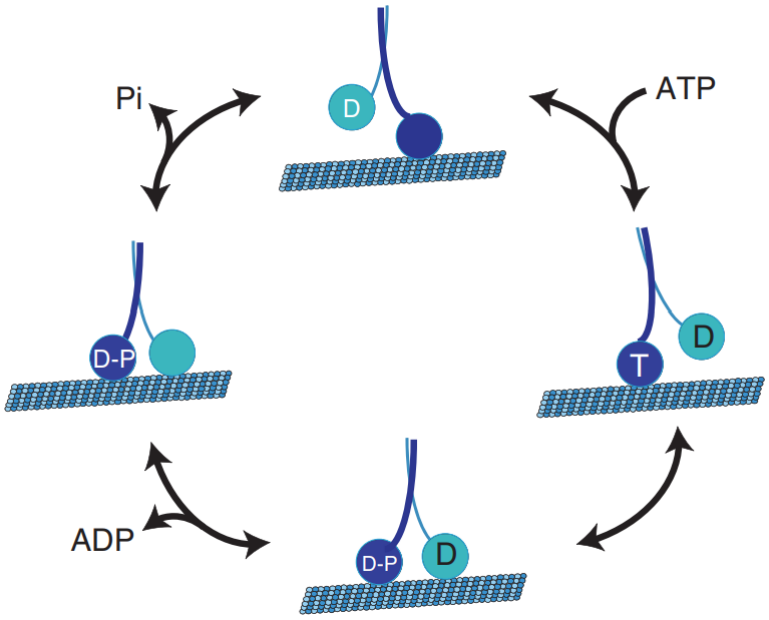

Figure 1 : Kinesin moves progressively along the microtubule through the coordinated stepping of the two motor domains. Binding of ATP (T) induces a high-affinity association of the head with the microtubule; release of the products of ATP hydrolysis, ADP (D) and Pi, allows dissociation of the head from the microtubule track. (Adapted from Sweeney et al. 2014.)[1]

The importance of motor proteins becomes clear when their specific role is considered. They are responsible for moving cargoes within the cell, organizing cell compartments. Without the motor proteins, the spatial organization of cellular components and the efficient executions of essential cellular processes would be severely compromised.[3]

It is important to note that the reliance of motor proteins and chemical molecular machines on chemical transformations to power their function invites parallels between them. These molecular systems serve as bridges between the domains of biology and chemistry.[3]

1.2 Non-equilibrium steady states (NESS)

To understand the concept of NESS, it is important to first explore different system types. Those systems are thermodynamically controlled, kinetically trapped, and non-equilibrium. Two main states are equilibrium and non-equilibrium steady states. Firstly, the two states are presented and then the three distinct systems are explained.

If two compounds **A** and **B** are in dynamic exchange and at equilibrium, there is no net exchange between their concentrations. Their concentrations can be predicted by their corresponding equilibrium constants. The same principles can be applied to cyclic exchange processes as depicted in **Figure 2,** at equilibrium the concentrations of **[A], [B]** and **[C]** follow the equilibrium constants K_{AB}, K_{BC}, K_{AC}. [4] Thus, these compounds are in a state of equilibrium.

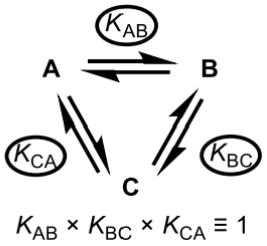

Figure 2 : Cyclic equilibrium system between A, B and C. (Adapted from Apprahamian et al. 2022)[4]

In contrast, non-equilibrium steady state (NESS) describes a dynamic state that is far-from-equilibrium. In a NESS, the concentrations of species involved in a coupled process deviate from what would be expected under equilibrium conditions, as defined by the equilibrium constant (K).[4]

Achieving a NESS involves coupling the out-of-equilibrium system to a spontaneous process. In this coupling the relative concentrations of the species involved in the coupled process differ from what would be expected at equilibrium (as defined by the equilibrium constant, K). This coupling relies on the educts and products within the network catalyzing the spontaneous process. It is important to mention that the concentrations of the species within the NESS network will only change if there is kinetic asymmetry.[4]

In a NESS, the relative concentrations of species within the part of the network connected to the spontaneous process can be altered from their equilibrium values. This leads to a net flux of molecules between these species. However, other species outside of these networks, which are not directly connected to the spontaneous reaction, remain unaffected.

A NESS can be harnessed to do continuous work at a steady state.

An example of NESS is depicted in **Figure 3. 4** is formed by reaction of **2** with **3,** followed by hydrolysis of **4** to regenerate **2.** The aldehyde substrate mediates this coupled reaction. If the relative concentrations of **3**, H_2O, AcOH and HCN are chemostated to values inconsistent with their equilibrium constant (K_{rxn}), this coupling will change the steady state concentrations of **[2]** and **[4]** from the values predicted by K_1 and therefore NESS will be achieved.[4]

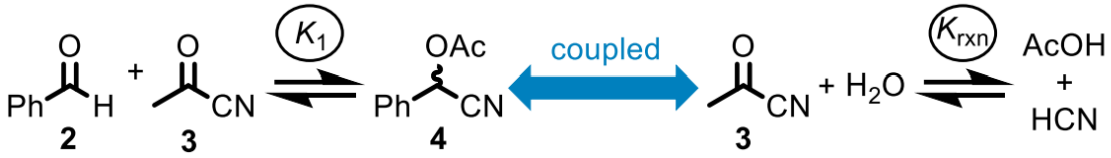

Figure 3 : Coupled reactions forming the NESS reaction network. (Adapted from Apprahamian et al. 2022)[4]

1.2.1. Classification of systems

The properties and characteristics of different systems depend on their molecular distribution and energy states, resulting in unique behaviors. Consequently, chemical systems can be categorized into three states, as illustrated in **Figure 4.** In thermodynamic equilibrium (**a**) the system is in its most stable configuration, no changes occur over time. In this state molecules occupy energy levels corresponding to a global minimum of Gibbs free energy. **b** represents a kinetically trapped state. In this case states are not occupied by their most favorable thermodynamic distribution; the molecules represent a state away from equilibrium. A NESS as shown in **c** exhibits compared to a kinetically trapped one a lower energy barrier. Far of equilibrium systems exhibit kinetic asymmetry, characteristic for these systems are the different reaction pathways. Therefore, a far from equilibrium system needs a constant flow of energy to be maintained otherwise molecules will go back to their most stable thermodynamic state.[5]

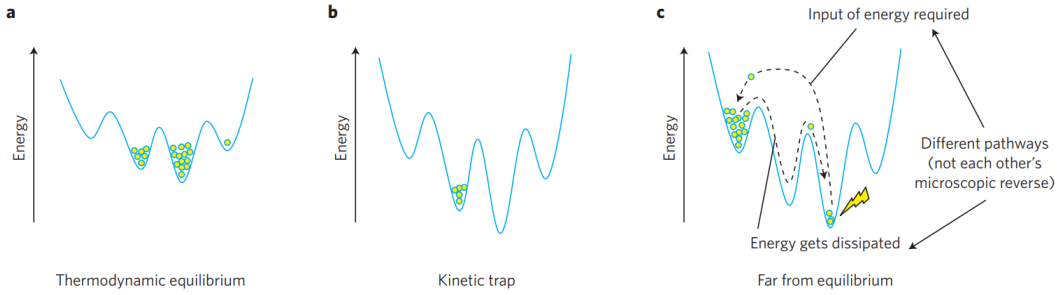

Figure 4 : Thermodynamic regimes of a chemical systems. Adapted from Mattia et al. 2015[5]

Two examples of NESS are depicted in **Figure 5.** The first example involves nanoparticles functionalized with azobenzene-containing thiol derivatives and is depicted in **Figure 5a**. The system self assembles when exposed to UV radiation. This is attributed to the increase in polarity resulting from the UV radiation, causing the azobenzene configuration to shift from Z to E.[5] When there is no more UV radiation, the self-assembled structures fall apart spontaneously and the nanoparticles disperse again in the solution, which is the most favorable thermodynamic state. To keep the azobenzene configuration shifting from Z to E continuous UV radiation is required. This far-from-equilibrium may be exploited for producing light-sensitive inks. The continuous utilization of energy in the form of UV light keeps the system in far-from-equilibrium state, if there wasn't any energy input the more stable isomer E would prevail and the assembly would disintegrate.[5]

The second example depicted in **Figure 5b** pertains to the process of gelation. In this case, a gel can be formed by continuously methylating a carboxylate acid precursor, which, on its own,

wouldn't undergo gelation due to electrostatic repulsion. When methyl iodide is introduced as fuel source, it triggers the gelation process. The gels disintegrate when there is no more fuel added to the system. Energy provided by the methyl iodide keeps the system in a gel state and it can be cycled between the solution and the gel by addition of fuel. The gel structure in this case exists because of the addition of the methyl iodide, which is the fuel and without adding it, the gel structure would disintegrate. The gel structure doesn't disintegrate because of the continuous transformation between the two different chemical structures, the carboxylate, and the methylated derivative. Without the energy input which is the fuel and keeps the far-from-equilibrium system, the system would fall apart, and the carboxylate would be the most thermodynamically stable species.[5]

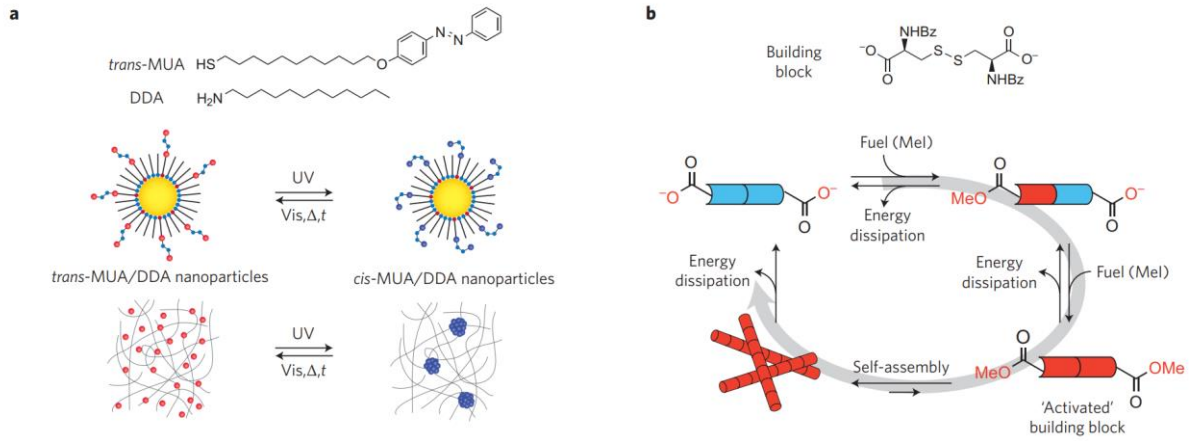

Figure 5 : Far from equilibrium supramolecular examples. adapted from Mattia et al. 2015[5]

1.2.2 Chemo mechanical cycle and the concept of kinetic asymmetry

Generally, a kinetically controlled system is in a "trapped" state, it is only one of the many possible states that exists in the potential energy landscape of the system. It requires specific conditions, such as catalyst. However, this system is limited by the lower thermodynamic more stable structures. In contrast, far from equilibrium systems derive their functionality from the ongoing transformation between multiples structures, rather than relying on the characteristics of a single assembly.[5]

A chemo mechanical cycle can be understood as a sequence of chemical reactions (reactions for the fuel-to-waste conversion) and mechanical processes (structural changes) driven by chemical energy. Chemo mechanical cycles can be found in various biological systems, as already mentioned with the kinesin, the mechanical movement along the microtubules is powered by the energy derived from the hydrolysis of ATP into ADP and Pi. [6]

Kinetic asymmetry refers to chemical processes where the rates of two opposing reactions aren't equal. The concept of kinetic asymmetry describes an imbalance in the kinetics of reactions which are opposite. In an equilibrium state the ratios of forward to backward equilibrium constants are controlled by thermodynamics and the sum of all the equilibrium constants is equal to 1. Out-of-equilibrium, however, the rate constants, hence, the kinetic asymmetry, can be controlled by evolution in biological systems or by choosing and designing the molecular components to achieve the wanted kinetic behavior of the system. Therefore, the products of "out-of-equilibrium" constants in such a chemical system is not equal to 1. [6]

For example, in the reaction cycle depicted in **Figure 6,** the kinetic asymmetry can be expressed in terms of the ratios of the "off" rates $\frac{k_{W,+2}}{k_{W,-1}}$ and $\frac{k_{B,+2}}{k_{B,-1}}$ of the reaction cycle depicted.

These ratios are independent of the concentration. [S] represents the substrate and [P] represents the product of the reaction cycle. If the ration $\frac{k_{w,+2}}{k_{w,-1}} \neq 1$, it signifies a situation where [S] binds and dissociates quickly.

The position dependance which can arise from allosteric interactions between the molecules controls the directionality of cycling of the reaction scheme.[7]

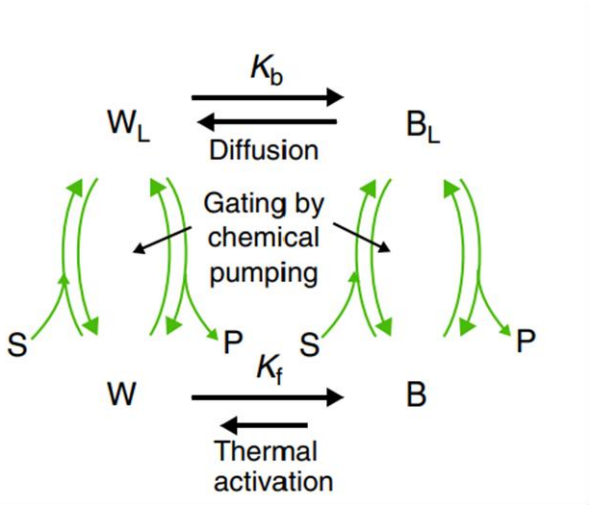

$$S + W \underset{}{\overset{K_{W,S}}{\rightleftharpoons}} W_L \overset{K^{-1}_{W,P}}{\rightleftharpoons} W + P$$

$$S + B \underset{}{\overset{K_{B,S}}{\rightleftharpoons}} B_L \overset{K^{-1}_{B,P}}{\rightleftharpoons} B + P$$

Figure 6 : Reaction cycle adapted from Astumian et al. 2019.[7]

1.3 Brownian ratchet mechanisms [8]

Brownian ratchet mechanism explains how seemingly chaotic movements in warm, random environments, combined with the presence of asymmetrical objects can give rise to mechanical motion. Brownian ratchet mechanism can be used for understanding and describing how biological molecular or synthetical chemical motors operate. They harness thermal fluctuations to drive directional motion by catalyzing fuel-to-waste conversion.[8]

When compared to biological Brownian ratchets, synthetic autonomous chemically fueled motors, are simpler. Nevertheless, they illustrate the fundamental roles of kinetic asymmetry and catalysis in achieving directed motion. Autonomous Brownian ratchets take the free energy necessary for operating out-of-equilibrium by facilitating the conversion of fuel into waste products. To achieve directional motion, they depend on kinetical asymmetry, which generates preference for movement in a specific direction as they progress through the chemomechanical cycle.[9]

In **Figure 8,** Feynman's ratchet is illustrated, it helps illustrate the fundamental principles behind Brownian ratchet mechanisms and the second law of thermodynamics. A crucial aspect to consider is the temperatures involved. When $T_1 = T_2$ the pawl is at the same temperature as the rest of the device therefore goes from open and close states failing to act as a ratchet.

However, when $T_1 > T_2$ and out-of-equilibrium is established. The significance lies in the creation of an out-of-equilibrium situation, which left to relax, can induce. This demonstrates a key principle: the input of energy is required to harness the potential to perform work, thereby illustrating the relation between thermal dynamics and the ability to achieve useful mechanical outcomes in accordance with the second law of thermodynamics.[9]

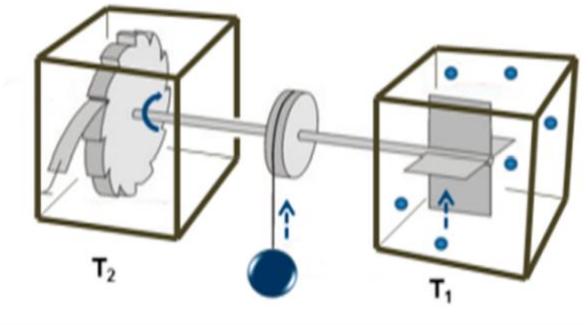

Figure 7 : Feynman's ratchet, adapted from Dave Leigh et al. (2015)[9]

Brownian ratchets mechanism can be separated into two general classes: energy ratchets and information ratchets.[9]

1.3.1 Brownian energy ratchets

Brownian energy ratchets use the energy fluctuations in a system to displace particles in a specific direction. They work by applying an external force or modifying the energy surface configuration, regardless of the particle's position. Pulsating and tilting ratchets are subcategories of energy ratchets. Pulsating ratchets change the energy configuration to create a directional movement, this can be compared to a pressing power switch on and off repeatedly. Tilting ratchets use external source of energy (ex: heat) to break the energy configuration and produce a directionality movement. [9,10]

Figure 8A depicts an on/off energy ratchet, in (a) particles are in an energy minimum, when the potential is turned off, diffusion causes the particles to move to the right. When potential is turned on again there is higher probability that particles are in an adjacent right well (compared to the one in (a) due to the potential asymmetry.) Relaxation into the minimal energy state of the systems(d) leads the particles moving to the right.[9]

Figure 8B depicts temperature or diffusion ratchet. In position (a) particles are in a minimum energy configuration, on (b) temperature rises, which in consequence reduces barrier energy heights, allowing short diffusion, (c) lowering temperature allows the particles to be in the adjacent right well, then (d) complete relaxation to a minimum energy traps the particles into a new position more on the right. This is due to the asymmetry of the energy surface which favors trapping the particles in the right wells adjacent to their initial position.[9]

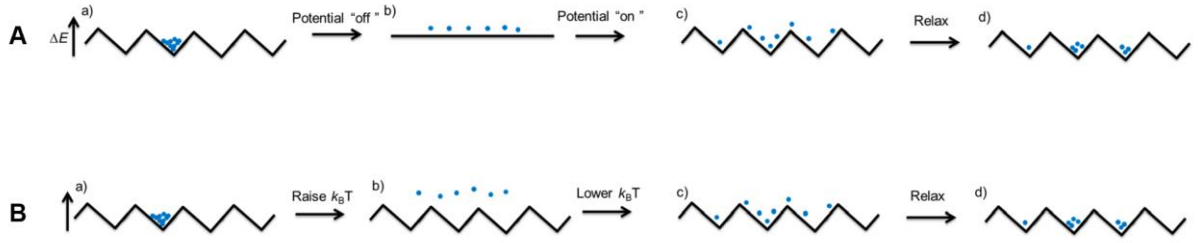

Figure 8 : A) Energy ratchet in simplest form on/off B) Information ratchet. Adapted from Leigh et al. (2015) [9]

1.3.2 Brownian information ratchets

Brownian information ratchet change energy configuration barriers based on the particle's position, which leads to the redistribution of particles, taking them "out-of-equilibrium". The information ratchet mechanism can be imagined as like particles communicating with the energy surface.

Depicted in **Figure 9** is an illustration of information ratchet, (a) particle is "sending" signals shown as dotted lines to let the energy barrier know where they are. When the particle is in certain position as shown in (b), it tells the barrier to move to the right but not to the left, then the particle moves due to random Brownian motion (c). In the subsequent stage (d), the particle has successfully moved to the right and the process can recommence from the initial configuration shown in (a). This cycle interaction between the particle and the energy barrier facilitates the information ratchet's operation, allowing particles to move in a directed way.[9]

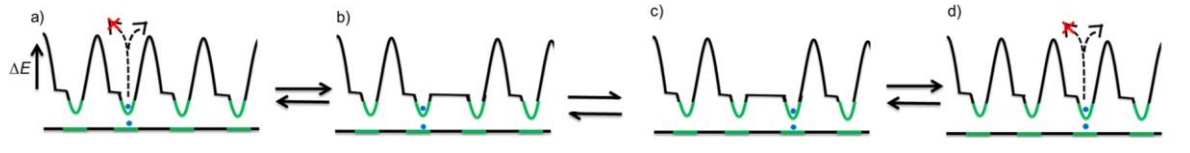

Figure 9 : Information ratchet. Adapted from Leigh et al. (2015) [9]

1.4 Molecular motors

The field of microscopic molecular machines has gained attention in recent years, marked by significant progress. The 2016 Nobel prize in Chemistry was awarded to the work of Jean-Pierre Sauvage, Fraser Stoddart and Ben Feringa for their work on the design and synthesis of molecular machines. Their work put molecular machines into the spotlight, unlocking new avenues for exploration and innovation. Nevertheless, the issue of achieving directional control in molecular machines remains a challenge.[11]

1.4.1 Nomenclature and definition

It is important to name and define molecular motors. Molecular switches, motors, rotors are made of a rotating unit (green) and a stator part (orange) which are connected by an axe as depicted in **Figure 10**.[12]

Molecular switch (**Figure 10A**), the rotator can change its position between two or more stable states. This change of position happens when an external stimulus in the form of light, chemical fuel, temperature, electricity is applied. Molecular rotor (**Figure 10B**) with the same configuration as the molecular switch, performs non-directional free rotation around the axis at room temperature. The speed of rotation can also be controlled by external stimulus. Molecular motor (**Figure 10C**) doesn't differ much from molecular rotor. When directionality is added to the rotation of the axis and 360° clockwise or counterclockwise rotation can be obtained, it becomes molecular motor. Autonomous molecular motor (**Figure 10D**) exhibits a unidirectional rotation which can be attained when fuel is present, the latter induces a net direction of rotation if it is not consumed.[12]

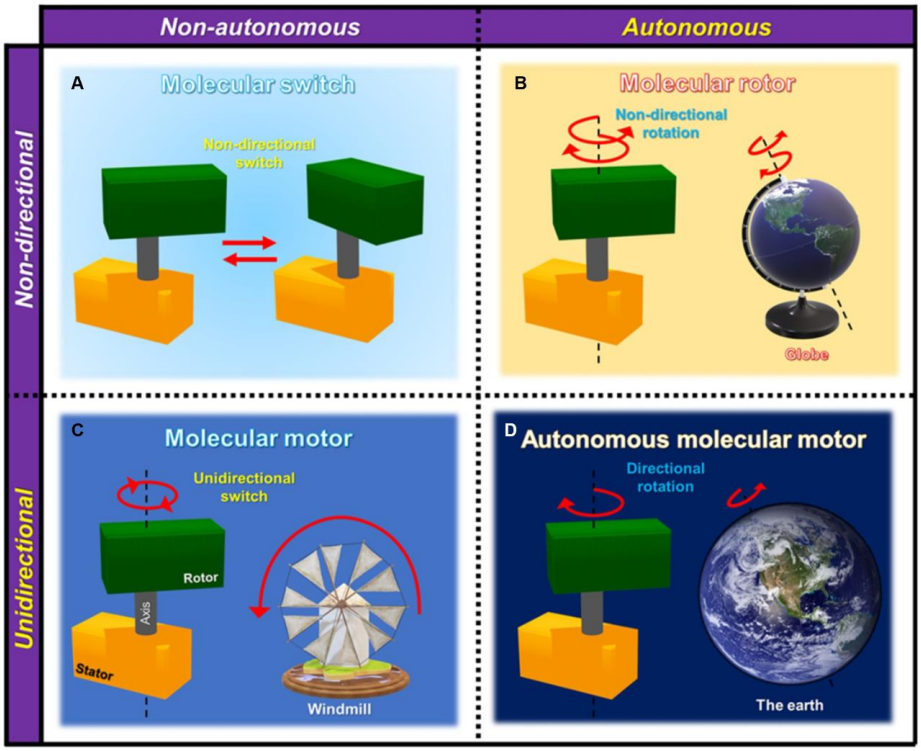

Figure 10 : Types of molecular machines. Adapted from Feringa et al (2022).[12]

1.4.2 Light- and redox-driven examples

Ferringa and co-workers reported the first light driven molecular motor in 1999[13]. UV radiation cause trans-cis isomerization and temperature variation controls helicity inversions. Firstly,

(P,P)-trans-1 is irradiated with UV and changes conformation to (M,M)-cis-2 ; then the latter is heated at 20°C and helical inversion occurs and (P,P)-cis-2 is formed. (P,P)-cis-2 is irradiated and transforms to (M,M)-trans-1 which than is heated at 60°C and helical inversion transforms it in (P,P)-trans-1. This last reaction closes the cycle.[13] This molecular motor is depicted in **Figure 11.**

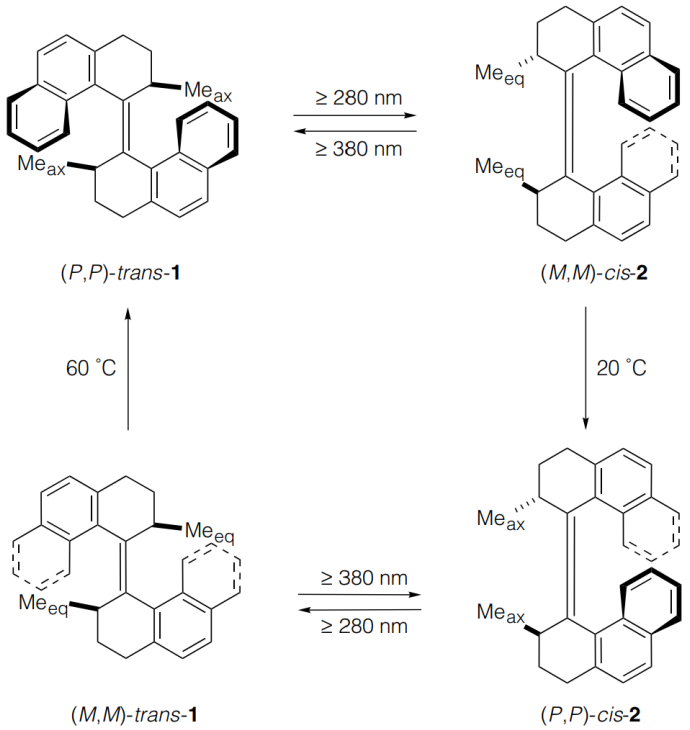

Figure 11 : First light driven molecular motor reported by Ferringa and co-workers in 1999.[13]

Ferringa and co-workers also reported a redox driven molecular motor in 2016,[14] the reaction scheme is depicted in **Figure 12.** Treating (S,M)-1 with [Pd(II)] they obtained axial rotation, and (S,M)-1 was transformed to (S,P)-1, then reducing the [Pd(II)] to [Pd(0)], (S,M)-1 is obtained again therefore 1 unidirectional 360° rotation is attained. This unidirectional rotation is done with the help of palladium oxidation states.

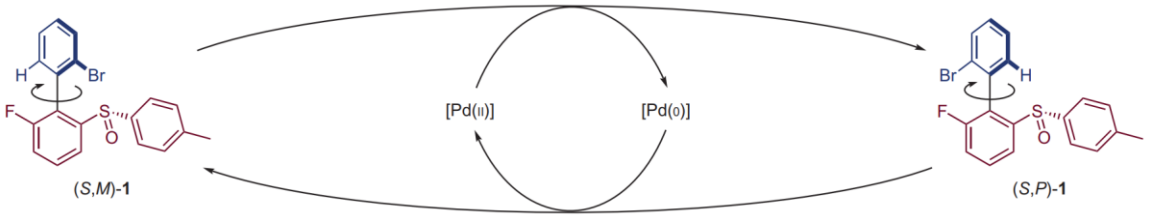

Figure 12 : Redox chemical driven molecular motor reported by Ferringa and co-workerrs Adapted from Ferrina et al. (2016)[14]

1.4.3 Chemically fueled rotary motors

In chemically fueled rotary motors, chemical reagents are used as fuel. These chemical motors rely on specific chemical reactions to convert the fuel molecules into waste while harvesting the energy released for inducing directional rotary motion. The chemical reactions are

designed in a way that the energy released propels the chemical motor in a desired reaction as that can be seen with the examples that follow. [15]

1.4.3.1 Sequential addition of fuels

Zhao, Ferringa and co-workers reported in 2020 a chemically fueled driven rotary molecular motor with 100% unidirectionality.[16] Depicted in **Figure 13A** is the biaryl structure of the molecule which was used for the experiment. The compound has one chiral center and shows axial chirality. On **Figure 13B** is shown the energy profile of the C-C bond that connects the stator and rotor without fuel. Then on the next figure is shown the energy profile of the unidirectional rotation of the C-C bond which undergoes 180° rotation with chemical fuels. Step A is cyclization, then helix inversion is depicted with step B and step C is the opening of the ring. These 3 steps represent the energy profile of a 360° rotation. **Figure 13D** shows a detailed scheme of the 360° rotation of the molecular motor (S,S')-M1 viewed from top.[16]

Cyclization (step 1) was done with EDC, which is the fuel of rotation. Step 2 consists of ring opening by nucleophilic substitution with MeONa and then (step 3) was cyclized again with EDC and then for step 4 the ring was again opened with MeONa.[16]

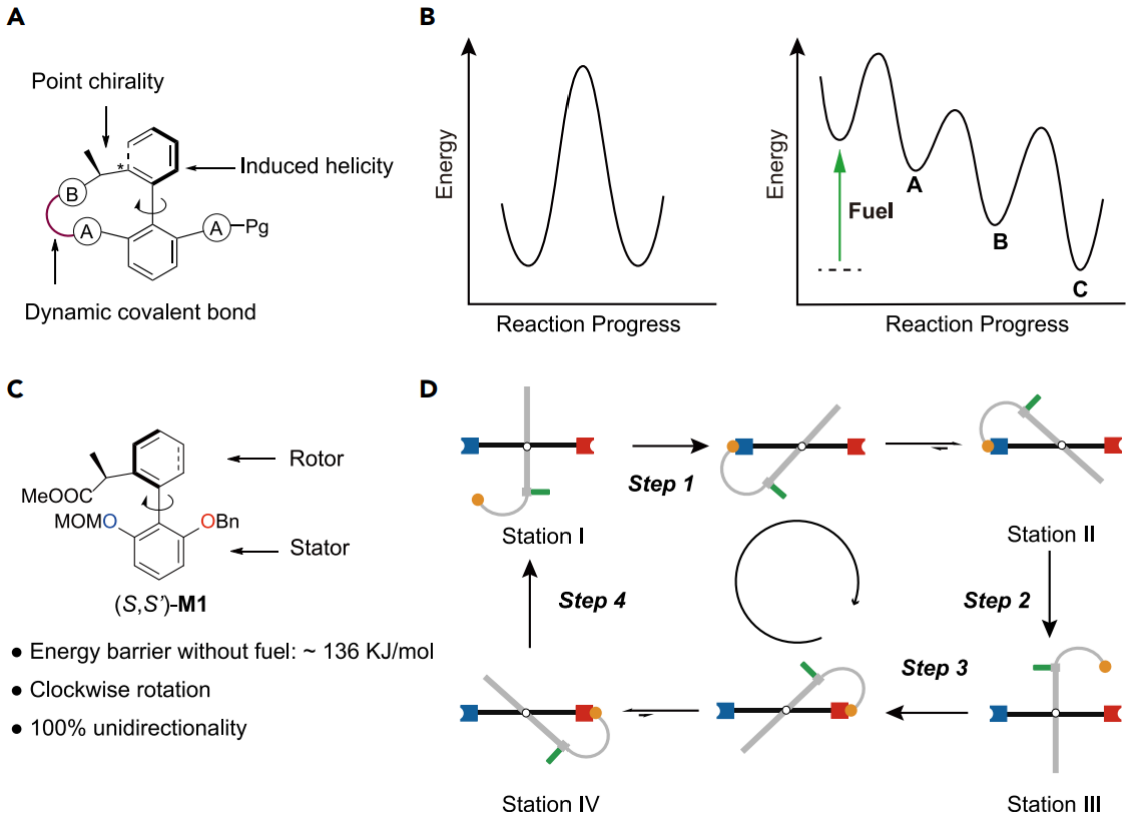

Figure 13 : Scheme of design and concept of the chemically driven rotary motor. Adapted from *Zhao, Ferringa and co-workers (2020).*[16]

1.4.3.2 Fuel pulses

An example of pulsed rotary motors was developed by *Leigh* and co-workers in 2017.[17] The system they designed relies on altering the binding affinity of the cycle for different binding sites. The binding affinity is influenced by the transition between acid and alkaline conditions.

Combination of these processes causes directional rotation of the components in [2]catenane as depicted in **Figure 14.** They used trichloroacetic acid as fuel, which undergoes efficient triethylamine-catalyzed decarboxylation to produce chloroform and carbon dioxide as waste. Under acidic conditions (**1·H$^+$**) the crown ether (red) resides on the protonated dibenzylammonium site (blue). When the conditions are basic and trichloroacetic acid is consumed, the dibenzylammmonium group is deprotonated (green). This is making the triazolium group (orange) the thermodynamically preferred binding site. [17]

When a pulse of trichloroacetic acid is added, it protonates the dibenzylammonium site in the motor and catalyzes hydrazone barrier exchange, this leads to 180° directional rotation of the crown ethers at the triazolium group. Meanwhile, triethylamine catalyzes decarboxylation of trichloroacetic acid and promotes disulfide exchange as required for the second 180° rotation of the motor, the combined quantity of base remains constant, as the fuel decarboxylates, there is more and more triethylamine in the free base form. One pulse of trichloroacetic acid drives a fully 360° rotation of the crown ethers, once the fuel is consumed another cycle can begin with the addition of a new aliquot of the fuel.[17]

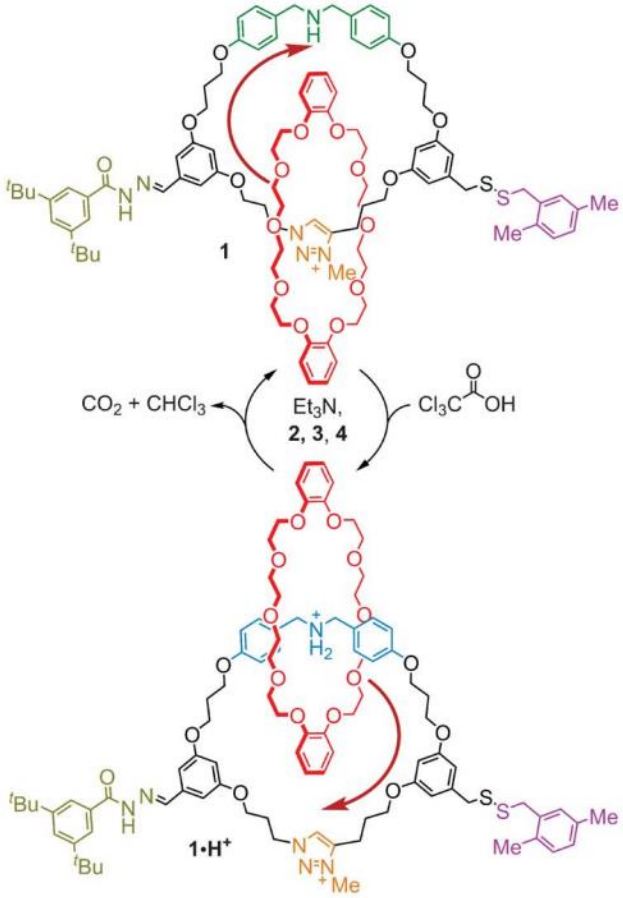

Figure 14 : [2]-Catenane pulsed rotary motor developed by Leigh and coworkers. Adapted from Leigh and co-workers (2017)[17].

1.4.3.3 Autonomous fuel consumption[18]

Leigh and co-workers reported in 2022 the first example of the autonomous operation of a chemically driven rotary motor.[18] The motor compound used in the experiment has a stator part, phenyl-2-carbonyl. The latter is attached to a rotor part, via a single C-N bond. The structure of the rotor is pyrrole-2-carbonyl. This autonomous operated rotary motor is fueled

with carbodiimides to form anhydrides. Directionality is achieved with the usage of chiral carbodiimide fuel for the activation and chiral hydrolysis agent for the deactivation. The chemical reaction cycle of this autonomous operated motor is shown in **Figure 16.**

The diacid (-)-**1** is converted to the anhydride (-)-**1'** by the reaction with the chiral fuel (R,R)-**3.** The carbodiimide allows the anhydride formation to be faster than hydrolysis (kinetical asymmetry) with completing the first cycle of the directed rotation. The grey arrows in **Figure 15** show slower transformations than black arrows. Formation of (-)-**1'** enables transformation of axially chiral forms by forming the anhydride tether which completes the second part of the rotation. The chiral catalyst (R)-**4** only hydrolyzes one tether anhydride enantiomer and controls directional motion during the hydrolysis of (+)-**1'** to (+)-**1.** Once the hydrolysis done, the rotor rotates past the **X** substituent in ortho position on the stator part and completes 360° rotation.[18]

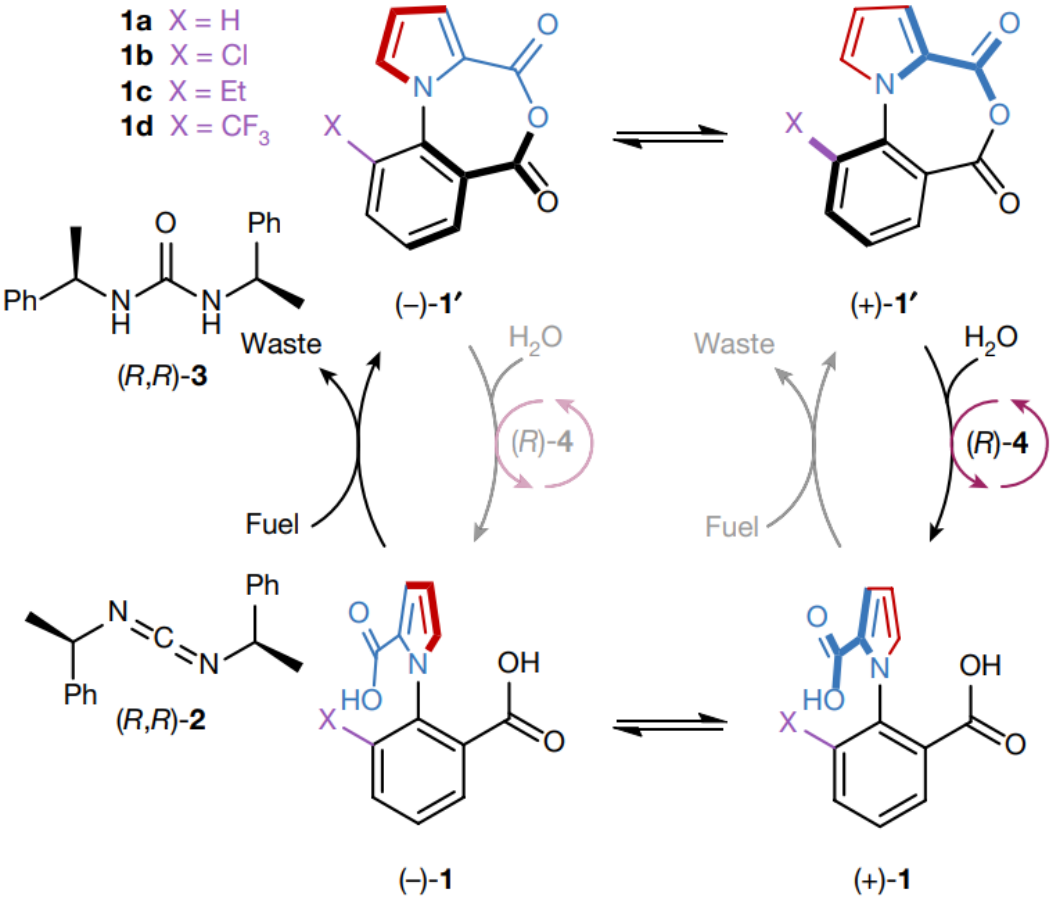

Figure 15 : Reaction cycle of the first autonomous reported fuelled chemical motor. Adapted from Leigh and coworkers (2022). [18]

2. Objectives

Non-equilibrium steady states (NESS) play a fundamental role in numerous cellular processes, driving essential activities such as intracellular transport, as exemplified by kinesin. Another class of compounds, acylphosphates, has recently come under scrutiny in the context of NESS. [19]

Acylphosphates hold an important role in nature, as they serve as vital intermediates in numerous biological processes. Given this context and the documented non-enzymatic processes for both formation and hydrolysis of acylphosphates hold significant promise as subject of investigation due to their potential connections to NESS. [20]

On the other hand, acylphosphonates which are similar structurally to acylphosphates, haven't yet been investigated. The aim of this thesis was to evaluate if NESS from acylphosphonates can be established and evaluate if acylphosphonates can be used in fueled reaction networks for the design of molecular motors. Additionally, evaluating various synthesis routes for molecular motors based on acylphosp(on)ates was an integral aspect of this research.

It is important to note that no autonomous molecular rotary motor containing a chiral center has been reported in the literature to this day.

In **Figure 16** is presented the motor compound, which is the aim of this thesis, the two moieties which are the stator (blue) and the rotor (red) are connected via a C-N bond, which is the axis that will rotate.

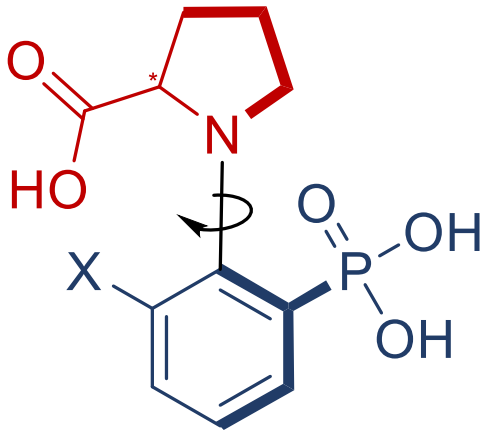

Figure 16 : The motor compound that is the aim of this thesis.

For the synthesis of the molecular motor various strategies were explored to synthetize using multiple strategies for coupling the rotor moiety (red) and the stator moiety (blue). Ulmann couplings were explored, classical and microwave mediated. Intramolecular Ulmann coupling was also tried. The last strategy that was used was to try to synthetize the compound using aromatic nucleophilic substitution followed by Sandmeyer reaction for the insertion of the phosphonate group.

3. Experimental

3.1 Chemicals and reagents

Table 1 : Chemicals and reagents.

Name	Reference	Lot	CAS	Purity	Hazard codes
L-Proline	P0380	BOOKD-LD	147-85-3	>99%	None
D-Proline	P0994	BOOKF-MD	344-25-2	>98%	None
2-Bromophenol	130915-10G	N/A	95-56-7	98%	H226 ;H302 ;H315 ;H319 ;H335 ;H400 ;H410
K_2CO_3	102553140	N/A	584-08-7	>99%	H302 ;H315 ;H318 ;H319 ;H335
Copper (I) iodide		S8394011314	7681-65-4	99%	H302 ;H315 ;H317 ;H318 ;H335 ;H400 ;H410
DMA	204-826-4	N/A	127-19-5	99%	H312 ;H319 ;H331 ;H332 ;H360 ;H373
Bromobenzene	16350-100ML	BCBQ6806V	108-86-1	99%	H226 ;H315 ;H411
Na_3PO_4	342483	CFKD7605	7601-54-9	96%	H290 ;H314 ;H315 ;H318 ;H319H331 ;H335 ; H412
DMF	23469.367	22H224002	68-12-2		H226 ;H312 ;H319 ;H332 ;H360
DMSO	348440010	2354503	67-68-5	99.7%	H225 ;H227 ;H302 ;H312 ;H315 ;H319 ;H332
AcCl	00990-250ML	BCBN9378V	75-36-5	>99%	H225 ;H302 ;H314 ;H318
Cyclohexane	486853034	43MS594	110-82-7	98%	H225 ;H250 ;H260 ;H304 ;H314 ;H315 ;H336 ;H400 ;H410
DMAP	6693548	32S32BBN	1122-58-3	>99%	H301 ;H310 ;H314 ;H315 ;H318 ;H319 ;H331 ;H335 ;H370 ;H411
DCM	568393	1495SJK	75-09-2	99%	H315 ;H319 ;H335 ;H336 ;H351 ;H371 ;H373
Pyridine	270970-100ML	STBK6990	110-86-1	99.8%	H225 ;H302 ;H312 ;H315 ;H319 ;H332
TMSCl	4958LS	GHRU5043	75-77-4	99.5%	H225 ;H301 ;H312 ;H314 ;H315 ;H318 ;H319 ;H331 ;H351
2-Bromoanisole	102530326	159239-25G	578-57-4	97%	H315 ;H319 ;H402 ;H412
Pheylphosphonic acid	P0204	QQ4YO-ND	1571-33-1	>98%	H302 ;H314 ;H318

Sodium benzoate	SB3954	SEEH423	532-32-1	99%	H319
Acetic anhydride	320102-100ML	STBK5431	108-24-7	>99%	H226 ;H302 ;H314 ;H315 ;H318 ;H319 ;H330 ;H331 ;H332 ;H335
Cu_2O	584HDF	FFHD21	1317-39-1	99%	H302 ;H319 ;H332 ;H400 ;H410
Potassium tert-butylate	8.04918.0250	S3943318410	865-47-4	96%	H228 ;H252 ;H260 ;H302 ;H314 ;H318
EtOAc	534785	SFHS2231	141-78-6	99%	H225 ;H319 ;H336
2-Iodophenol	58492FJA	PIVJ2.2	533-58-4	99.8%	H302 ;H312 ;H315 ;H319 ;H332 ;H335
MES	M0707	L2KXI-SH	4432-31-9	>99%	None
MOPS	M0606	TLOSICS	1132-61-2	>99%	None
CS2CO3	441902-250G	BCCB0308	534-17-8	99%	H315 ;H318 ;H319 ;H335 ;H361 ;H373
$Cu(Ac)_2$	14263	G6754A	6046-93-1	99%	H302 ;H314 ;H318 ;H400 ;H410 ;H411
Ethyl Imidazole	E0132	JJUBJ-AQ	7098-07-9	>98%	H302 ;H315 ;H318 ;H319 ;H412
PEG 400	P1187	3XTBE-GC	25322-68-3	>99%	None
Dioxane	D293421	D3AW3-CS	123-91-1	99%	H225 ;H319 ;H335 ;H351
$AlCl_3$	2050432-5G	SHHS2123	7784-13-6	99%	H314 ;H318 ;H372 ;H373
BBr_3	202207-25G	SHBF2067		99.9%	H300 ;H314 ;H315 ;H318 ;H319 ;H330 ;H336 ;H351
2-bromo-3-methylanisole	AS114946	24052023	38197-43-2	95%	H302
PPTS	232238-25G	0000108033	24057-28-1	98%	H315 ;H319 ;H335
HBr	268003-1L	STBK6323	10035-10-6	48%	H226 ;H290 ;H314 ;H315 ;H318 ;H319 ;H335
Sodium tert-butoxide	359270-100G	STBF0165V	865-48-5	97%	H228 ;H251 ;H314
Diphenylphosphine	4EFHDS22	SFTRW42	829-85-6	95%	H250 ;H315 ;H319 ;H335
$NaHCO_3$	65HDIFK34	DDFK332	144-55-8	95%	None
$MgSO_4$	0682.3	209284188	7487-88-9	>99%	H302 ;H312 ;H332
L-Proline methyl ester	287067-5G	STBK9405	2133-40-6	98%	None

hydrochloride					
Triethylamine	423234-25ML	HGZF3542	121-44-8	95%	H225 ;H302 ;H311 ;H312 ;H314 ;H318 ;H331 ;H332 ;H335
3,4-dihydro-2H-pyran	D106208-100ML	STBH7052	110-87-2	97%	H225 ;H315 ;H317 ;H319 ;H335 ;H412
MOMCl	100331-25G	SLCK2437	107-30-2	>99%	H225 ;H302 ;H312 ;H330 ;H332 ;H350
NaH	452912-500G	STBK2890	7646-69-7	60%	H228 ;H260 ;H290 ;H314 ;H318
POCl3	201170-250G	STBK6492	10025-87-3	99%	H300 ;H302 ;H314 ;H330 ;H372
2-Hydroxyphenylacetic acid	H0340	4AF5M-KO	614-75-5	99%	H315 ;H319 ;H335
1-fluoro-2-nitrobenzene	F10801-50G	BCCH3951	1493-27-2	99%	H302 ;H311 ;H319 ;H332 ;H372 ;H411
4-methoxypyridine	SDJFJ50G	VVHF212	620-08-6	99%	H227 ;H315 ;H319 ;H335
Pd/C	75990-10G	BCCB9732	7440-05-3	99%	H228 ;H315 ;H319 ;H335 ;H413
Ammonium Formate	798568-100G	1002382324	540-69-2	97%	H319
Dimethyl sulfone	102431615	BCBZ3940	67-71-0	>99%	None
Phosphonoacetic acid	102513099	BCCD8577	4408-78-0	>99%	None
Imidazole	I2401-5G	STBG8647	271-44-3	98%	None
Purine	SIIFK-25G	SITJ45322	120-73-0	99%	None
Pyrazine	SHVK232	UGUD342J	290-37-9	99%	H228
Boc-Pro-OH	8.53003.0025	S6598303801	15761-39-4	>95%	None
Benzoic anhydride	385980-100G	BCBK8739V	93-97-0	>95%	H315 ;H318 ;H319 ;H335
TFA	T6508-100ML	STBF6942V	76-05-1	99%	H314 ;H318 ;H332 ;H412
EDC	BD19757	BTA659	25952-53-8	99.52%	H302 ;H311 ;H315 ;H317 ;H318 ;H319 ;H335 ;H373 ;H400 ;H410
n-Hexane	DHF98DF	BBHEX20	110-54-3	99%	

3.2 Instrumentation

The usual laboratory material was used for all the experiments. Specific lab equipment which was used is displayed in the tables below.

All chemicals were purchased from Merck Sigma Aldrich, TCI, AcrosOrganics, FisherScientific, Enamine, ABCR, VWR or chemPUR and were used without further purification.

BrukerAvance 400 and 600 NEO spectrometers were used to record NMR spectra (1H: 400 or 600 Hz, 13C: 101 Hz or 151 Hz, 31P: 162 or 243 Hz). The respective spectra were referenced to the residual solvent peaks (Chemical shifts (δ) are denoted in ppm and coupling constants (J) in Hz.

MestReNova software was used for displaying and analyzing NMR spectra.

OriginPro 2022b (version 9.8.5.201) and Python 3.11.4 were used for analyzing and displaying data.

OpenLab CDS and MassHunter Instruments software was used for analyzing HPLC UV and qTOF data.

ChemDraw 22.2.0 32-bit was used for the drawing of molecules and reactions.

Table 2 : Lab equipement used.

Name	Company	Product	Reference
Analytical balance	Mettler Toledo	XA105 DualRange	XA105DU
Balance	Kern ACJ/ACS	ACS 220-4	WB12AF0261
pH meter	Mettler Toledo	SevenCompact	200720030
Pipettes	Eppendorf	0-10 uL	G36723I
		10-100 uL	G38348I
		100-1000uL	G43657I
UV lamp	Idessaga	MinUVIS	-
Vortex Machine	Scientific Industries	Vortex-Genie 2	F22423GKI
Rotavap	Heidolph	Hei-VAP Value Digital	OCI0750
Freeze-Dryer	Christ	Alpha 3-4 LSCbasic	24949243
Solvent purification	MBraun	MB SPS 5	EPS 15 ATEX 2080X
Flash Chromatography	Büchi Switzerland	Pure C-850 FlashPrep	1100089180

Table 3 : HPLC-UV instrument.

HPLC Agilent 1260 Infinity II		
Modules	**Reference**	**LOT**

Multisampler	1260 Multisampler	G716A	Serial No. DEAGY02724
Pump	1260 Flexible Pump	G7104C	Serial No. DEAGZ03073
Column	1260 MCT	G7116A	Serial No. DEAEM10740
Detector	1260 DAD HS	G7117C	Serial No. DEAEK10901

Table 4 : HPLC-qTOF apparatus.

HPLC Agilent 1260 Infinity II			
Modules	**Reference**		**LOT**
Pump	1260 Flexible Pump	G7104C	Serial No. DEAG200347
Column	1260 MCT	G7116A	Serial No. DEAEM04445
Detector	1260 DAD HS	G7117C	Serial No. DEAEK05216
Multisampler	1260 Multisampler	G7167A	Serial No. DEAGY01139
Agilent 6546 LC/Q-TOF			
qTOF detector	G1958-65271		Serial #SG19169025

Table 5 : Columns used for HPLC and Flash Chromatography.

Columns used for HPLC	
Producer	**Column specifications**
Waters	ACQUITY Premier Oligonucleotide C18, 130Å, 1.7 µm, 2.1 x 100 mm
Agilent	InfinityLab Poroshell 120 Aq-C18 (100 x 2.1 mm, 2.7 µm)
Columns used for Flash Chromatography	
Producer	**Column specifications**
FlashPure	FlashPure EcoFlex Silica 4g, 12g, 25g, Irregular particle shape 55-75Å, 40-64 µm
	FlashPure Select C18 12g, 80g, Spherical particle shape, 92-108Å, 20-35 µm

3.3 Stock solutions and sample preparation

3.3.1 $PhPO_3$ 0.25 M stock solution

Weigh 1 g of phenylphosphonic acid in a 25 mL volumetric flask. Put 10 mL H_2O in the flask and dissolve everything. Adjust the volume to 25 mL with H_2O. Mix the solution thoroughly and store it at 5 °C when not in use.

3.3.2 Sodium benzoate 1 M stock solution

Weigh 720 mg of sodium benzoate in a 5 mL volumetric flask. Put 3 mL H_2O in the flask and dissolve everything. Adjust the volume to 5 mL with H_2O. Mix the solution thoroughly and store it at 5 °C when not in use.

3.3.3 Sodium benzoate 10 M stock solution

Weigh 14.4 g of sodium benzoate in a 10 mL volumetric flask. Put 5 mL H_2O in the flask and dissolve everything. Adjust the volume to 10 mL with H_2O. Mix the solution thoroughly and store it at 5 °C when not in use.

3.3.4 MOPS (3 M) pH 7.5 buffer solution

Weigh 15.6 g MOPS in a 25 mL volumetric flask. Put 10 mL H_2O in the flask to dissolve everything, adjust the pH using concentrated HCl or NaOH to 7.5 and then adjust the volume to 25 mL with H_2O.

3.3.5 MOPS (30 M) pH 7.5 buffer solution

Weigh 31.2 g MOPS in a 50 mL volumetric flask. Put 25 mL H_2O in the flask to dissolve everything, adjust the pH using concentrated HCl or NaOH to 7.5 and then adjust the volume to 50 mL with H_2O.

3.3.6 MOPS (2 M) pH 6.5 buffer solution

Weigh 10.4 g MOPS in a 25 mL volumetric flask. Put 10 mL H_2O in the flask to dissolve everything, adjust the pH using concentrated HCl or NaOH to 6.5 and then adjust the volume to 25 mL with H_2O.

3.3.7 MES (1.5 M) pH 6.5 buffer solution

Weigh 7.3 g MES in a 25 mL volumetric flask. Put 10 mL H_2O in the flask to dissolve everything, adjust the pH using concentrated HCl or NaOH to 6.5 and then adjust the volume to 25 mL with H_2O.

3.3.8 $PhOHPhPO_3$ 0.1 M stock solution

Weigh 6.5 mg $PhOHPhPO_3$ in an HPLC 1 mL vial and pipet 250 uL of H_2O. Mix the solution thoroughly and store it at 5 °C when not in use.

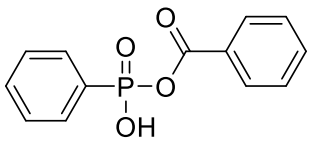

$PhOHPhPO_3$

Figure 17 : Structure $PhOHPhPO_3$

3.3.9 300 mM NH_4HCO_2 HPLC buffer solution

Weigh 18.9 g of NH_4HCO_2 in a 1000 mL volumetric flask. Put 500 mL H_2O in the flask to dissolve everything, adjust the pH using NaOH or concentrated HCl to 8.5 and then adjust the volume to 1000 mL with H_2O. Mix the solution thoroughly and add it to the HPLC recipient.

4.3.3 TFA 0.2 % HPLC buffer solution

In a 300 mL volumetric flask put 299.4 mL of H_2O. Using an Eppendorf 1 mL pipet, take 600 uL of TFA and add it to the solution in the volumetric flask. Mix the solution thoroughly and add it to the HPLC recipient.

4.3.4 Sample preparation for $PhPO_3$ reaction cycle

In a 1 mL HPLC vial pipet 100 uL from the $PhPO_3$ 0.25 M stock solution, pipet 9.5 uL acetic anhydride, pipet 50 uL pyridine, pipet 334 uL of the MOPS (3 M) pH 7.5 solution, adjust the pH to 6.5 with NaOH and adjust the volume to 1 mL with H_2O

4.3.5 Sample preparation for catalyst evaluation for acylphosphonate anhydride hydrolysis

For imidazole, purine, pyrazine stock solutions were prepared because they are solids with concentration of 0.5 M. For imidazole 8 mg were dissolved in 250 uL H_2O. For purine 15 mg were dissolved in 250 uL H_2O. For pyrazine 10 mg were dissolved in 250 uL H_2O. For pyridine, 4-methoxypyridine, DMAP and ethyl imidazole pure solutions of the compounds were used.

Without catalyst: In a 1 mL HPLC vial with 100 uL inlet pipet 25 uL $PhOHPhPO_3$ 1 M stock solution, pipet 25 uL MOPS pH 6.5 buffer solution, adjust the pH to 6.5 with NaOH or HCl and adjust to 100 uL with H_2O. The sample is ready for HPLC analytics measurements.

Pyridine: In a 1 mL HPLC vial with 100 uL inlet pipet 25 uL $PhOHPhPO_3$ 1 M stock solution, pipet 25 uL MOPS pH 6.5 buffer solution, pipet 10.1 uL Pyridine, adjust the pH to 6.5 with NaOH or HCl and adjust to 100 uL with H_2O. The sample is ready for HPLC analytics measurements.

4-methoxypyridine: In a 1 mL HPLC vial with 100 uL inlet pipet 25 uL $PhOHPhPO_3$ 1 M stock solution, pipet 25 uL MOPS pH 6.5 buffer solution, pipet 12.7 uL 4-methoxypyridine, adjust the pH to 6.5 with NaOH or HCl and adjust to 100 uL with H_2O. The sample is ready for HPLC analytics measurements.

Imidazole: In a 1 mL HPLC vial with 100 uL inlet pipet 25 uL $PhOHPhPO_3$ 1 M stock solution, pipet 25 uL MOPS pH 6.5 buffer solution, pipet 20 uL of the stock solution imidazole, adjust the pH to 6.5 with NaOH or HCl and adjust to 100 uL with H_2O. The sample is ready for HPLC analytics measurements.

DMAP: In a 1 mL HPLC vial with 100 uL inlet pipet 25 uL $PhOHPhPO_3$ 1 M stock solution, pipet 25 uL MOPS pH 6.5 buffer solution, pipet 13 uL DMAP, adjust the pH to 6.5 with NaOH or HCl and adjust to 100 uL with H_2O. The sample is ready for HPLC analytics measurements.

Purine: In a 1 mL HPLC vial with 100 uL inlet pipet 25 uL $PhOHPhPO_3$ 1 M stock solution, pipet 25 uL MOPS pH 6.5 buffer solution, pipet 20 uL of the stock solution purine, adjust the pH to 6.5 with NaOH or HCl and adjust to 100 uL with H_2O. The sample is ready for HPLC analytics measurements.

Ethyl imidazole: In a 1 mL HPLC vial with 100 uL inlet pipet 25 uL $PhOHPhPO_3$ 1 M stock solution, pipet 25 uL MOPS pH 6.5 buffer solution, pipet 12 uL ethyl imidazole, adjust the pH to 6.5 with NaOH or HCl and adjust to 100 uL with H_2O. The sample is ready for HPLC analytics measurements.

Pyrazine: In a 1 mL HPLC vial with 100 uL inlet pipet 25 uL $PhOHPhPO_3$ 1 M stock solution, pipet 25 uL MOPS pH 6.5 buffer solution, pipet 20 uL of the stock solution pyrazine, adjust the pH to 6.5 with NaOH or HCl and adjust to 100 uL with H_2O. The sample is ready for HPLC analytics measurements.

4.3.6 Sample preparation for optimization of NESS acylphosphonate reference system

Run 1: In a 1 mL HPLC vial pipet: 100 uL of the $PhPO_3$ 0.25 M stock solution, 100 uL of the sodium benzoate 1 M stock solution, 167 uL of the MOPS 3 M pH 6.5 stock solution, pipet 78 uL of pyridine, adjust the pH to 7.5 with NaOH or HCl, adjust to 1 mL with H_2O. Mix the solution thoroughly and put it aside. Weigh in another 1 mL HPLC vial, 14.4 mg of EDC. Prepare the

HPLC instrument, 2 minutes before injecting the sample, pipet the solution from the first HPLC vial and put it in the vial with the EDC, mix everything thoroughly for 1 min and inject the sample.

Run 2: In a 1 mL HPLC vial pipet: 100 uL of the $PhPO_3$ 0.25 M stock solution, 100 uL of the sodium benzoate 1 M stock solution, 167 uL of the MOPS 3 M pH 6.5 stock solution, pipet 78 uL of pyridine, adjust the pH to 6.5 with NaOH or HCl, pipet 78 uL of pyridine, adjust to 1 mL with H_2O. Mix the solution thoroughly and put it aside. Weigh in another 1 mL HPLC vial, 14.4 mg of EDC. Prepare the HPLC instrument, 2 minutes before injecting the sample, pipet the solution from the first HPLC vial and put it in the vial with the EDC, mix everything thoroughly for 1 min and inject the sample.

Run 3: In a 1 mL HPLC vial pipet: 100 uL of the $PhPO_3$ 0.25 M stock solution, 100 uL of the sodium benzoate 1 M stock solution, 167 uL of the MOPS 3 M pH 6.5 stock solution, pipet 85 uL of 4-methoxypyridine, adjust the pH to 7.5 with NaOH or HCl, adjust to 1 mL with H_2O. Mix the solution thoroughly and put it aside. Weigh in another 1 mL HPLC vial, 14.4 mg of EDC. Prepare the HPLC instrument, 2 minutes before injecting the sample, pipet the solution from the first HPLC vial and put it in the vial with the EDC, mix everything thoroughly for 1 min and inject the sample.

Run 4: In a 1 mL HPLC vial pipet: 100 uL of the $PhPO_3$ 0.25 M stock solution, 100 uL of the sodium benzoate 1 M stock solution, 167 uL of the MOPS 3 M pH 6.5 stock solution, pipet 43 uL 4-methoxypyridine, pipet 39 uL pyridine, adjust the pH to 6.5 with NaOH or HCl, adjust to 1 mL with H_2O/DMF (7:3) prepared previously. Mix the solution thoroughly and put it aside. Weigh in another 1 mL HPLC vial, 14.4 mg of EDC. Prepare the HPLC instrument, 2 minutes before injecting the sample, pipet the solution from the first HPLC vial and put it in the vial with the EDC, mix everything thoroughly for 1 min and inject the sample.

Run 5: In a 1 mL HPLC vial pipet: 100 uL of the $PhPO_3$ 0.25 M stock solution, 100 uL of the sodium benzoate 1 M stock solution, 167 uL of the MOPS 3 M pH 6.5 stock solution, pipet 43 uL 4-methoxypyridine, pipet 39 uL pyridine, adjust the pH to 6.5 with NaOH or HCl, adjust to 1 mL with H_2O/DMF (1:1) prepared previously. Mix the solution thoroughly and put it aside. Weigh in another 1 mL HPLC vial, 14.4 mg of EDC. Prepare the HPLC instrument, 2 minutes before injecting the sample, pipet the solution from the first HPLC vial and put it in the vial with the EDC, mix everything thoroughly for 1 min and inject the sample.

Run 6: In a 1 mL HPLC vial pipet : 100 uL of the $PhPO_3$ 0.25 M stock solution, 100 uL of the sodium benzoate 1 M stock solution, 167 uL of the MOPS 3 M pH 6.5 stock solution, pipet 43 uL 4-methoxypyridine, pipet 39 uL pyridine, adjust the pH to 7.5 with NaOH or HCl, pipet 43 uL 4-methoxypyridine, pipet 39 uL pyridine adjust to 1 mL with H_2O prepared previously. Mix the solution thoroughly and put it aside. Weigh in another 1 mL HPLC vial, 14.4 mg of EDC. Prepare the HPLC instrument, 2 minutes before injecting the sample, pipet the solution from the first HPLC vial and put it in the vial with the EDC, mix everything thoroughly for 1 min and inject the sample.

Run 7: In a 1 mL HPLC vial pipet: 100 uL of the $PhPO_3$ 0.25 M stock solution, 100 uL of the sodium benzoate 1 M stock solution, 167 uL of the MOPS 3 M pH 6.5 stock solution, pipet 43 uL 4-methoxypyridine, pipet 39 uL pyridine, adjust the pH to 6.5 with NaOH or HCl, adjust to 1 mL with H_2O prepared previously. Mix the solution thoroughly and put it aside. Weigh in another 1 mL HPLC vial, 14.4 mg of EDC. Prepare the HPLC instrument, 2 minutes before injecting

the sample, pipet the solution from the first HPLC vial and put it in the vial with the EDC, mix everything thoroughly for 1 min and inject the sample.

Run 8: In a 1 mL HPLC vial pipet: 100 uL of the $PhPO_3$ 0.25 M stock solution, 100 uL of the sodium benzoate 1 M stock solution, 167 uL of the MOPS 3 M pH 6.5 stock solution, pipet 85 uL of 4-methoxypyridine, adjust the pH to 6.5 with NaOH or HCl, adjust to 1 mL with H_2O. Mix the solution thoroughly and put it aside. Weigh in another 1 mL HPLC vial, 14.4 mg of EDC. Prepare the HPLC instrument 2 minutes before injecting the sample, pipet the solution from the first HPLC vial and put it in the vial with the EDC, mix everything thoroughly for 1 min and inject the sample.

4.3.7 Parameters screening

1 equiv. EDC: In a 1 mL HPLC vial pipet: 100 uL of the $PhPO_3$ 0.25 M stock solution, 100 uL of the sodium benzoate 1 M stock solution, 167 uL of the MOPS 3 M pH 6.5 stock solution, pipet 85 uL of 4-methoxypyridine, adjust the pH to 6.5 with NaOH or HCl, adjust to 1 mL with H_2O. Mix the solution thoroughly and put it aside. Weigh in another 1 mL HPLC vial, 4.8 mg of EDC. Prepare the HPLC instrument 2 minutes before injecting the sample, pipet the solution from the first HPLC vial and put it in the vial with the EDC, mix everything thoroughly for 1 min and inject the sample.

2 equiv. EDC: In a 1 mL HPLC vial pipet: 100 uL of the $PhPO_3$ 0.25 M stock solution, 100 uL of the sodium benzoate 1 M stock solution, 167 uL of the MOPS 3 M pH 6.5 stock solution, pipet 85 uL of 4-methoxypyridine, adjust the pH to 6.5 with NaOH or HCl, adjust to 1 mL with H_2O. Mix the solution thoroughly and put it aside. Weigh in another 1 mL HPLC vial, 9.6 mg of EDC. Prepare the HPLC instrument 2 minutes before injecting the sample, pipet the solution from the first HPLC vial and put it in the vial with the EDC, mix everything thoroughly for 1 min and inject the sample.

3 equiv. EDC: In a 1 mL HPLC vial pipet: 100 uL of the $PhPO_3$ 0.25 M stock solution, 100 uL of the sodium benzoate 1 M stock solution, 167 uL of the MOPS 3 M pH 6.5 stock solution, pipet 85 uL of 4-methoxypyridine, adjust the pH to 6.5 with NaOH or HCl, adjust to 1 mL with H_2O. Mix the solution thoroughly and put it aside. Weigh in another 1 mL HPLC vial, 14.4 mg of EDC. Prepare the HPLC instrument 2 minutes before injecting the sample, pipet the solution from the first HPLC vial and put it in the vial with the EDC, mix everything thoroughly for 1 min and inject the sample.

$PhPO_3$ 5 mM: In a 1 mL HPLC vial pipet: 20 uL of the $PhPO_3$ 0.25 M stock solution, 100 uL of the sodium benzoate 1 M stock solution, 167 uL of the MOPS 3 M pH 6.5 stock solution, pipet 85 uL of 4-methoxypyridine, adjust the pH to 6.5 with NaOH or HCl, adjust to 1 mL with H_2O. Mix the solution thoroughly and put it aside. Weigh in another 1 mL HPLC vial, 14.4 mg of EDC. Prepare the HPLC instrument 2 minutes before injecting the sample, pipet the solution from the first HPLC vial and put it in the vial with the EDC, mix everything thoroughly for 1 min and inject the sample.

$PhPO_3$ 25 mM: In a 1 mL HPLC vial pipet: 100 uL of the $PhPO_3$ 0.25 M stock solution, 100 uL of the sodium benzoate 1 M stock solution, 167 uL of the MOPS 3 M pH 6.5 stock solution, pipet 85 uL of 4-methoxypyridine, adjust the pH to 6.5 with NaOH or HCl, adjust to 1 mL with H_2O. Mix the solution thoroughly and put it aside. Weigh in another 1 mL HPLC vial, 14.4 mg of EDC. Prepare the HPLC instrument 2 minutes before injecting the sample, pipet the solution

from the first HPLC vial and put it in the vial with the EDC, mix everything thoroughly for 1 min and inject the sample.

$PhPO_3$ 50 mM: In a 1 mL HPLC vial pipet: 200 uL of the $PhPO_3$ 0.25 M stock solution, 100 uL of the sodium benzoate 1 M stock solution, 167 uL of the MOPS 3 M pH 6.5 stock solution, pipet 85 uL of 4-methoxypyridine, adjust the pH to 6.5 with NaOH or HCl, adjust to 1 mL with H_2O. Mix the solution thoroughly and put it aside. Weigh in another 1 mL HPLC vial, 14.4 mg of EDC. Prepare the HPLC instrument 2 minutes before injecting the sample, pipet the solution from the first HPLC vial and put it in the vial with the EDC, mix everything thoroughly for 1 min and inject the sample.

4-methoxypyridine 100 mM: In a 1 mL HPLC vial pipet: 100 uL of the $PhPO_3$ 0.25 M stock solution, 100 uL of the sodium benzoate 1 M stock solution, 167 uL of the MOPS 3 M pH 6.5 stock solution, pipet 85 uL of 4-methoxypyridine, adjust the pH to 6.5 with NaOH or HCl, adjust to 1 mL with H_2O. Mix the solution thoroughly and put it aside. Weigh in another 1 mL HPLC vial, 14.4 mg of EDC. Prepare the HPLC instrument 2 minutes before injecting the sample, pipet the solution from the first HPLC vial and put it in the vial with the EDC, mix everything thoroughly for 1 min and inject the sample.

4-methoxypyridine 200 mM: In a 1 mL HPLC vial pipet: 100 uL of the $PhPO_3$ 0.25 M stock solution, 100 uL of the sodium benzoate 1 M stock solution, 167 uL of the MOPS 3 M pH 6.5 stock solution, pipet 170 uL of 4-methoxypyridine, adjust the pH to 6.5 with NaOH or HCl, adjust to 1 mL with H_2O. Mix the solution thoroughly and put it aside. Weigh in another 1 mL HPLC vial, 14.4 mg of EDC. Prepare the HPLC instrument 2 minutes before injecting the sample, pipet the solution from the first HPLC vial and put it in the vial with the EDC, mix everything thoroughly for 1 min and inject the sample.

4-methoxypyridine 1000 mM: In a 1 mL HPLC vial pipet: 100 uL of the $PhPO_3$ 0.25 M stock solution, 10 uL of the sodium benzoate 10 M stock solution, 16.7 uL of the MOPS 30 M pH 6.5 stock solution, pipet 850 uL of 4-methoxypyridine, adjust the pH to 6.5 with NaOH or HCl, adjust to 1 mL with H_2O. Mix the solution thoroughly and put it aside. Weigh in another 1 mL HPLC vial, 14.4 mg of EDC. Prepare the HPLC instrument 2 minutes before injecting the sample, pipet the solution from the first HPLC vial and put it in the vial with the EDC, mix everything thoroughly for 1 min and inject the sample.

pH = 7.5 MOPS: In a 1 mL HPLC vial pipet: 100 uL of the $PhPO_3$ 0.25 M stock solution, 100 uL of the sodium benzoate 1 M stock solution, 167 uL of the MOPS 3 M pH 6.5 stock solution, pipet 85 uL of 4-methoxypyridine, adjust the pH to 7.5 with NaOH or HCl, adjust to 1 mL with H_2O. Mix the solution thoroughly and put it aside. Weigh in another 1 mL HPLC vial, 14.4 mg of EDC. Prepare the HPLC instrument 2 minutes before injecting the sample, pipet the solution from the first HPLC vial and put it in the vial with the EDC, mix everything thoroughly for 1 min and inject the sample.

pH = 5.5 MES: In a 1 mL HPLC vial pipet: 100 uL of the $PhPO_3$ 0.25 M stock solution, 100 uL of the sodium benzoate 1 M stock solution, 84 uL of the MES 1 M pH 6.5 stock solution, pipet 85 uL of 4-methoxypyridine, adjust the pH to 5.5 with NaOH or HCl, adjust to 1 mL with H_2O. Mix the solution thoroughly and put it aside. Weigh in another 1 mL HPLC vial, 14.4 mg of EDC. Prepare the HPLC instrument 2 minutes before injecting the sample, pipet the solution from the first HPLC vial and put it in the vial with the EDC, mix everything thoroughly for 1 min and inject the sample.

T = 5 °C: In a 1 mL HPLC vial pipet: 100 uL of the $PhPO_3$ 0.25 M stock solution, 100 uL of the sodium benzoate 1 M stock solution, 167 uL of the MOPS 3 M pH 6.5 stock solution, pipet 85 uL of 4-methoxypyridine, adjust the pH to 6.5 with NaOH or HCl, adjust to 1 mL with H_2O. Mix the solution thoroughly and put it aside. Weigh in another 1 mL HPLC vial, 14.4 mg of EDC. Prepare the HPLC instrument 2 minutes before injecting the sample, pipet the solution from the first HPLC vial and put it in the vial with the EDC, mix everything thoroughly for 1 min and inject the sample.

T = 25 °C: In a 1 mL HPLC vial pipet: 100 uL of the $PhPO_3$ 0.25 M stock solution, 100 uL of the sodium benzoate 1 M stock solution, 167 uL of the MOPS 3 M pH 6.5 stock solution, pipet 85 uL of 4-methoxypyridine, adjust the pH to 6.5 with NaOH or HCl, adjust to 1 mL with H_2O. Mix the solution thoroughly and put it aside. Weigh in another 1 mL HPLC vial, 14.4 mg of EDC. Prepare the HPLC instrument 2 minutes before injecting the sample, pipet the solution from the first HPLC vial and put it in the vial with the EDC, mix everything thoroughly for 1 min and inject the sample.

T = 40 °C: In a 1 mL HPLC vial pipet: 100 uL of the $PhPO_3$ 0.25 M stock solution, 100 uL of the sodium benzoate 1 M stock solution, 167 uL of the MOPS 3 M pH 6.5 stock solution, pipet 85 uL of 4-methoxypyridine, adjust the pH to 6.5 with NaOH or HCl, adjust to 1 mL with H_2O. Mix the solution thoroughly and put it aside. Weigh in another 1 mL HPLC vial, 14.4 mg of EDC. Prepare the HPLC instrument 2 minutes before injecting the sample, pipet the solution from the first HPLC vial and put it in the vial with the EDC, mix everything thoroughly for 1 min and inject the sample.

4.3.8 Quantitative NMR for $PhOHPhPO_3$

NMR sample was measured once the $PhOHPhPO_3$ was separated and isolated according to protocol **4.8.2.1** and then a ^{31}P-NMR was done to find its concentration (**Figure 18**).

Concentration was calculated using the following equations (**Figure 19**):

$$\frac{\frac{A(ISDT)}{n_{prot}(ISDT)}}{\frac{A(Sample)}{n_{prot}(Sample)}} = \frac{n(ISDT)}{n(Sample)}$$

$$\downarrow$$

$$n(Sample) = \frac{n_{prot}(ISDT) * A(Sample) * c(ISDT)}{n_{prot}(Sample) * A(ISDT)}$$

Figure 18 : Equations used for finding concentration of the compound.

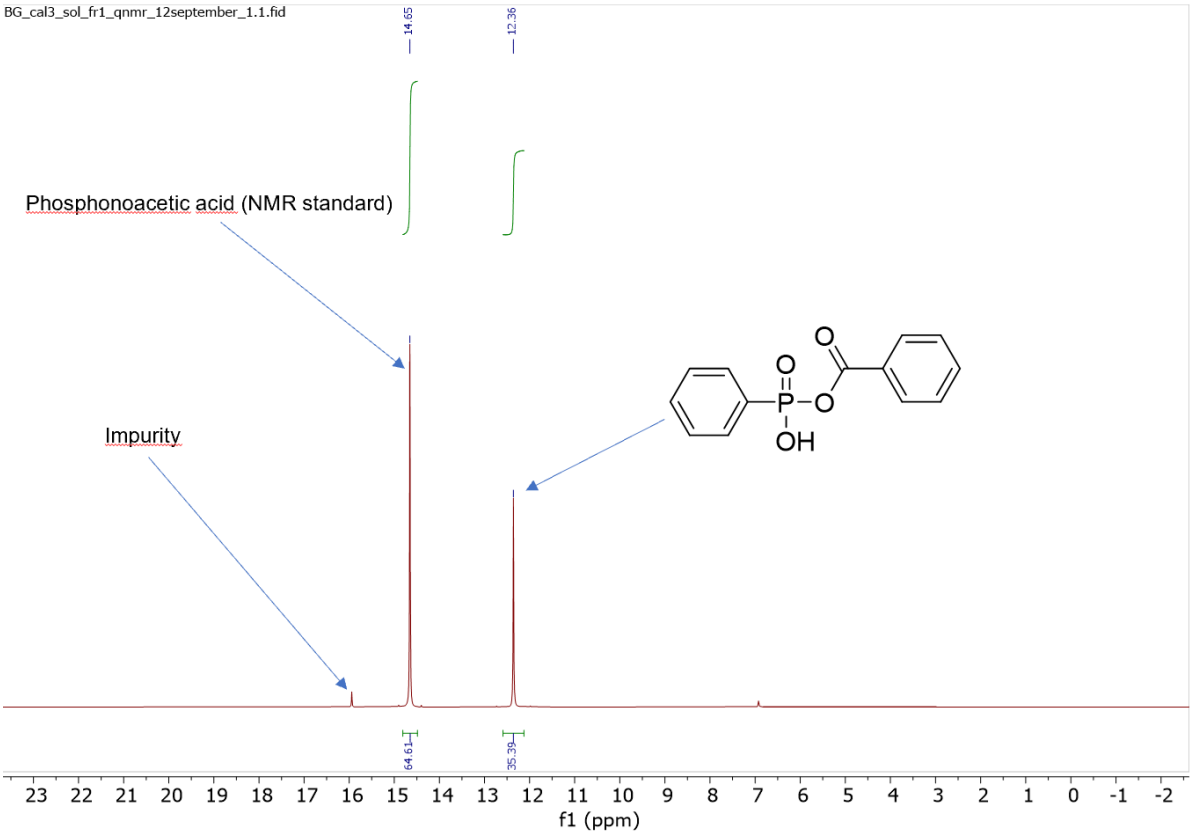

Figure 19 : ^{31}P-NMR of $PhOHPhPO_3$ that was used for the quantitative NMR.

4.3.9 HPLC calibration for $PhOHPhPO_3$

For the calibration samples of $PhOHPhPO_3$ seven calibration points were spiked: 0, 1, 5, 10, 25, 50, 75 mM of $PhOHPhPO_3$ were prepared. In an HPLC vial with an inlet of 100 uL, pipet the corresponding volume from the 0.1 M stock solution of $PhOHPhPO_3$. For 0 mM of $PhOHPhPO_3$, add 100uL H_2O. For 1 mM $PhOHPhPO_3$ pipet 1 uL from the 0.1 M stock solution of $PhOHPhPO_3$, add 99 uL H_2O. For 5 mM $PhOHPhPO_3$ pipet 5 uL from the 0.1 M stock solution of $PhOHPhPO_3$, add 95 uL H_2O. For 10 mM $PhOHPhPO_3$ pipet 10 uL from the 0.1 M stock solution of $PhOHPhPO_3$, add 90 uL H_2O. For 25 mM $PhOHPhPO_3$ pipet 25 uL from the 0.1 M stock solution of $PhOHPhPO_3$, add 75 uL H_2O. For 50 mM $PhOHPhPO_3$ pipet 50 uL from the 0.1 M stock solution of $PhOHPhPO_3$, add 50 uL H_2O. For 75 mM $PhOHPhPO_3$ pipet 75 uL from the 0.1 M stock solution of $PhOHPhPO_3$, add 25 uL H_2O. Mix thoroughly all the samples and they are ready for HPLC-UV analysis. Details of the calibration curve, R^2, can be found in chapter **10.6.**

4.4 HPLC methods

Table 6 : HPLC-qTOF method for monitoring coupling reactions.

Entry	Method			
Type	Gradient			
Stationary phase	ACQUITY Premier Oligonucleotide C18, 130Å, 1.7 µm, 2.1 x 100 mm			
Temp. [C°]	40			
Flowrate [ml/min]	0.7			
Mobile phase	A : H2O B :ACN C : 300mM NH4 buffer			
Timetable	Time [min]	A [%]	B [%]	C [%]
	0	92	3	5
	2	92	3	5
	8	25	7	5
	8.1	5	90	5
	10.5	5	90	5
	1	92	3	5
	16	92	3	5
Injection volume [µL]	4			
Solvent for dilution of sample	H2O/ACN (1 :1)			
DAD wavelength detection [nm]	254, 220			
Reference wavelength [nm]	360			
q-TOF ion polarity	Positive			
ESI gas temp. [°C]	320			
MS TOF Fragmentor [V]	175			
Mass range [m/z]	100-3200			

In the case of analyzing acylphophonates or any phosphonate compound the ion polarity of q-TOF was changed from positive to negative.

Table 7 : Qualitative method for monitoring acylphosphonates reaction cycles.

Entry	Method			
Type	Gradient			
Stationary phase	InfinityLab Poroshell 120 Aq-C18 (100 x 2.1 mm, 2.7 µm)			
Temp. [C°]	40			
Flowrate [ml/min]	0.3			
Mobile phase	A : H2O B :ACN D : 2% TFA			
Timetable	Time [min]	A [%]	B [%]	D [%]
	0	85	3	12
	2	85	3	12
	10	8	80	12
Injection volume [µL]	0.2			
Solvent for dilution of sample	H2O/ACN (1 :1)			
DAD wavelength detection [nm]	254			
Reference wavelength [nm]	360			

Table 8 : Optimized HPLC method for monitoring acylphosphonates reactions.

Entry	Method			
Type	Isocratic			
Stationary phase	InfinityLab Poroshell 120 Aq-C18 (100 x 2.1 mm, 2.7 µm)			
Temp. [C°]	40			
Flowrate [ml/min]	0.3			
Mobile phase	A : H2O B :ACN D : 2% TFA			
Timetable	Time [min]	A [%]	B [%]	D [%]
	0	68	20	12
	6	68	20	12
Injection volume [µL]	0.2			
Solvent for dilution of sample	H2O/ACN (1 :1)			
DAD wavelength detection [nm]	254			
Reference wavelength [nm]	360			

4.5 Flash chromatography methods

The list of all flash chromatography methods used for the purification of the compounds which were synthetized.

Table 9 : List of all flash chromatography method used for the purification of the synthetized compounds.

N° 1	
Type	Gradient
Stationary phase	Silica column
Mobile phase	A : Cyclohexane B: Ethyl acetate
Timetable	T [min] A [%] B [%]

	0	95	5
	4	95	5
	9	90	10
	10	0	100
	15	0	100
Type of injection	Liquid injection		
DAD wavelength detection [nm]	254, 220, 280		
N° 2			
Type	Gradient		
Stationary phase	Silica column		
Mobile phase	A : Petroleum ether B: Ethyl acetate		
Timetable	T [min]	A [%]	B [%]
	0	90	10
	25	60	40
	35	40	60
	40	0	100
Type of injection	Liquid injection		
DAD wavelength detection [nm]	254, 220, 280		
N° 3			
Type	Gradient		
Stationary phase	Silica column		
Mobile phase	A : n-Hexane B: Ethyl acetate		
Timetable	T [min]	A [%]	B [%]
	0	98	2
	5	98	2
	7	90	10
	12	90	10
	15	75	25
	16	75	25
	18	10	90
	20	10	90
Type of injection	Liquid injection		
DAD wavelength detection [nm]	254, 220, 280		
N° 4			
Type	Gradient		
Stationary phase	C-18 column		
Mobile phase	A : Water B: ACN		
Timetable	T [min]	A [%]	B [%]
	0	95	5
	2	95	5
	8	70	30
	10	70	30
	14	40	60

	19	40	60
	24	10	90
	30	10	90
	31	0	100
	36	0	100
Type of injection	Liquid injection		
DAD wavelength detection [nm]	254, 220, 280		
N° 5			
Type	Gradient		
Stationary phase	C-18 column		
Mobile phase	A : Water B: ACN		
Timetable	T [min]	A [%]	B [%]
	0	97	3
	10	97	3
	30	10	90
	10	10	90
Type of injection	Liquid injection		
DAD wavelength detection [nm]	254, 220, 280		

4.8 Synthesis and characterization

4.8.2 Synthesis protocols and characterization

The synthesis protocols that were used for the reactions are presented here; all the spectra of the compounds if there was a possibility to isolate and characterize them can be found under the general procedure of the reaction in the synthesis chapter.

4.8.2.1 Synthesis of Benzoic phenylphosphonic anhydride

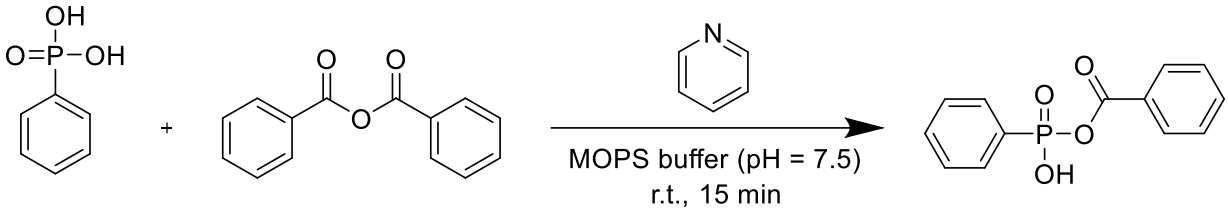

Benzoic phenylphosphonic anhydride was synthesized by mixing phenylphosphonic acid (250 mg, 1 equiv.) with benzoic anhydride (1430 mg, 4 equiv.) in 8 mL of a 1 molar MOPS buffer solution (pH adjusted to 7.5 using NaOH) containing pyridine (50.0 µL, 0.4 equiv.). The reaction was stirred vigorously at RT for 15 min. Purification via flash chromatography (**method 5**) yielded 28 mg (11.2%) of benzoic phenylphosphonic anhydride as a colorless solid.

^{31}P-NMR (243 MHz, D_2O): δ [ppm] = 12.36 (s)

HRMS (ESI negative mode): -m/z = 261.03 (calculated for C8H8O5P- m/z = 261.0322)

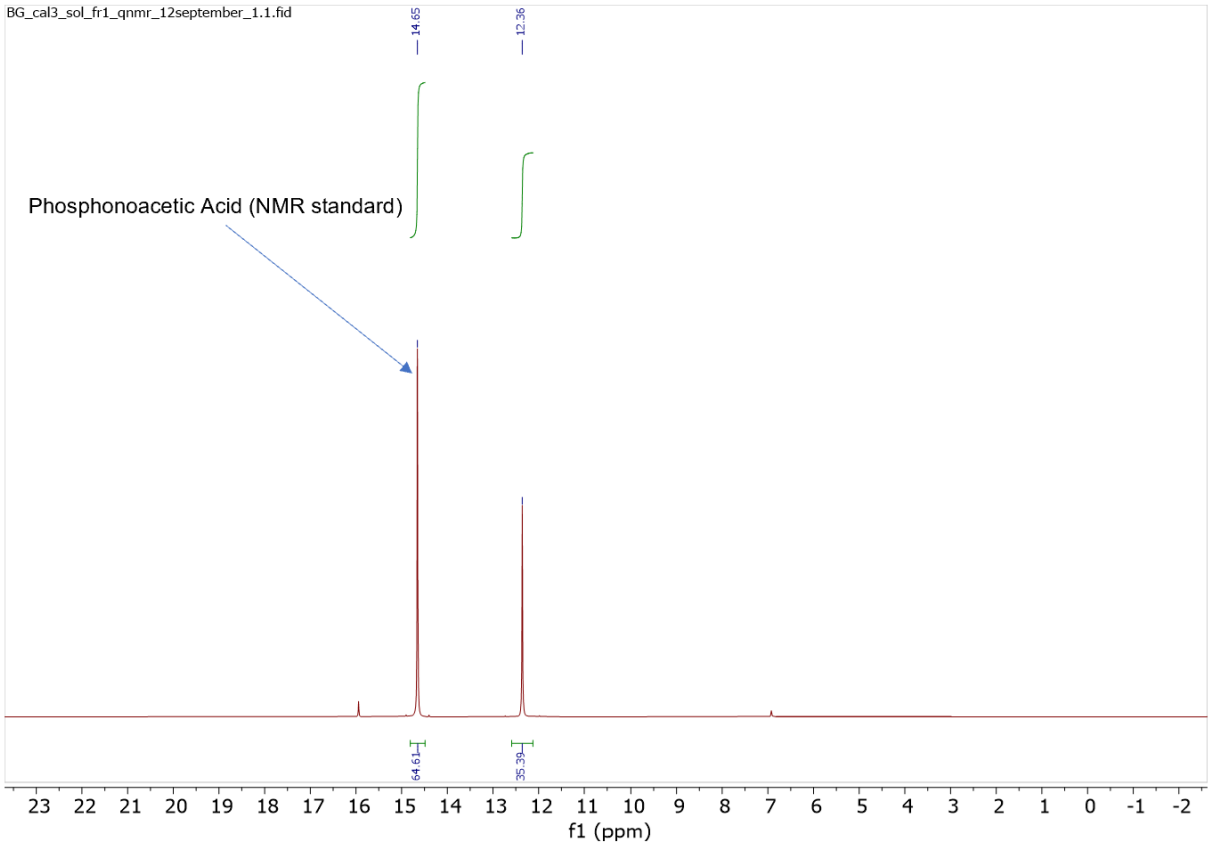

Figure 20 : ^{31}P-NMR spectrum of **benzoic phenylphosphonic anhydride.**

4.8.2.2 Synthesis of Phenyl-L-proline (3)

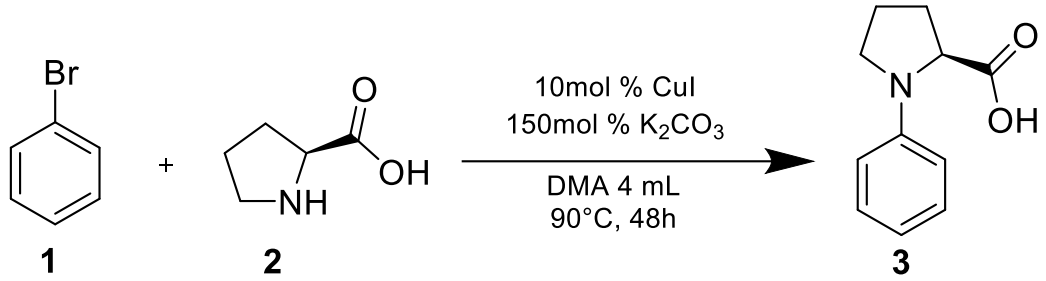

1 **2** **3**

In a Schlenk tube, under N_2 atmosphere, 100 mg of L-Proline (**2**) (0.867 mmol, 1 equiv.) and 136 mg of Bromobenzene (**1**) (0.867 mmol, 1 equiv.) were dissolved in 4 ml DMA. Under stirring 1.6 mg of copper iodide (0.00867 mmol, 10 mol %) and 180 mg of potassium carbonate (1.3 mmol, 150 mol %) were added to the solution. The reaction mixture was stirred on 90°C for 48 hours. After 48 hours the reaction mixture was cooled down to room temperature, then 10 mL of ethyl acetate were added. Under cooling with ice and water, concentrated HCl was added to acidify the mixture to pH 2-3. Then the organic layer was separated, and the aqueous layer was extracted with ethyl acetate (5 x 10 mL). The combined organic layers were washed with brine, dried over anhydrous magnesium sulfate, and concentrated by rotavapor. ^{1}H and ^{13}C characterization wasn't done since the compound wasn't isolated.

HRMS (ESI negative mode): -m/z = 190.09 (theoretical - m/z = 190.0946)

4.8.2.2 Synthesis of (2-hydroxyphenyl)-L-proline (6)

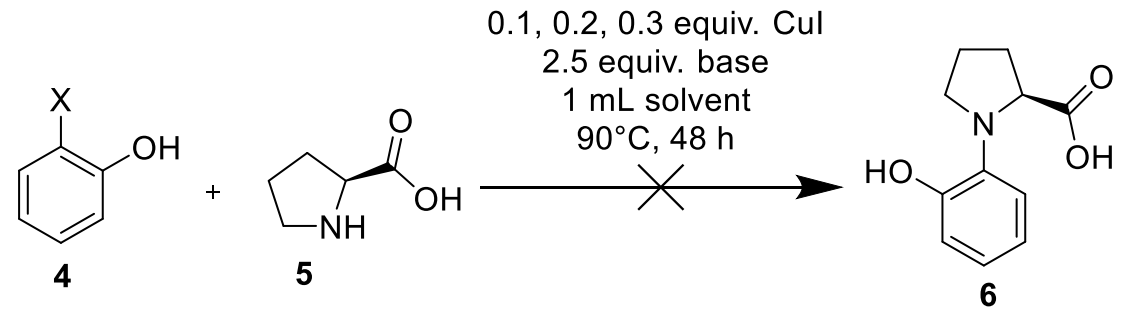

4 **5** **6**

X = Br or I

In a Schlenk tube, under N_2 atmosphere, 126 mg of L-Proline (**5**) (1.1 mmol, 1.2 equiv.) and 1 mmol of **4** were dissolved either in 1 ml DMA, ACN/H_2O, DMF/H_2O, Dioxane or DMSO. Under stirring 2.1, 4.2 or 6.3 mg of copper iodide (0.1, 0.2 or 0.3 equiv.) and 2.5 equiv. of base (K_2CO_3, Na_3PO_4, Cs_2CO_3 or ^{k}OtBu were added to the solution. The reaction mixture was stirred on 90°C for 48 hours. After 48 hours the reaction mixture was cooled down to room temperature, then 10 mL of ethyl acetate were added. Under cooling with ice and water, concentrated HCl was added to acidify the mixture to pH 2-3. Then the organic layer was separated, and the aqueous layer was extracted with ethyl acetate (5 x 10 mL). The combined organic layers were washed with brine, dried over anhydrous magnesium sulfate, and concentrated by rotavapor. No product was observed, therefore ^{1}H and ^{13}C characterization couldn't be done.

4.8.2.3 Synthesis of (2-methoxyphenyl)-L-proline (12)

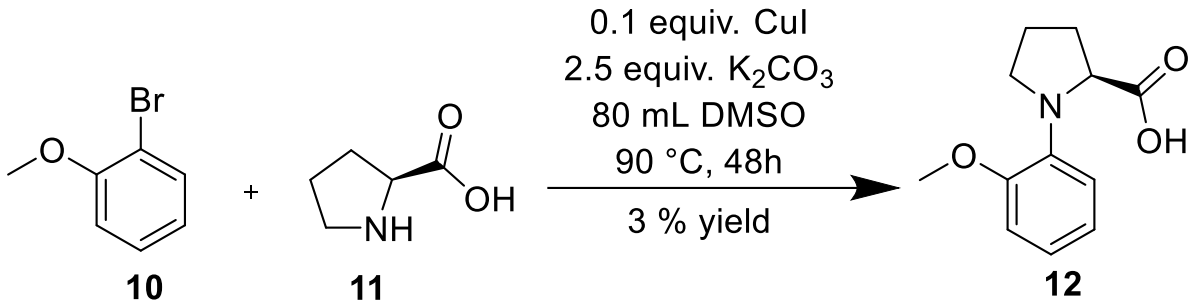

10 **11** **12**

In a Schlenk tube, under N_2 atmosphere, 1.8 g of L-Proline (**11**) (16 mmol, 1 equiv.) and 3 g of 1-bromo-2-methoxybenzene (**10**) (16 mmol, equiv.) were dissolved either in 80 ml DMSO. Under stirring 0.3 g of copper iodide (1.6 mmol, 0.1 equiv.) and 5.5 g of potassium carbonate (40 mmol, 2.5 equiv.) were added to the solution. The reaction mixture was stirred on 90°C for 48 hours. After 48 hours the reaction mixture was cooled down to room temperature, then 100 mL of ethyl acetate were added. Under cooling with ice and water, concentrated HCl was added to acidify the mixture to pH 2-3. Then the organic layer was separated, and the aqueous layer was extracted with ethyl acetate (5 x 100 mL). The combined organic layers were washed with brine, dried over anhydrous magnesium sulfate, and concentrated by rotavapor. Purification was done via flash chromatography (**flash chromatography method 1**) yielded 3% product as pink solid. **12** was characterized using ^{1}H-NMR, ^{13}C-NMR. See **Figure 21** for ^{1}H-NMR spectrum and **Figure 22** for ^{13}C-NMR spectrum.

^{1}H-NMR (600 MHz, DMSO): δ [ppm] = 6.85 (dd, ^{3}J = 6.84, 1H, aryl), 6.79 (td, ^{3}J = 6.79, 1H, aryl), 6.67 (td, ^{3}J = 6.67, 1H, aryl), 6.61 (dd, ^{3}J = 6.61, 1H, aryl), 4.46 (m, 1H, 2), 3.65 (s, 3H, 3), 3.39 (m, 1H, 4), 3.24 (m, 1H, 4), 2.20 (m, 1H, 5/6), 1.87 (m, 3H, 5/6)

^{13}C-NMR (151 MHz, DMSO): δ [ppm] = 175.31, 148.45, 137.76, 121.20, 117.97, 114.49, 112.36, 61.80, 55.49, 50.00, 30.74, 22.87.

HRMS (ESI negative mode): -m/z = 220.098 (theoretical - m/z = 220.1052)

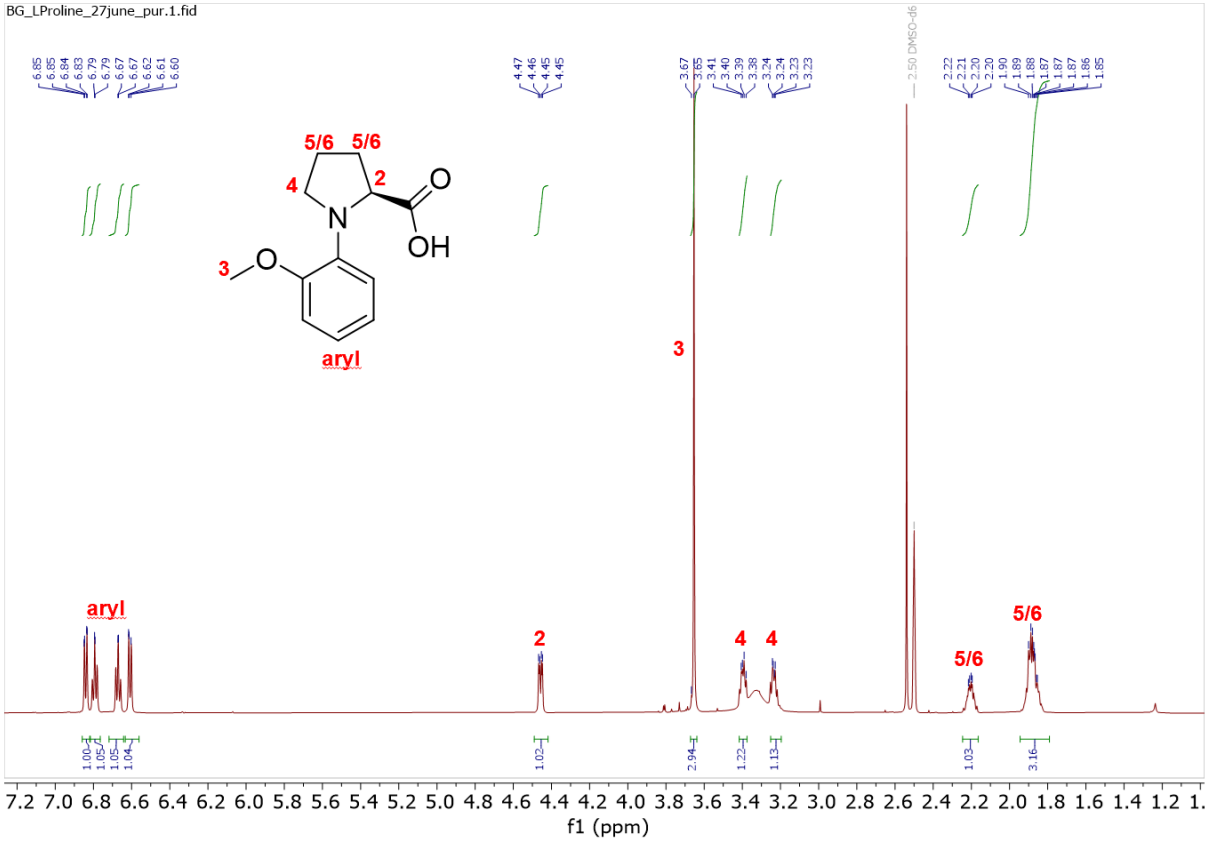

Figure 21 : ^{1}H-NMR spectrum of **12** in DMSO.

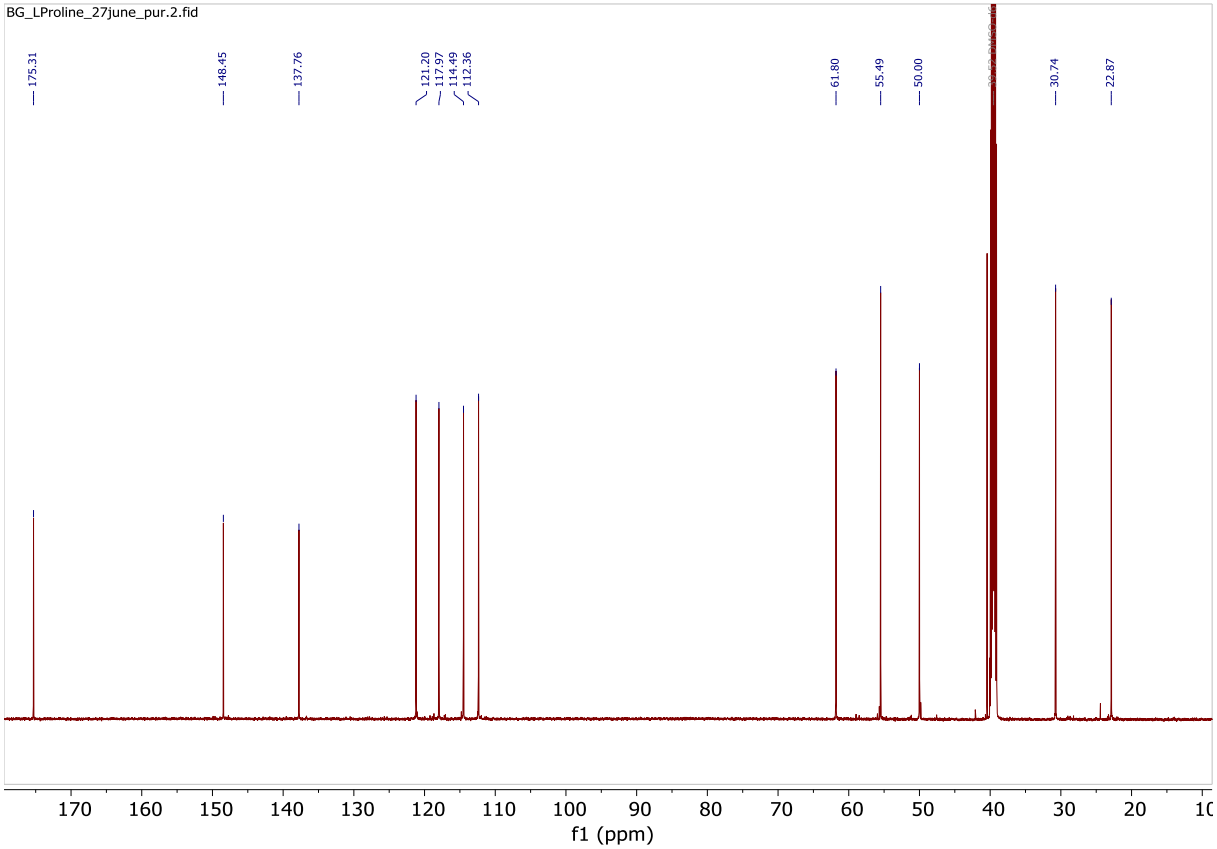

Figure 22 : ^{13}C-NMR spectrum of **12** in DMSO.

4.8.2.4 Synthesis of protected bromophenols - (2-bromophenoxy)trimethylsilane (10a)

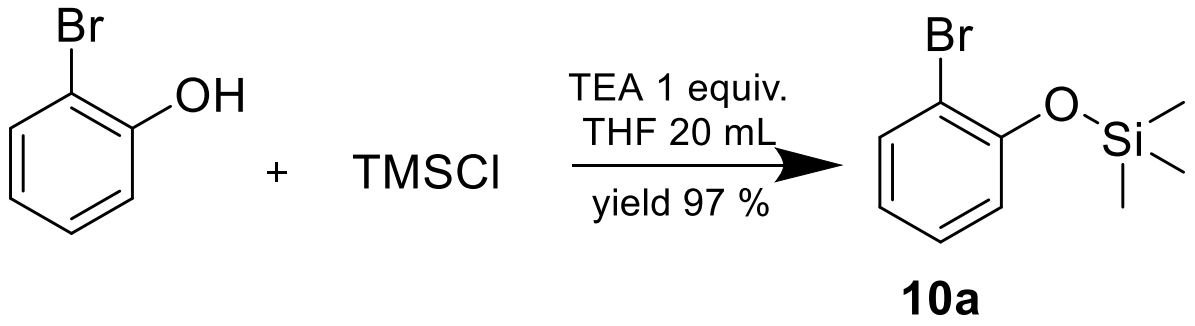

10a

In a Schlenk tube, under N_2 atmosphere, 2.5 g of 2-Bromophenol (15 mmol, 1 equiv.) were dissolved in 20 mL anhydrous THF. To the solution were added 1.4 g of triethylamine (15 mmol, 1 equiv.) and 1.5 g trimethylsilyl chloride (15 mmol, 1 equiv.). The solution was stirred for 18 hours. After 18 hours the mixture was concentrated to remove THF. The resultant oil was purified via flash chromatography (**flash chromatography method 1**) yielded 97 % product as colorless oil. **10a** was characterized using ^{1}H-NMR. See **Figure 23** for ^{1}H-NMR spectrum.

^{1}H-NMR (600 MHz, $CDCl_3$): δ [ppm] = 7.54 (dd, ^3J = 7.53, 1H, aryl), 7.18 (m, 2H, aryl), 6.90 (dd, ^3J = 6.89, 1H, aryl), 0.32 (s, 9H, 1).

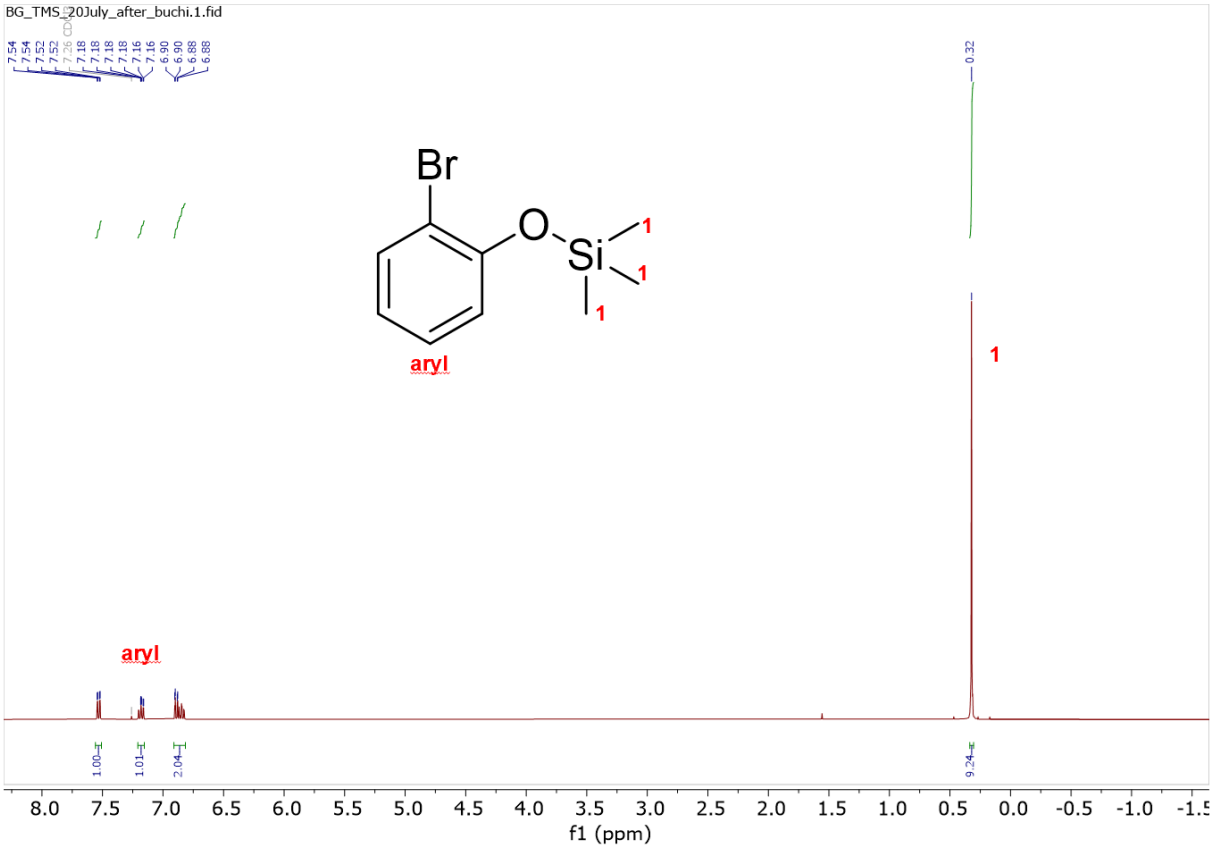

Figure 23 : ^{1}H-NMR spectrum of **10a.**

4.8.2.5 Synthesis of protected bromophenols - 2-(2-bromophenoxy)tetrahydro-2H-pyran (10b)

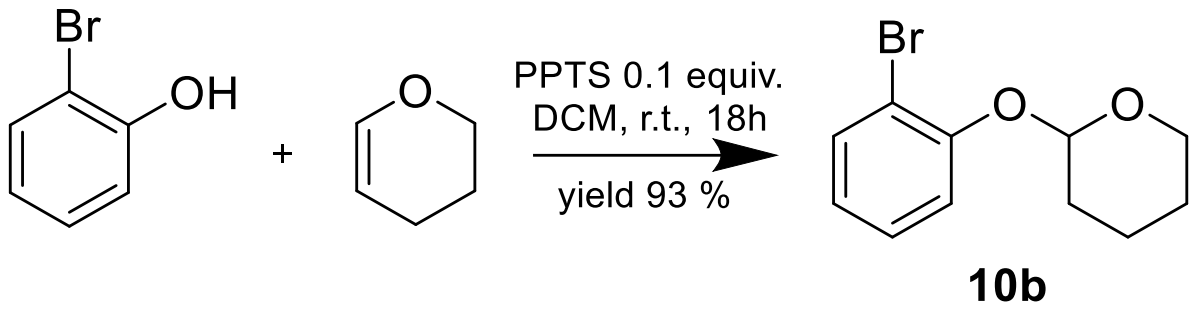

10b

1 g of 2-bromophenol was dissolved in 30 mL dichloromethane, to the mixture was added 800 mg 3,4-dihydro-2H-pyran (10 mmol, 1.7 equiv.) and 145 mg pyridinium p-toluenesulfonate (0.6 mmol, 0.1 equiv.). The mixture was stirred at room temperature for 18 hours. After 18 hours the reaction was quenched with H_2O. The product was extracted with dichloromethane (3 x 25 mL). The combined organic layer was washed with brine, dried over anhydrous $MgSO_4$ and evaporated. Purification was done via flash chromatography (**flash chromatography method 1**) to afford 93 % product as a colorless oil. **10b** was characterized using ^{1}H-NMR. See **Figure 24** for ^{1}H-NMR spectrum.

^{1}H-NMR (600 MHz, $CDCl_3$): δ [ppm] = 7.55 (dd, ^3J = 7.54, 1H, aryl), 7.29 (m, 2H, aryl), 6.87 (dd, ^3J = 6.87, 1H, aryl), 5.52 (t, 1H, 1), 3.91 (m, 1H, 2/3), 3.63 (m, 1H, 2/3), 1.72 (m, 6H, 4/5/6).

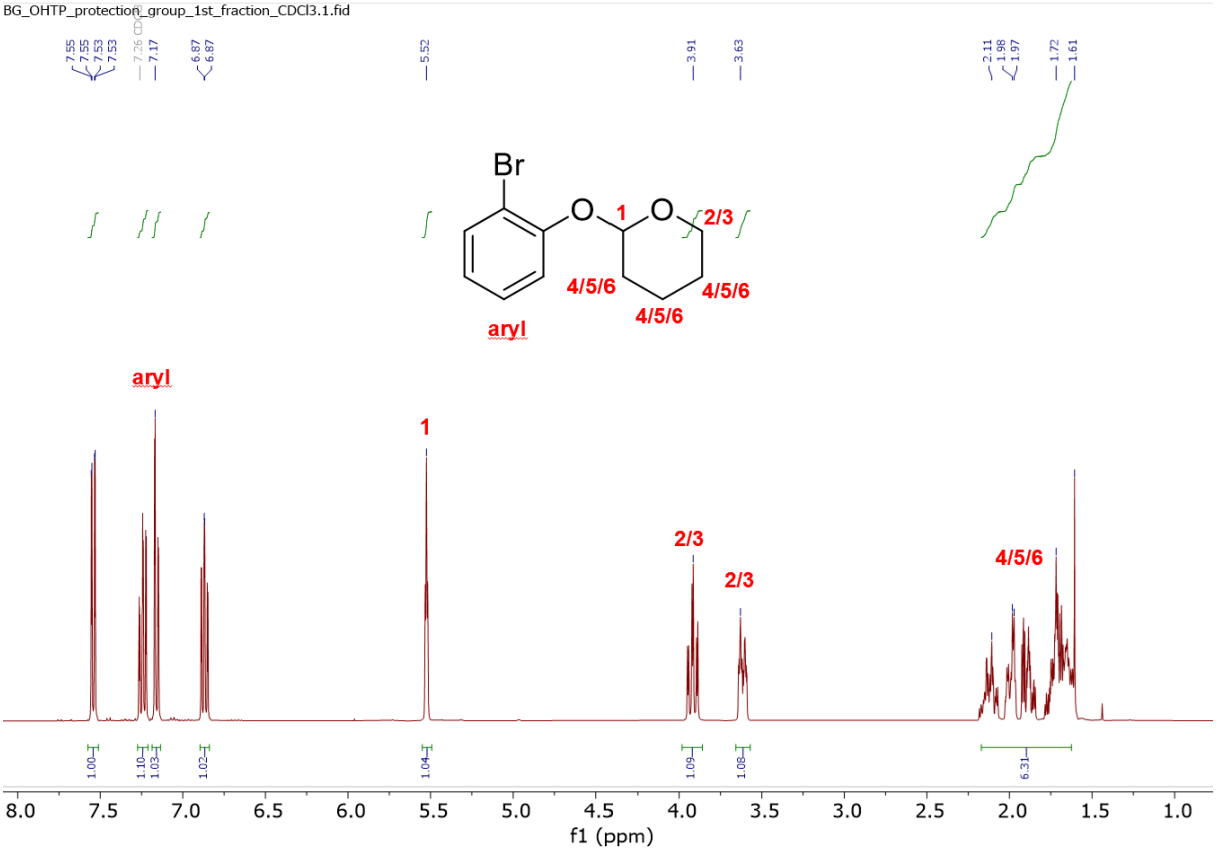

Figure 24 : ^{1}H-NMR spectrum of **10b.**

4.8.2.6 Synthesis of protected bromophenols - 1-bromo-2-(methoxymethoxy)benzene (10c)

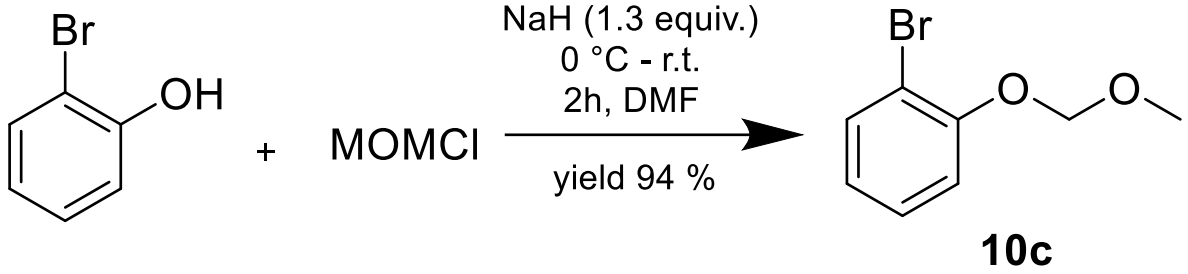

10c

In a flask, 1 g 2-bromophenol (6 mmol, 1 equiv.) was dissolved in 10 mL anhydrous DMF. The mixture was cooled to 0 °C and then 180 mg NaH (8 mmol, 1.3 equiv.) was added. Then 860 mg chloromethyl methyl ether (7 mmol, 1.2 equiv.) was added dropwise to the mixture. The ice batch was removed, and the mixture was stirred at room temperature for 2 hours. Then cooled again and quenched with water. The product was extracted with diethyl ether (3 x 25 mL), the combined organic layers were dried over anhydrous $MgSO_4$, concentrated under vacuum. Purification was done via flash chromatography (**flash chromatography method 1**) to afford 94 % product as a colorless oil. **10c** was characterized using ^{1}H-NMR. See **Figure 25** for ^{1}H-NMR spectrum.

^{1}H-NMR (600 MHz, $CDCl_3$): δ [ppm] = 7.56 (dd, ^3J = 7.55, 1H, aryl), 7.25 (m, 1H, aryl), 7.16 (m, 1H, aryl), 6.89 (dd, ^3J = 6.89, 1H, aryl), 5.25 (s, 2H, 1), 3.53 (s, 3H, 2).

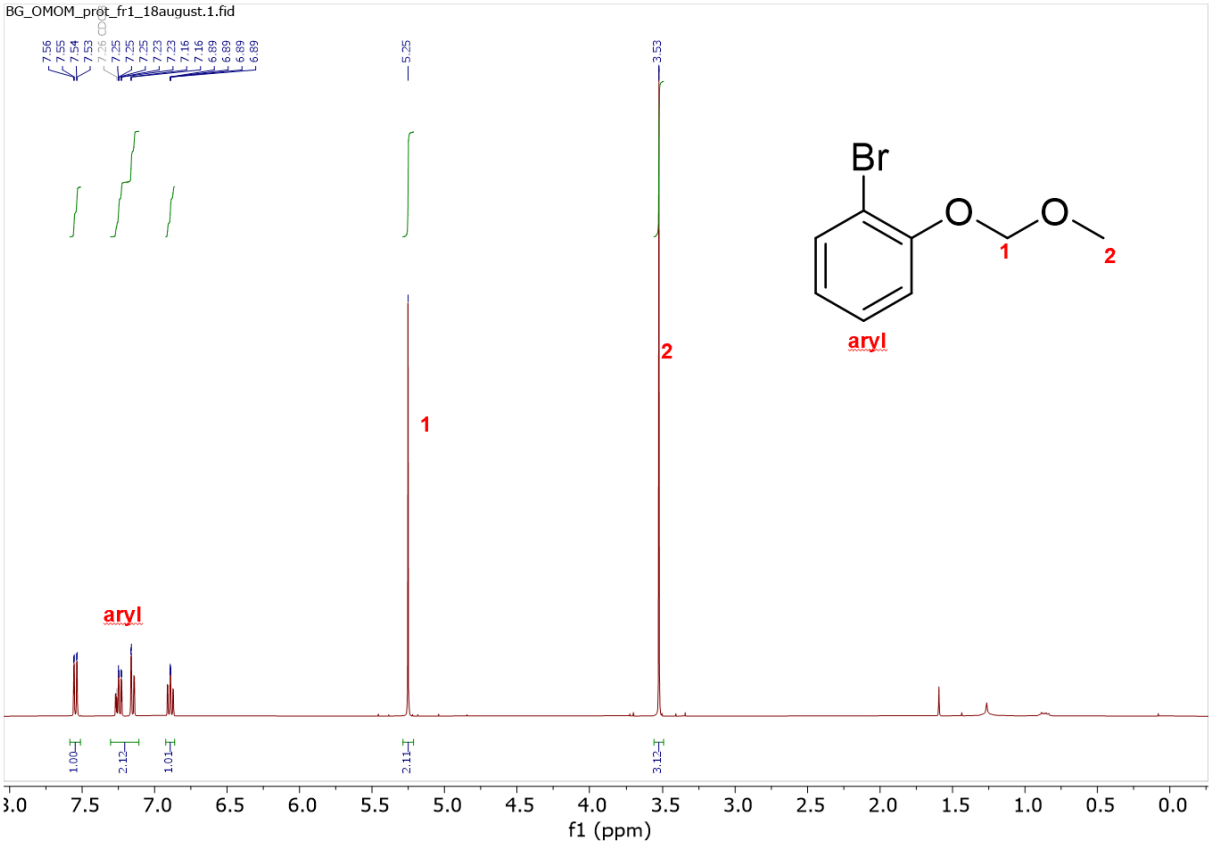

Figure 25 : ^{1}H-NMR spectrum of **10c.**

4.8.2.7 Deprotection of (2-methoxyphenyl)-L-proline (13) to (2-hydroxyphenyl)-L-proline (14)

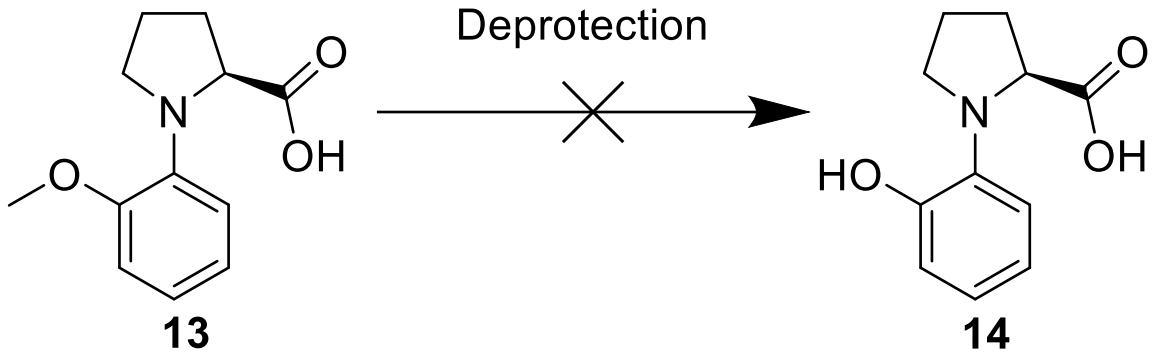

Entry 1: In a Schlenk tube, under N_2 atmosphere, 6 mg (2-methoxyphenyl)-L-proline (**13**) (0.025 mmol, 1 equiv.) were dissolved in 3 mL DCM. The solution was cooled to -78°C with dry ice and acetone. Once at -78 °C, to the solution were added 1.1 equiv. BBr_3 and the mixture was stirred for 1 hour.

Entry 2: In a Schlenk tube, under N_2 atmosphere, 6 mg (2-methoxyphenyl)-L-proline (**13**) (0.025 mmol, 1 equiv.) were dissolved in 3 mL H_2O. Under stirring to the solution were added 5 equiv. of HBr. The mixture was heated to 115 °C and stirred for 16 hours.

Entry 3: In a Schlenk tube, under N_2 atmosphere, 6 mg (2-methoxyphenyl)-L-proline (**13**) (0.025 mmol, 1 equiv.) were dissolved in 3 mL DCM. The solution was cooled to 0 °C with ice and water. Once at 0 °C, to the solution were added 9 equiv. $AlCl_3$ and the mixture was stirred for 24 hours.

Entry 4: In a Schlenk tube, under N_2 atmosphere, 6 mg (2-methoxyphenyl)-L-proline (**13**) (0.025 mmol, 1 equiv.) were dissolved in 3 mL DMSO. Under stirring to the solution were added 4 equiv. ^{t}BuONa. The mixture was heated to 115 °C and stirred for 16 hours.

Entry 5: In a Schlenk tube, under N_2 atmosphere, 6 mg (2-methoxyphenyl)-L-proline (**13**) (0.025 mmol, 1 equiv.) were dissolved in 0.5 mL DMF. Under stirring to the solution were added, ^{t}BuOK 2 equiv. and $HPPh_2$ 2 equiv. The mixture was heated to 80 °C and stirred for 8 hours.

All the entries didn't give the product (**14**), therefore ^{1}H and ^{13}C characterization couldn't be done.

4.8.2.8 Synthesis 2-(2-bromophenyl) 1-(tert-butyl) pyrrolidine-1,2-dicarboxylate (17)

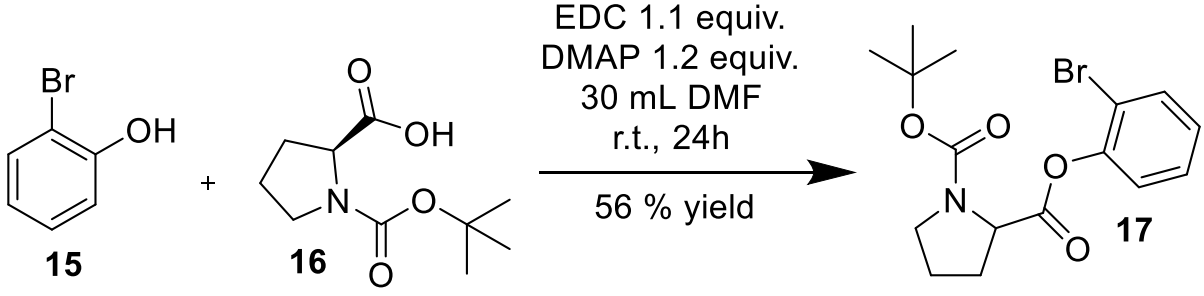

In a flask, 1 g of 2-Bromophenol (**15**) (5.8 mmol, 1 equiv.) and (tert-butoxycarbonyl)-L-proline (**16**) (5.8 mmol, 1 equiv.) were dissolved in 30 mL DMF. Under stirring 1.2 g EDC (6.4 mmol, 1.1 equiv.) and 0.9 g DMAP (7.6 mmol, 1.2 equiv.) were added to the solution. The reaction mixture was stirred at room temperature for 24 hours. After 24 hours, 10 mL of water was added. The mixture was extracted with diethyl ether (3 x 50 mL). The combined organic layers were washed with brine, dried over anhydrous magnesium sulfate, and concentrated by rotavapor. Purification was done via flash chromatography (**flash chromatography method 3**) yielded 56 % product as a brown solid. **17** was characterized using ^{1}H-NMR, ^{13}C-NMR. See **Figure 26** for ^{1}H-NMR spectrum and **Figure 27** for ^{13}C-NMR spectrum.

^{1}H-NMR (600 MHz, $CDCl_3$): δ [ppm] = 7.62 (dd, ^{3}J = 7.61, 1H, aryl), 7.35 (m, 1H, aryl), 7.17 (m, 2H,aryl), 4.55 (m, 1H, 2), 3.52 (m, 2H, 3), 2.40 (m, 2H, 4), 2.11 (m, 1H, 5), 1.96 (m, 1H, 5), 1.48 (s, 9H, 6).

^{13}C-NMR (151 MHz, $CDCl_3$): δ [ppm] = 170.54, 153.89, 133.68, 128.69, 123.58, 116.02, 80.41, 59.28, 46.57, 31.08, 28.63, 23.75.

HRMS (ESI positive mode): +m/z = 371.26 (theoretical +m/z = 370.0576)

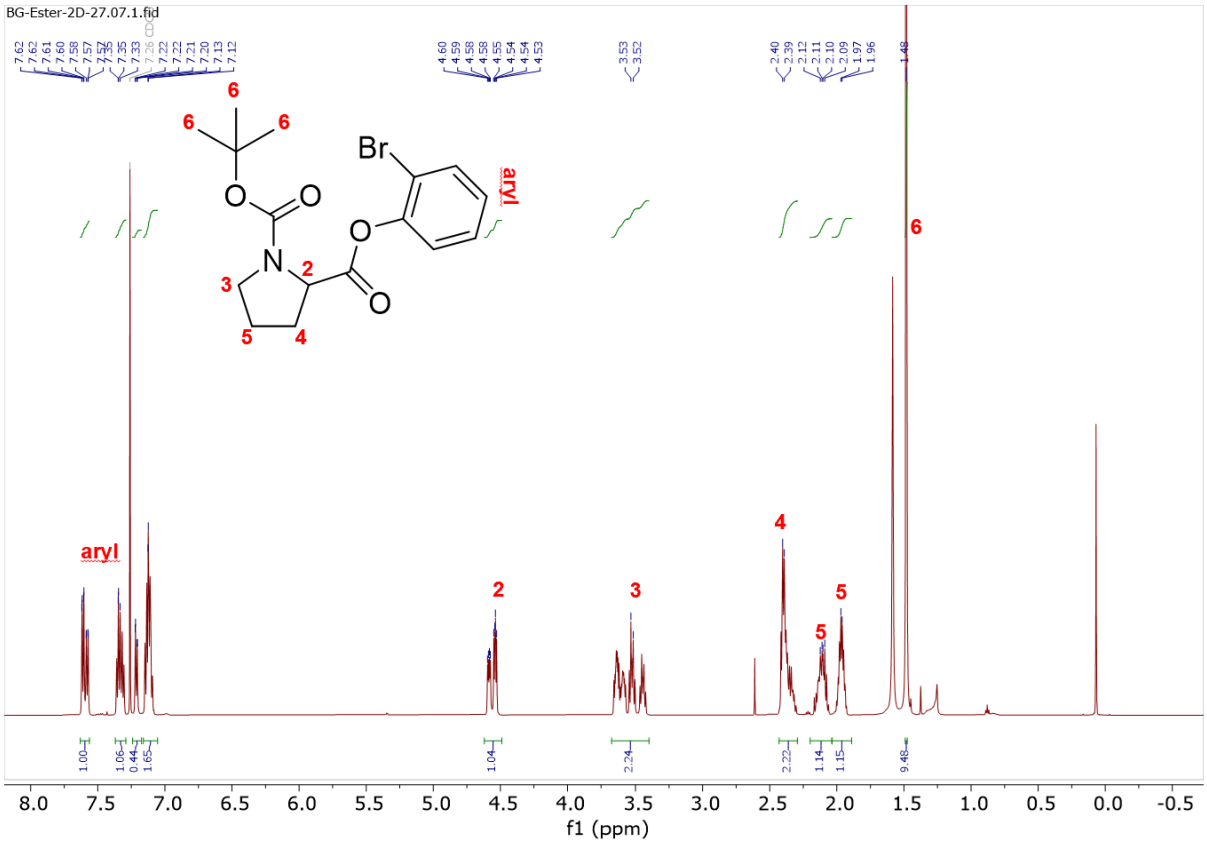

Figure 26 : ^{1}H-NMR spectrum of **17** in $CDCl_3$.

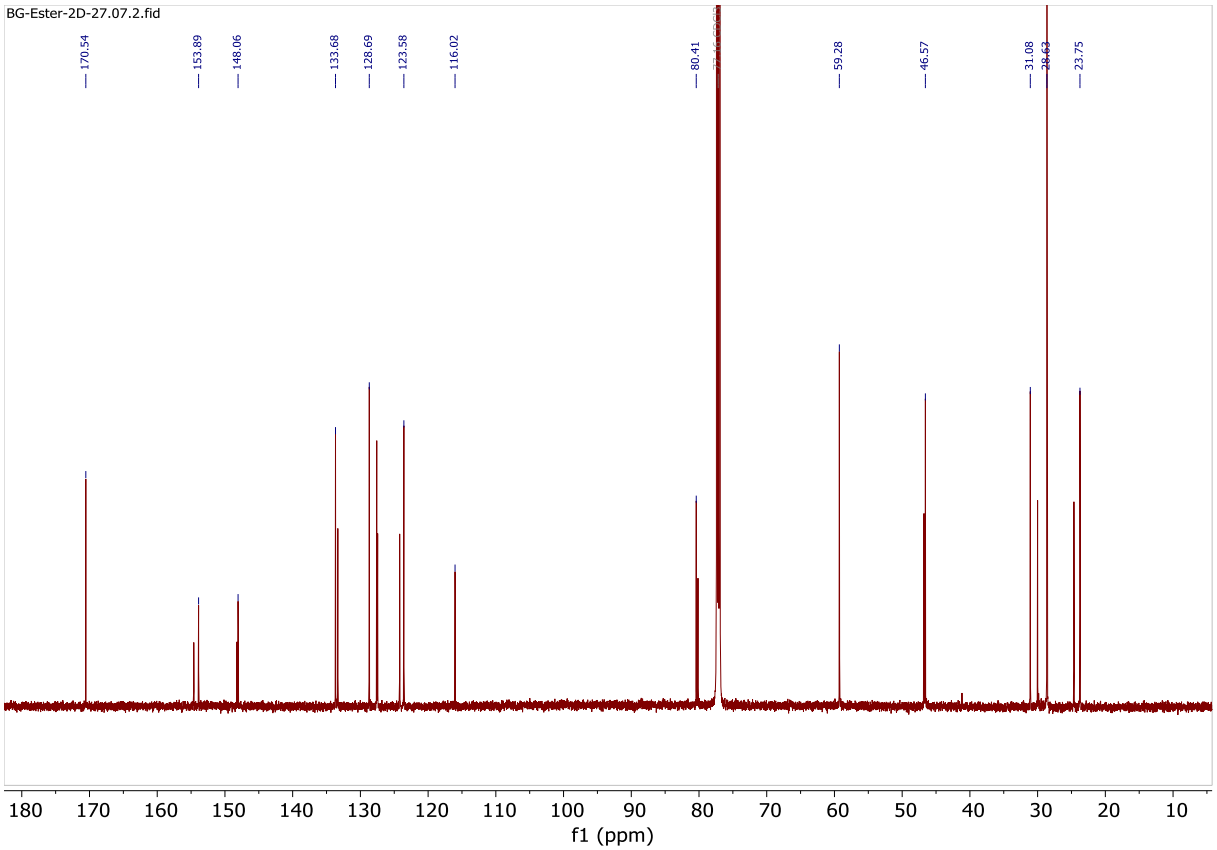

Figure 27 : ^{13}C-NMR spectrum of **17** in $CDCl_3$.

4.8.2.9 Deprotection of 2-(2-bromophenyl) 1-(tert-butyl) pyrrolidine-1,2-dicarboxylate (17) to 2-bromophenyl prolinate (18)

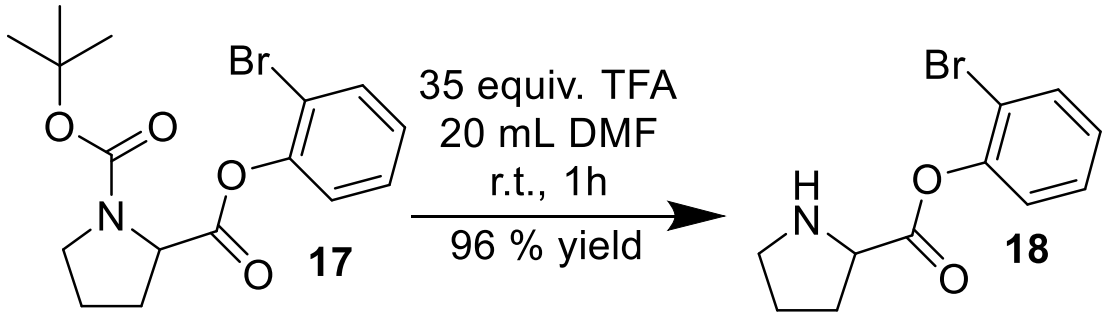

In a flask 100 mg of 2-(2-bromophenyl) 1-(tert-butyl) pyrrolidine-1,2-dicarboxylate (**17**) (0.3 mmol) were dissolved in 20 mL DCM. Under stirring 3 g TFA (25 mmol, 35 equiv.) were added to the solution. The reaction mixture was stirred at room temperature for 1 hour. After 1 hour, the mixture was concentrated by rotavapor. Further purification wasn't necessary, the overall yiel was 96% of the product as white solid. **18** was characterized using ^{1}H-NMR, ^{13}C-NMR. See **Figure 28** for ^{1}H-NMR spectrum and **Figure 29** for ^{13}C-NMR spectrum.

^{1}H-NMR (600 MHz, $CDCl_3$): δ [ppm] = 7.62 (d, ^{3}J = 7.61, 1H, aryl), 7.35 (m, ^{3}J = 7.35, 1H, aryl), 7.18 (m, ^{3}J = 7.35, 2H, aryl), 4.81 (m, 1H, 2), 3.54 (m, 2H, 3), 2.60 (m, 2H, 4), 2.18 (m, 2H, 5)

^{13}C-NMR (151 MHz, $CDCl_3$): δ [ppm] = 167.22, 160.07, 146.93, 133.45, 128.9, 128.37, 123.29, 59.37, 46.42, 39.54 (impurity), 28.89, 23.81.

HRMS (ESI positive mode): +m/z = 270.01 (theoretical +m/z = 270.0124)

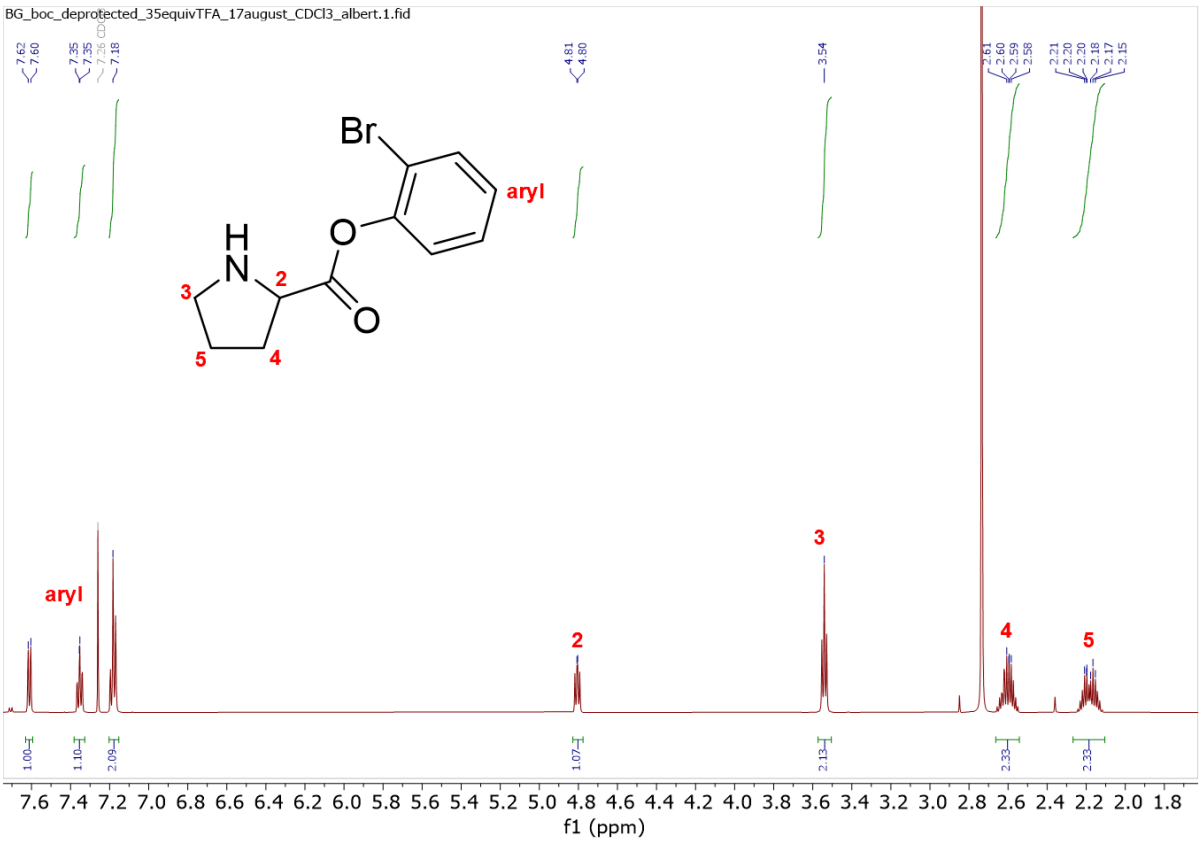

Figure 28 : ^{1}H-NMR spectrum of **17** in $CDCl_3$.

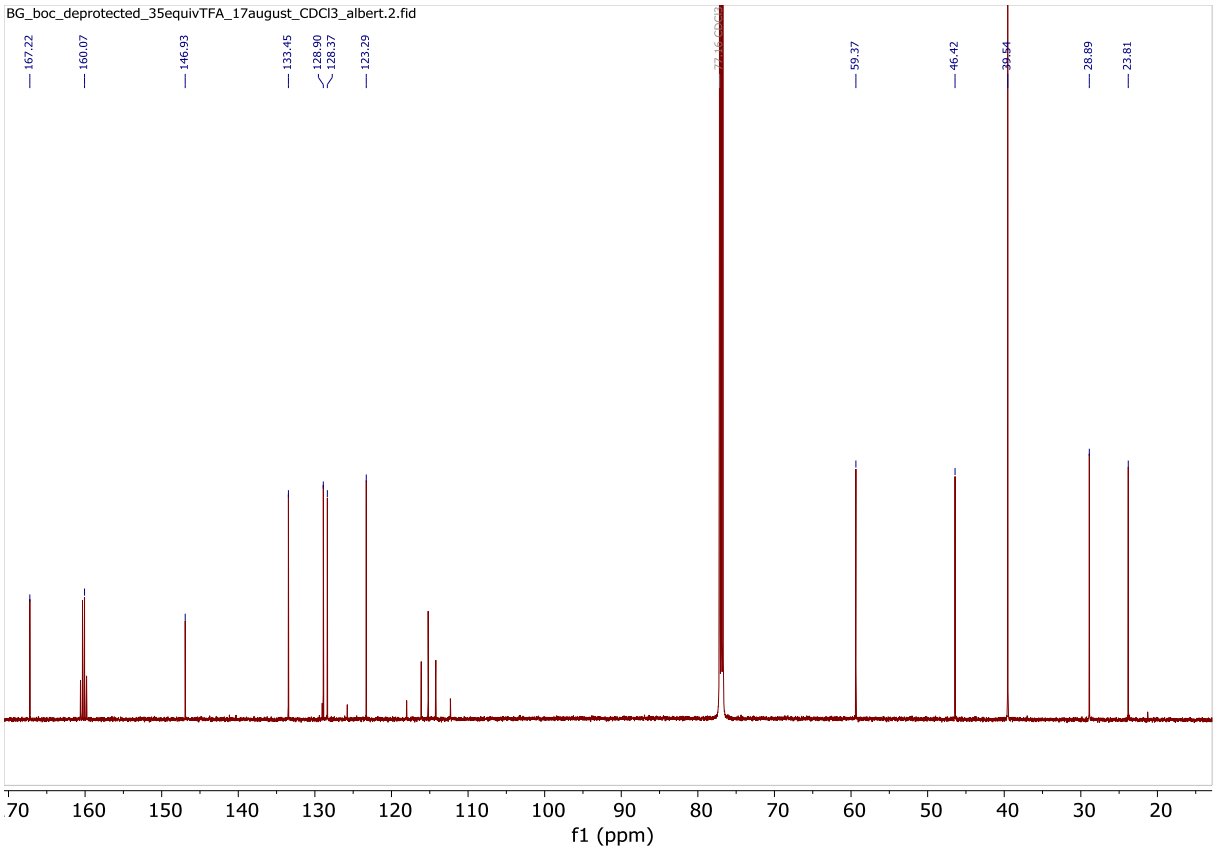

Figure 29 : ^{13}C-NMR spectrum of **17** in $CDCl_3$.

4.8.2.10 Intramolecular Ulmann coupling 2-bromophenyl prolinate (19)

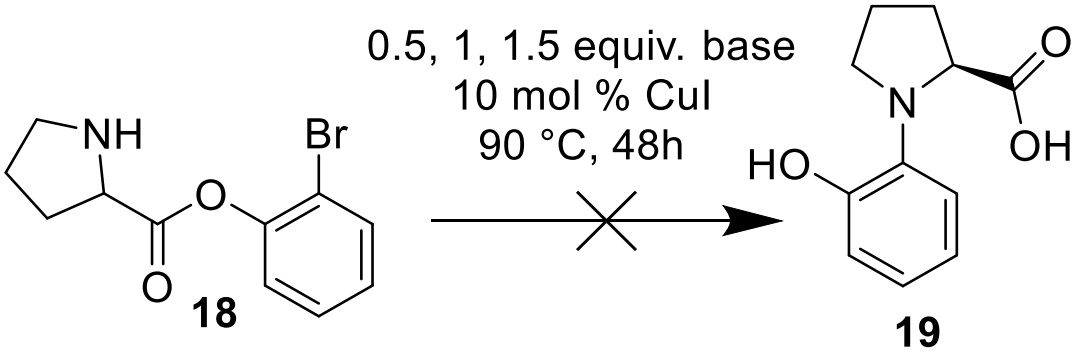

In a Schenk tube, under N_2 atmosphere, 50 mg of 2-bromophenyl prolinate (**18**) (0.18 mmol) were dissolved in 3 mL DMSO. Under stirring no base, 0.5, 1.5 or 2.5 equiv. K_2CO_3 or 1.5 equiv. TEA and 10 mol % CuI were added. The reaction mixture was stirred on 90°C for 48 hours. After 48 hours the reaction mixture was cooled down to room temperature, then 10 mL of ethyl acetate were added. Under cooling with ice and water, concentrated HCl was added to acidify the mixture to pH 2-3. Then the organic layer was separated, and the aqueous layer was extracted with ethyl acetate (5 x 15 mL). The combined organic layers were washed with brine, dried over anhydrous magnesium sulfate, and concentrated by rotavapor. No product was observed, therefore ^{1}H and ^{13}C characterization couldn't be done.

4.8.2.11 Synthesis of (2-methyl-6-nitrophenyl)-L-proline (22)

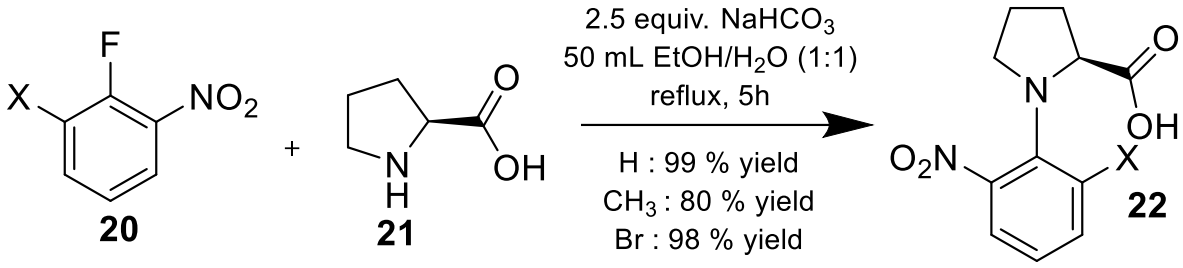

X = H, CH_3 or Br

In a flask, 1 g of 1-fluoro-2-nitrobenzene **(X= H, CH_3 or Br)** (**20**) (7 mmol, 1 equiv.) was dissolved in 50 mL H_2O/EtOH (1:1). Under stirring to the solution was added 1.5 g $NaHCO_3$ (17.8 mmol, 2.5 equiv.) followed by 0.8 g L-Proline (**21**) (7 mmol, 1 equiv.). The mixture was refluxed for 5 hours and then cooled down to room temperature. After removing EtOH by rotavapor, the remaining solution was acidified with concentrated HCl to pH 2-3 and extracted with EtOAc (3 x 70 mL). The combined organic layer was washed with brine, dried over anhydrous $MgSO_4$, and concentrated under reduced pressure. The residue was dried under vacuum to give, in quantitative yield, a yellow oil for all three *ortho* substituents were obtained. **22** was characterized using ^{1}H-NMR, ^{13}C-NMR. See **Figure 30** for ^{1}H-NMR spectrum and **Figure 31** for ^{13}C-NMR spectrum.

^{1}H-NMR (600 MHz, $CDCl_3$): δ [ppm] = 7.53 (dd, ^3J = 7.52, 1H, aryl), 7.41 (dd, ^3J = 7.40, 1H, aryl), 7.15 (t, ^3J = 7.15, 2H, aryl), 3.95 (m, 1H, 2), 3.54 (m, 1H, 3), 3.21 (m, 1H, 3), 2.39 (s, 3H, 4), 2.35 (m, 1H, 5/6), 2.17 (m, 1H, 5/6), 2.05 (m, 2H,5/6).

^{13}C-NMR (151 MHz, $CDCl_3$): δ [ppm] = 179.10, 148.95, 140.78, 138.76, 135.45, 125.39, 122.87, 62.95, 52.85, 31.38, 25.32, 18.51.

HRMS (ESI positive mode): +m/z = 251.096 (theoretical +m/z = 251.10)

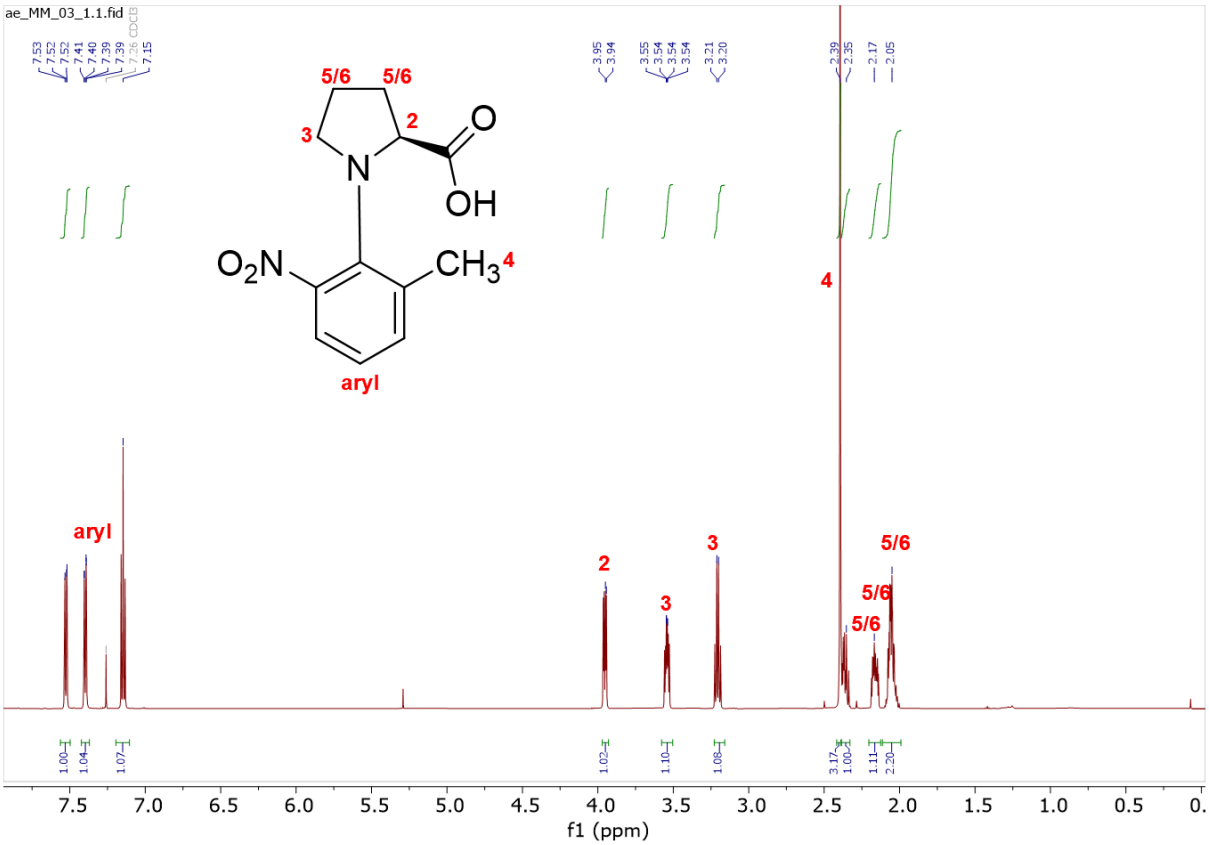

Figure 30 : ^{1}H-NMR spectrum of **22** in $CDCl_3$.

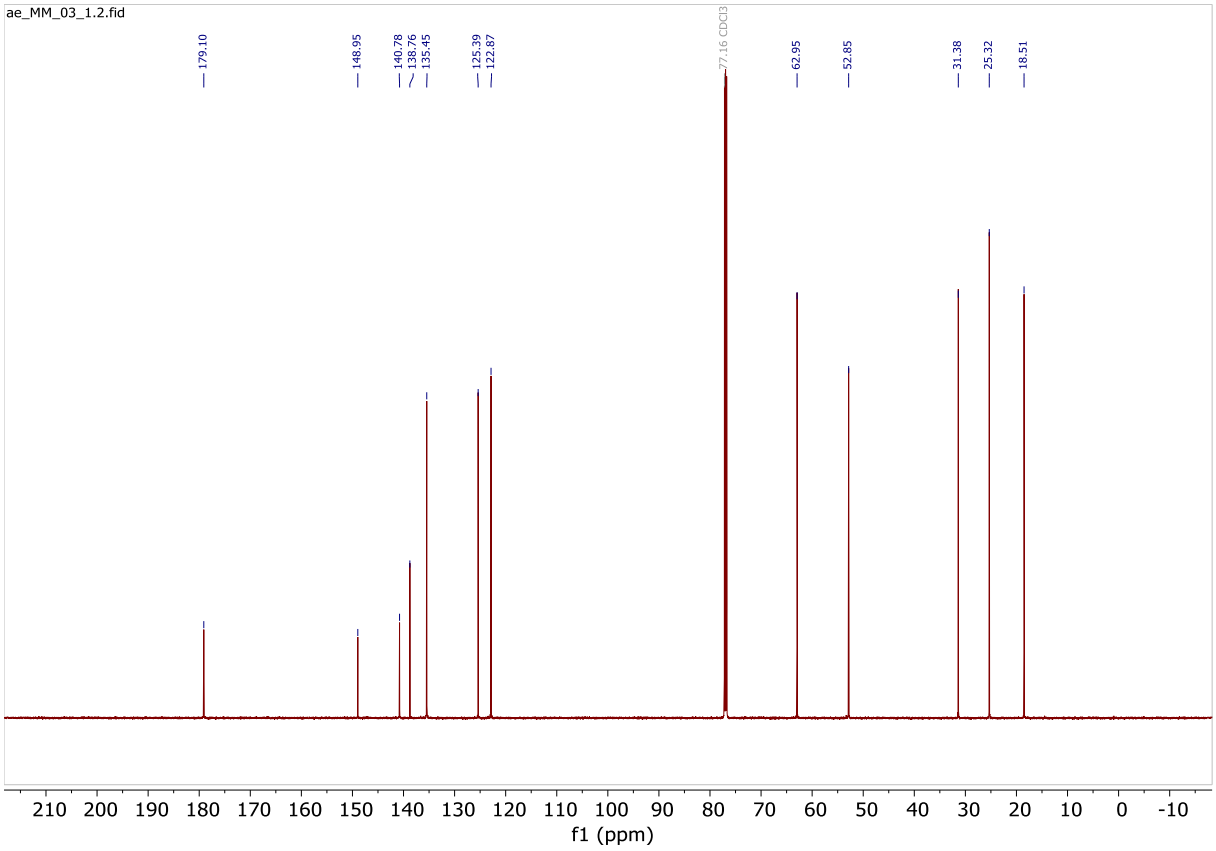

Figure 31 : ^{13}C-NMR spectrum of **22** in $CDCl_3$.

4.8.2.12 Reduction of (2-methyl-6-nitrophenyl)-L-proline (22) to (2-amino-6-methylphenyl)-L-proline (23)

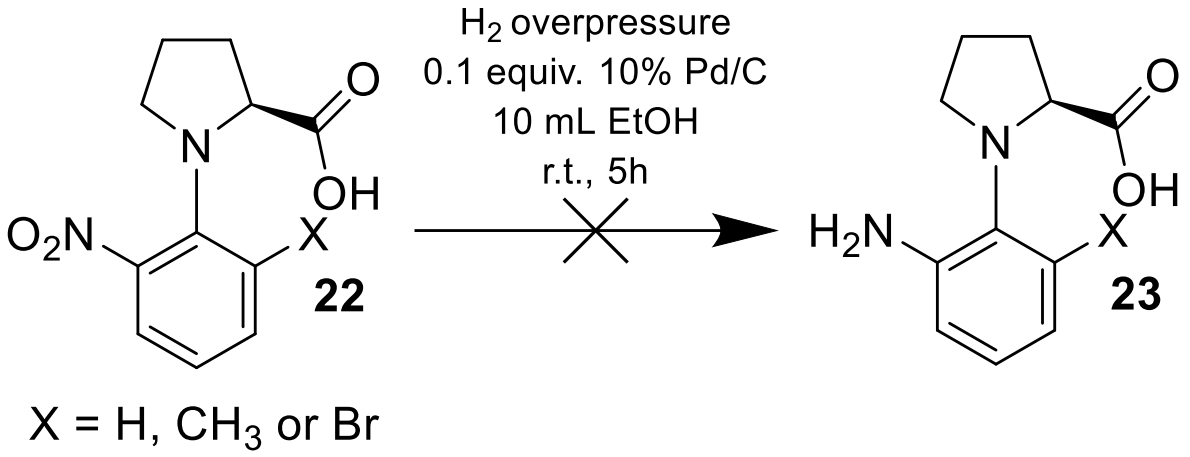

X = H, CH_3 or Br

In a flask, 50 mg **(X= H, CH_3 or Br)** (**22**) (0.2 mmol) 2-methyl-6-nitrophenyl)-L-proline and 2.2 mg of 10% Pd/C (0.02 mmol, 0.1 equiv.) were dissolved in 10 mL EtOH under an atmosphere of H_2 at room temperature under stirring for 5 hours. The mixture was filtered, and the filtrate was concentrated under vacuum. No product (**23**) formation was observed, therefore ^{1}H and ^{13}C characterization couldn't be done.

4.8.2.13 Hydrolysis of (1,2,3,3a-tetrahydropyrrolo[1,2-a] quinoxalin-4(5H)-one) (22b) to (2-aminophenyl)-L-proline (23).

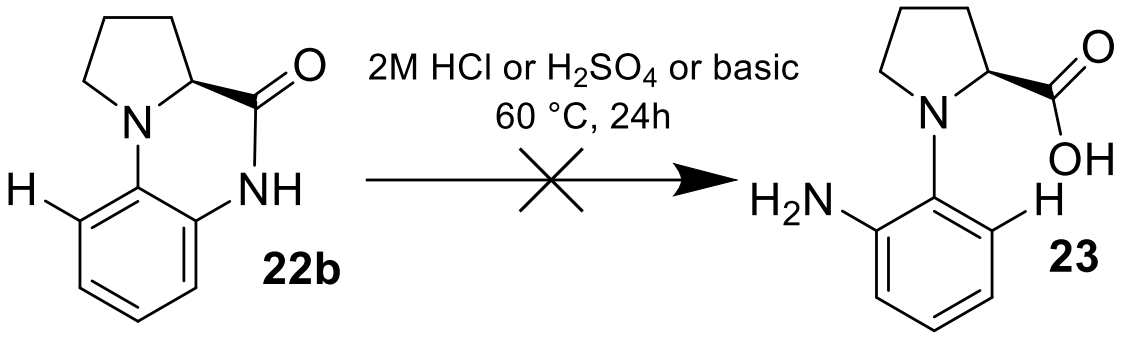

In a flask, 19 mg of (1,2,3,3a-tetrahydropyrrolo[1,2-a] quinoxalin-4(5H)-one) (**22b**) (0.1 mmol) was dissolved in acidic solutions (2M HCl, 2M H_2SO_4), and in basic solutions (0.25, 0.5, 1, 1.5, 2 M NaOH). The mixture was stirred for 24 hours on 60°C. Reaction control was taken at the end without purification. The product (**23**) wasn't observed.

4.8.2.14 Synthesis of tert-butyl (2-methyl-6-nitrophenyl)-L-prolinate (23b)

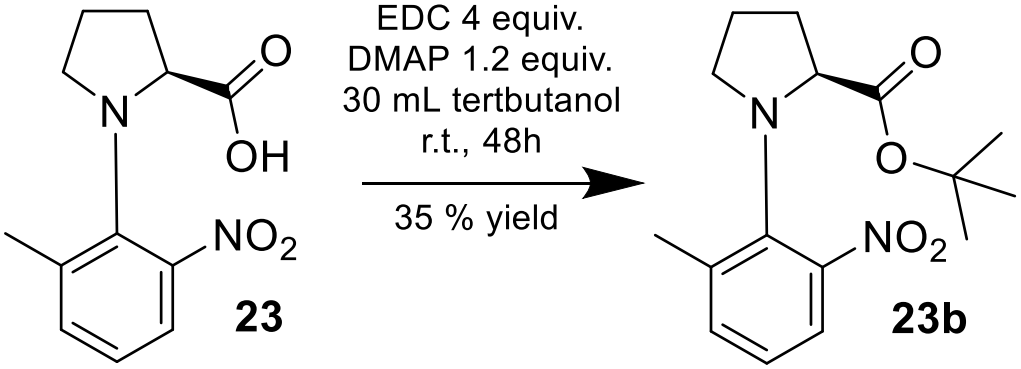

In a flask, 1 g of (2-methyl-6-nitrophenyl)-L-proline (**23**) (4 mmol, 1 equiv.) was dissolved in 30 mL Tertbutanol. Under stirring 2.45 g EDC (16 mmol, 4 equiv.) and 0.6 g DMAP (4.8 mmol, 1.2 equiv.) were added to the solution. The reaction mixture was stirred at room temperature for 48 hours. After 48 hours, 10 mL of water was added. The mixture was extracted with diethyl ether (3 x 50 mL). The combine organic layer were washed with brine, dried over anhydrous magnesium sulfate, and concentrated by rotavapor. Purification was done via flash chromatography (**flash chromatography method 3**) yielded 35 % product as a yellow liquid. **23b** was characterized using ^{1}H-NMR, ^{13}C-NMR. See **Figure 32** for ^{1}H-NMR spectrum and **Figure 33** for ^{13}C-NMR spectrum.

^{1}H-NMR (600 MHz, $CDCl_3$): δ [ppm] = 7.50 (dd, ^{3}J = 7.50, 1H, aryl), 7.38 (dd, ^{3}J = 7.37, 1H, aryl), 7.09 (m, 1H, aryl), 3.76 (m, 1H, 2), 3.52 (m, 1H, 3), 3.18 (m, 1H, 3), 2.39 (s, 3H, 7), 2.20 (m, 1H, 5/6), 2.05 (m, 3H, 5/6), 1.24 (s, 9H, 4).

^{13}C-NMR (151 MHz, $CDCl_3$): δ [ppm] = 172.43, 141.03, 139.58, 134.78, 124.37, 122.58, 80.39, 63.27, 52.11, 30.34, 27.64, 18.53.

HRMS (ESI positive mode): +m/z = 307.16 (theoretical +m/z = 307.1652)

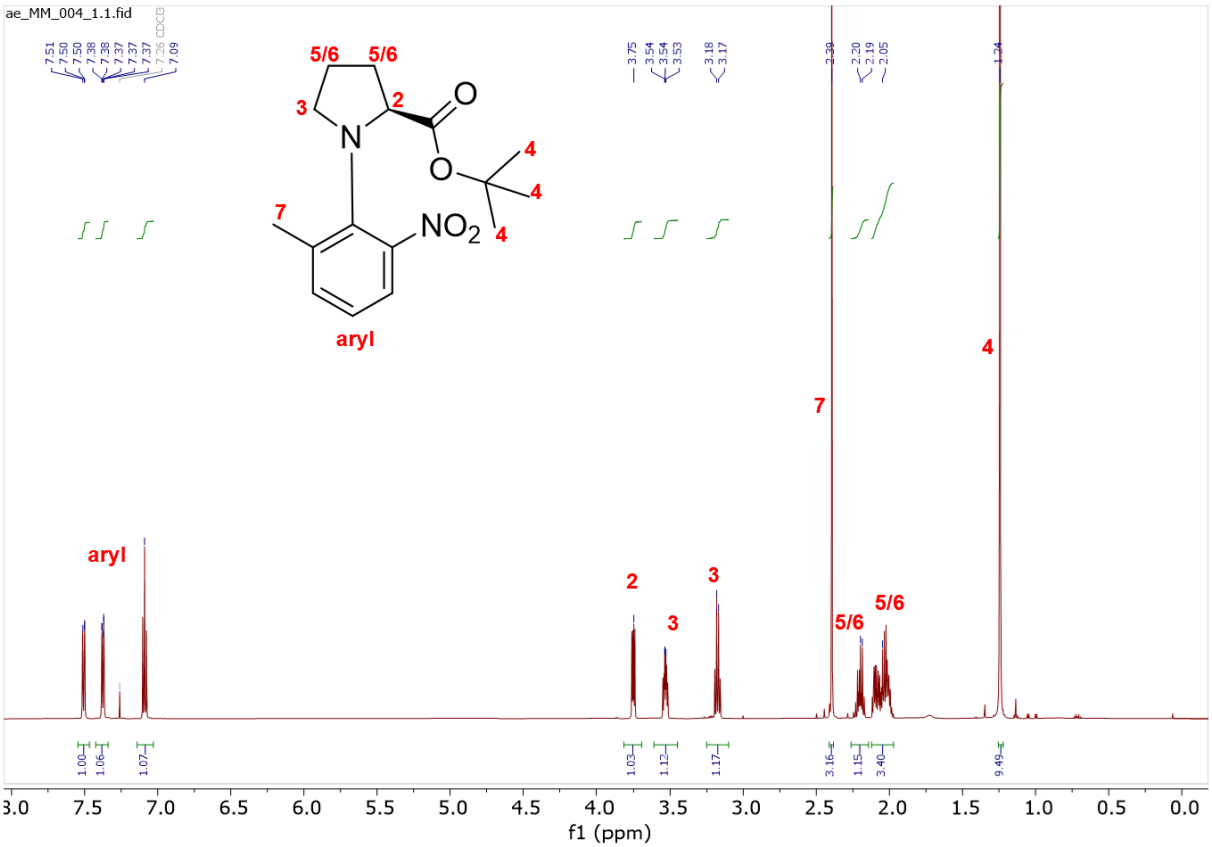

Figure 32 : ^{1}H-NMR spectrum of **23b** in $CDCl_3$.

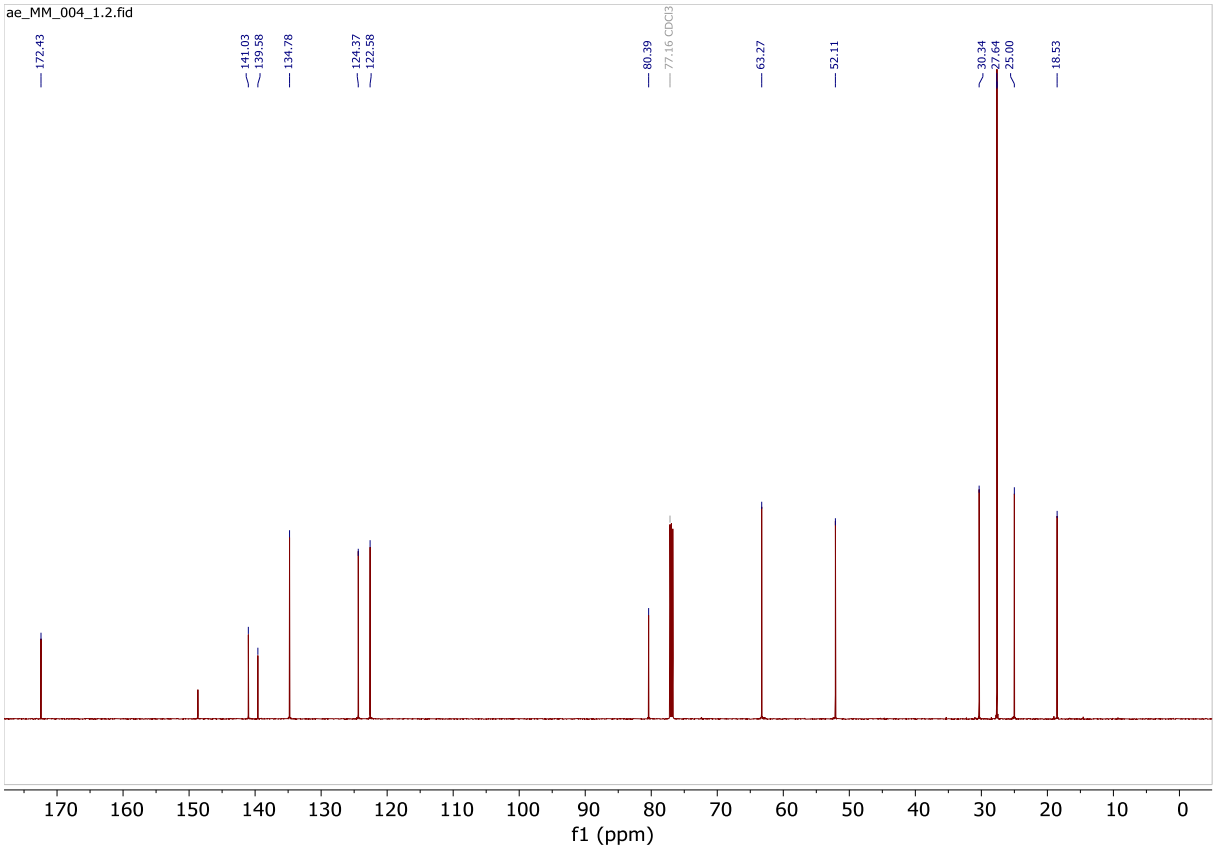

Figure 33 : ^{13}C-NMR spectrum of **23b** in $CDCl_3$.

4.8.2.15 Reduction of tert-butyl (2-methyl-6-nitrophenyl)-L-prolinate to tert-butyl (2-amino-6-methylphenyl)-L-prolinate (24)

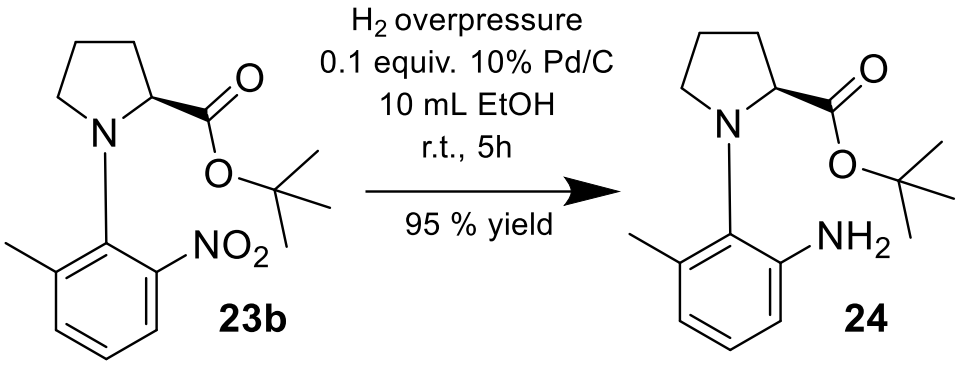

In a flask, 500 mg (1.7 mmol) tert-butyl (2-methyl-6-nitrophenyl)-L-prolinateand 18 mg of 10% Pd/C (0.17 mmol, 0.1 equiv.) were dissolved in 50 mL EtOH under an atmosphere of H_2 at room temperature under stirring for 5 hours. The mixture was filtered, and the filtrate was concentrated under vacuum. A qualitative yield of 95% was achieved. ^{1}H-NMR was done for characterization(**Figure 34).**

^{1}H-NMR (600 MHz, $CDCl_3$): δ [ppm] = 7.52 (dd, ^3J = 7.53, 1H, aryl), 7.38 (m, 1H, aryl), 7.10 (m, 1H, 1), 3.72 (m, 1H, 2/3), 3.18 (m, 1H, 2/3), 2.41 (s, 3H, 4), 2.11 (m, 4H, 5/6), 1.25 (s, 9H, 7)

HRMS (ESI positive mode): +m/z = 277.186 (theoretical +m/z = 277.19)

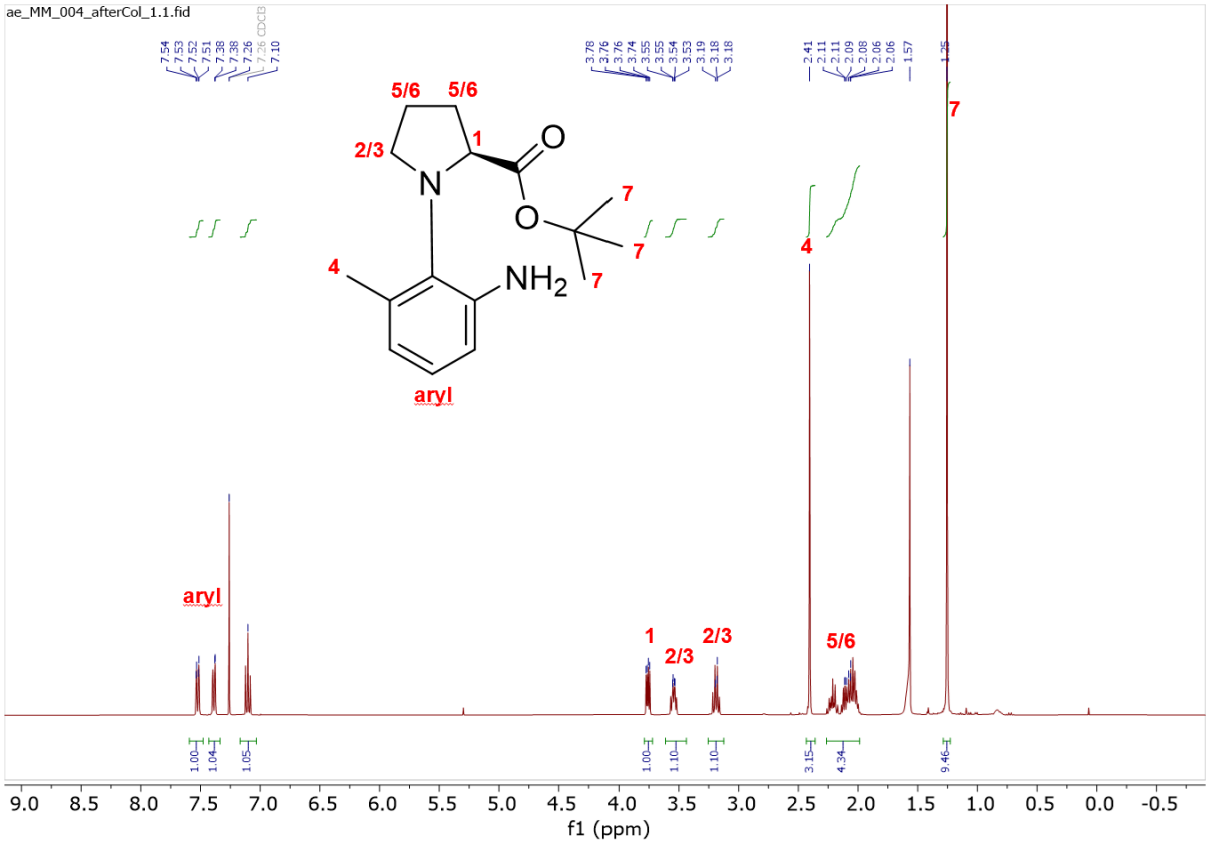

Figure 34 : ^{1}H-NMR spectrum of **24** in $CDCl_3$.

4.8.2.16 Synthesis of tert-butyl (2-(diphenoxyphosphoryl)-6-methylphenyl)-L-prolinate (24)

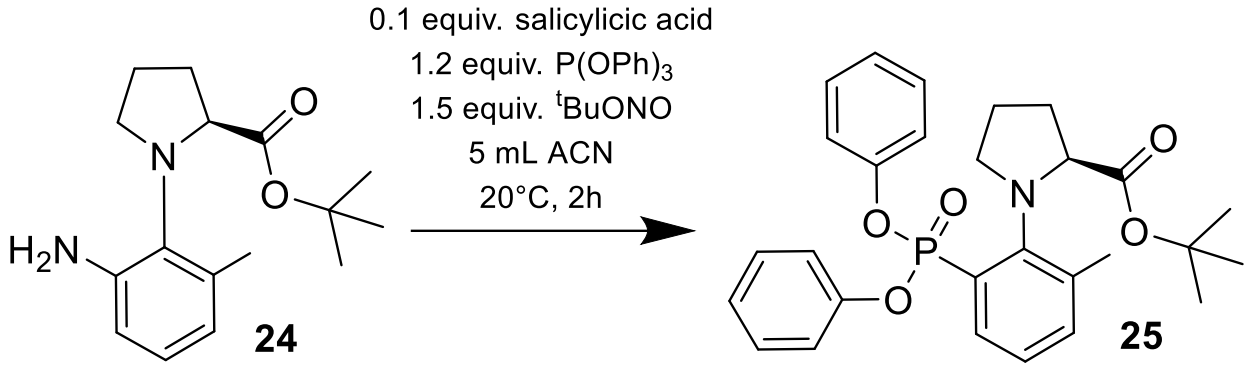

In a Schlenk tube, under N_2 atmosphere, 25 mg (0.09 mmol, 1 equiv.) tert-butyl (2-amino-6-methylphenyl)-L-prolinate (**24)** and salicylic acid 1.7 mg (0.009 mmol, 0.1 equiv.) were dissolved in 5 mL ACN. Then 34 mg (0.11 mmol, 1.2 equiv.) $P(OPh)_3$ were added. The reaction mixture was stirred until a homogenous solution was obtained. Then 14 mg (0.14 mmol, 1.5 equiv.) ^{t}BuONO was added, and the mixture was stirred for 2 hours at 20°C. After 2 hours, the mixture was diluted with 30 mL EtOAc, concentrated under vacuum. Purification was done using flash chromatohraphy (**flash chromatography method 2**). Qualitative yield estimated was around 5-10 %. Due to the instability and impurities **24** couldn't be characterized using ^{1}H-NMR and ^{13}C-NMR.

HRMS (ESI positive mode): +m/z = 494.218 (theoretical +m/z = 494.21)

4.8.2.17 Deprotection of tert-butyl (2-(diphenoxyphosphoryl)-6-methylphenyl)-L-prolinate (25) to (2-(2-(tert-butoxycarbonyl) pyrrolidin-1-yl)-3-methylphenyl)phosphonic acid (26)

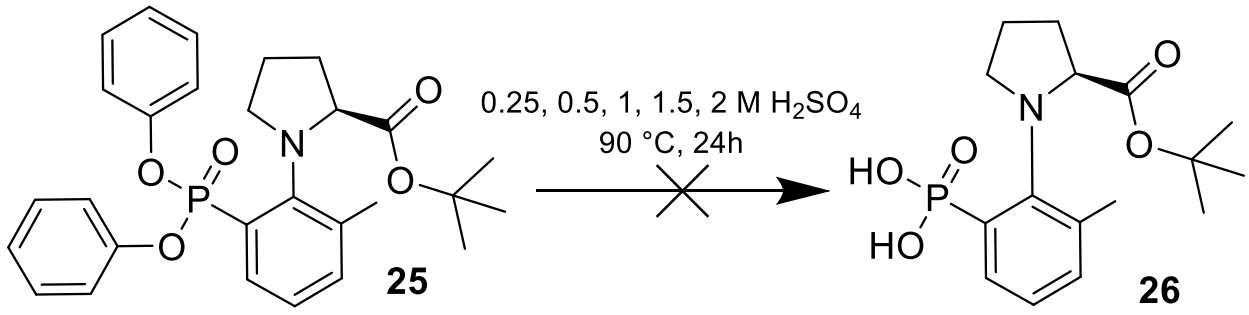

In a flask, 10 mg of tert-butyl (2-(diphenoxyphosphoryl)-6-methylphenyl)-L-prolinate **(25)** (0.03 mmol) was dissolved in acidic solutions (0.25, 0.5, 1, 1.5, 2 M H_2SO_4). The mixture was stirred for 24 hours on 90°C. Reaction control was taken at the end without purification. The product wasn't observed.

4.8.2.18 Synthesis of (2-(2-(tert-butoxycarbonyl)pyrrolidin-1-yl)-3-methylphenyl)phosphoramidic acid (25b)

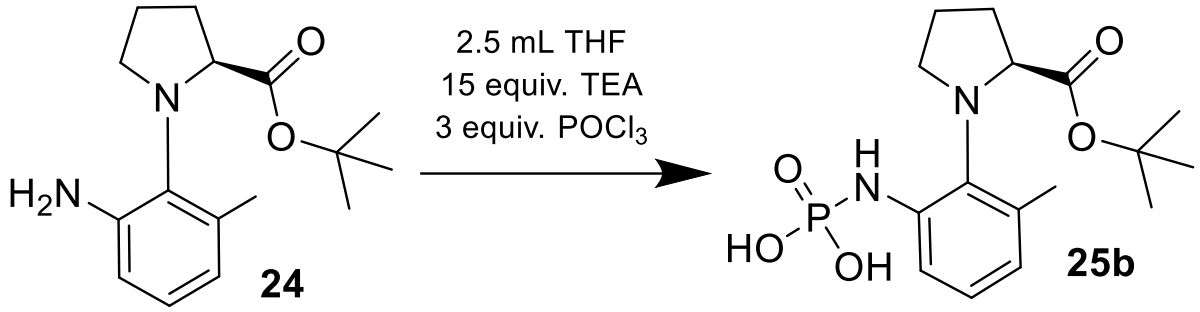

In a flask 250 mg (**24**) (0.9 mmol, 1 equiv.) tert-butyl (2-amino-6-methylphenyl)-L-prolinate in a 2.5 mL THF was dissolved. In another flask was dissolved 1.4 g (13.5 mmol, 15 equiv.) triethylamine and 420 mg (2.7 mmol, 3 equiv.) $POCl_3$ in 2.5 mL THF. Then the second solution was added to the first solution dropwise at 0°C. The mixture was stirred for 15 minutes and added to 15 mL ACN/H_2O (1:1) dropwise. Purification was done using flash chromatography (**flash chromatography method 5**). Qualitative yield obtained was around 3-5%, therefore **25b** couldn't be characterized using ^{1}H-NMR, ^{13}C-NMR.

HRMS (ESI positive mode): +m/z = 357.156 (theoretical +m/z = 357.12)

5. Results and discussion

5.1 NESS based on acylphosphonates [22,23]

Non-equilibrium steady states are a fundamental prerequisite for the design of molecular motors. While acylphosphate steady states were previously shown to be accessed in carbodiimide and carboxylic anhydride driven reaction cycles, very little focus was set towards acylphosphonates. For this reason, non-equilibrium steady states based on phosphonates were investigated. The kinetic profiles of acylphosphates are compared to the ones of acylphosphonates. The latter compounds are intriguing because dephosphorylation of C-P bond is not a concern and can be used to advantage. [24]

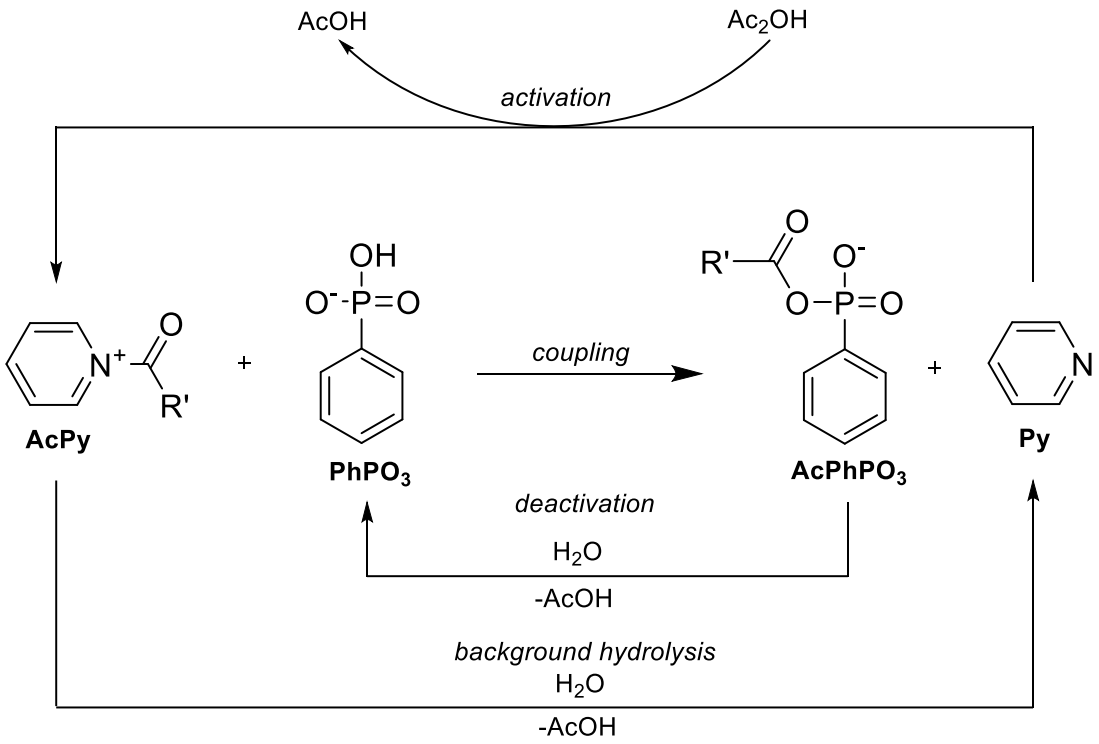

Figure 35 : Detailed reaction scheme of acylphosphonate reaction cycle. See chapter **4.3** for additional information about sample preparation.

In aqueous media acylphosphonates undergo hydrolysis towards their phosphonic and carboxylic acid moieties.[24] Acylation agents, however, can be used to maintain the system in a non-equilibrium steady state, as schematically shown in **Figure 35**. Here acetic anhydride (Ac_2O) is used to directly acetylate the $PhPO_3$ precursor. The acylation efficiency of this reaction can be highly influenced by means of organocatalysis. As can also be seen in more details in **Figure 35**, Py reacts in a first step with Ac_2O to form a reactive acyl pyridinium species (PyAc). This intermediate then reacts with $PhPO_3$ leading to the formation of $PhAcPO_3$ as steady state species. Since this forward reaction pathway is competing with the hydrolysis of $PhAcPO_3$, the product is transient nature. After fuel consumption the steady states species completely hydrolyses back to $PhPO_3$, and two equivalents of acetic acid are generated as waste.

Quantitative ^{31}P-NMR was used for the investigation of the $PhPO_3$ reaction cycle. TMP was used as an internal standard, and the course of the reaction is depicted in **Figure 35.**

The spectra at 0 min, contained no Ac_2O. After fuel addition, further ^{31}P-NMRs were measured at 2 min, 75 min and 105 min. Over the course of the reaction a new species ($PhAcPO_3$) with a downfield shift was observed (12.2 ppm). Quantitative activation yield was achieved after 2 minutes. It is also noteworthy that the $PhPO_3$ peak experiences an up-field shift after anhydride addition. This shift is most likely due to a change in the pH of the reaction media caused by production of acetic acid as a waste product.

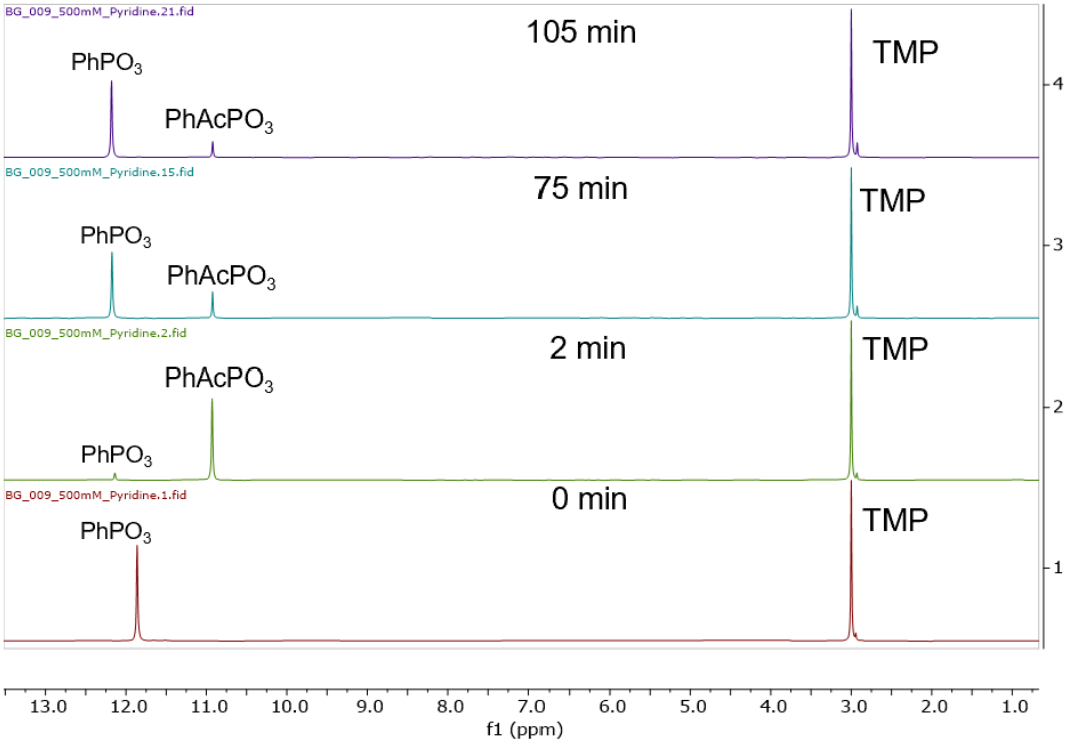

Figure 36 : ^{31}P-NMR of the PhPO3 reaction cycle over the course of 2 hours. 25 mM of $PhPO_3$ was used, 4 equiv. Ac2O, MOPS 500 mM diluted in water, pH was adjusted to 7.5 with HCl.

To get a better understanding of the tuneability of the system, the influence of Py was investigated by means of ^{31}P-NMR. As shown in **Figure 36,** two runs where the concentration of the Py was set to 50 mM for the first run and 500 mM for the second run were conducted. The exponential decay of $PhAcPO_3$ concentration after addition of Ac_2O was fitted according to the following regression function:

$$Acp[t] = A_1 \times e^{-t \times k} \quad \textbf{(1)}$$

The half-life ($t_{1/2}$) and rate constant (k) were calculated according to the following equations:

$$k = \frac{1}{t} \quad \textbf{(2)}$$

$$t_{1/2} = \frac{\ln(2)}{k} \quad \textbf{(3)}$$

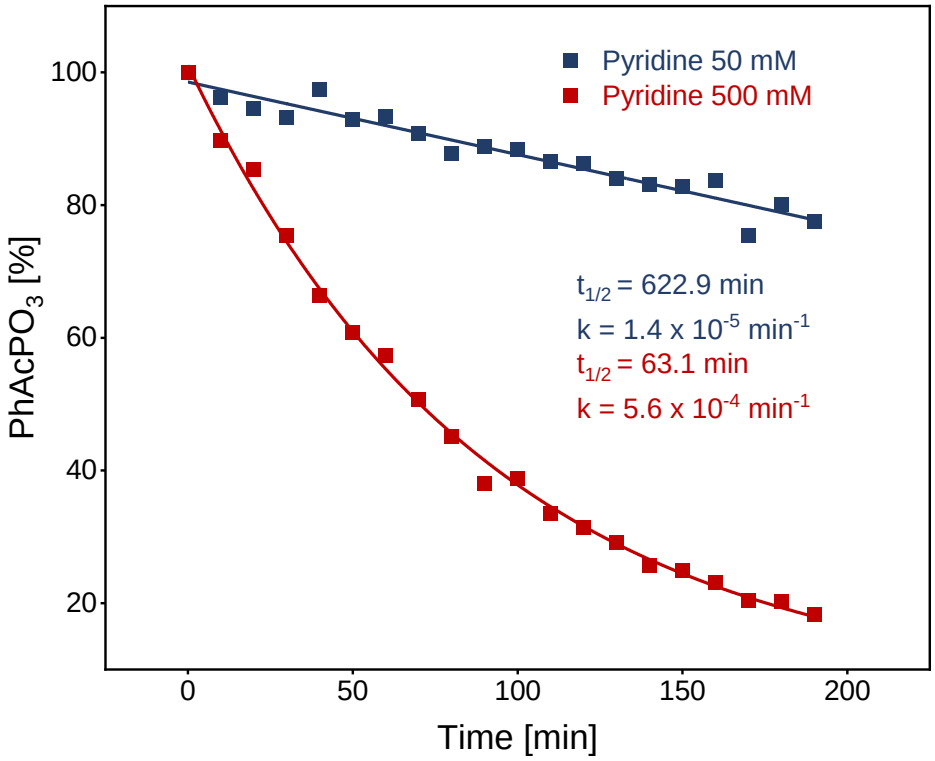

Figure 37 : Kinetic profile of $PhPO_3$ reaction cycle with varying Py concentrations. 25 mM of $PhPO_3$ was used, 50 (blue) and 500 (red) mM of Py, MOPS 500 mM diluted in water, pH was adjusted to 7.5 with HCl, 100 mM of Ac2O was used for activation.

Figure 37 represents the percentage of hydrolysis of $PhAcPO_3$ plotted over time. Respective half-lives and hydrolysis rates are shown in the plot for each Py concentration. The reaction cycle with 50 mM of Py exhibits a ten times lower half-life than the reaction cycle with 500 mM of catalyst. This means an increase in pyridine concentration accelerates the backward reaction. This is not surprising since pyridine can react with $AcPhPO_3$ to from AcPy which than hydrolysis back to the respective precursors.

5.1.1 Comparison of NESS based on acylphosphates and acylphosphonates

To further explore the distinctions between the acylation of phosphates and phosphonates, an experiment was conducted using similar reaction conditions as described previously. However, instead of $PhPO_3$, phenylphosphoric acid ($PhPO_4$) was used as precursor. The Py mediated hydrolysis half-life of $PhAcPO_4$ is 5.85 min, which is in comparison to the hydrolysis of $PhAcPO_3$ nearly 10 times faster. ($t_{1/2}$ = 63.1 min)

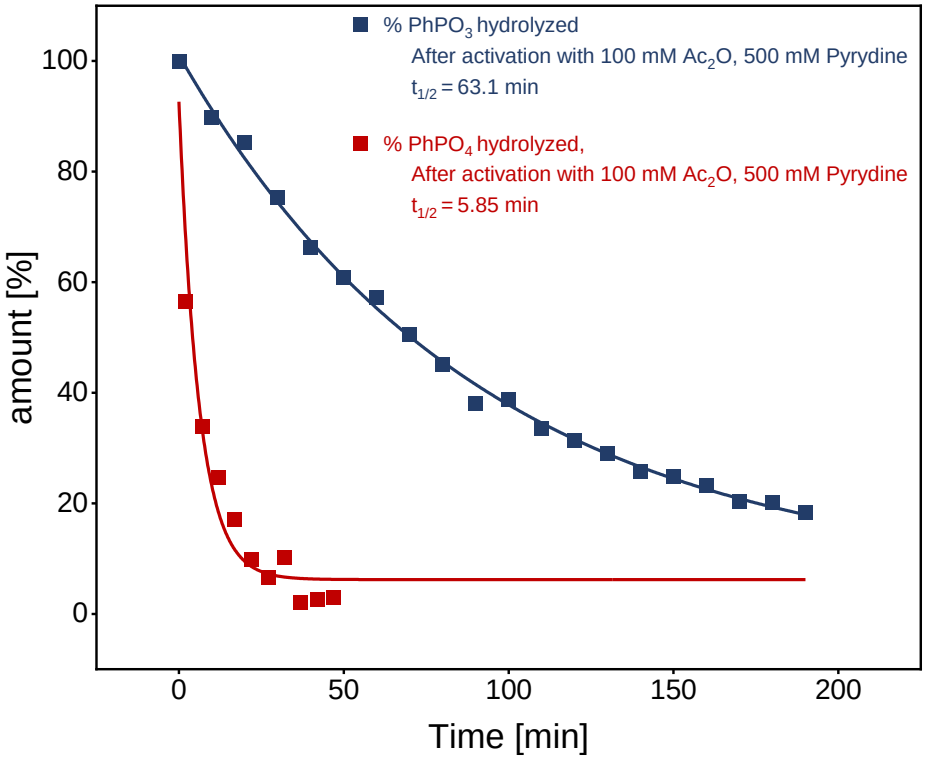

Figure 38 : Percentage of $PhPO_3$ (blue) and PhPO4 (red) hydrolyzed with the values of half-life and rate of the reaction, using 500 mM Py as catalyst, pH=7.5.

One plausible explanation for the difference in hydrolysis rate and half-life between the acylphosphonate anhydrides and acylphosphate anhydrides is that the first ones are more reactive than phosphonates. The acetic acylphosphonate anhydride has the direct P-C bond which stabilizes them more due to the bond strength, potentially explaining the higher stability in water compared to the acylphosphates.[25]

5.1.2 HPLC qualitative method development for NESS acylphosphonate reference system

While NMR analytics provide reliable insights into kinetics, this analytical method demands extended sample preparation time, and it isn't optimal for high throughput screenings. To address this issue a standard HPLC-UV method was established and used for evaluation of the system. First, a qualitative HPLC method was established (**Table 7** in chapter chemicals and reagents) for the $PhPO_3$ reference system. The solvents used were water and ACN. The HPLC analysis starts with 85% of water and 3% of ACN with 12% of TFA for 2 minutes.

TFA is used during the whole run as a strong acid to protonate the phosphonate moiety and to improve the separation. All the peaks were identified with injections of the stock solutions (see chapter **4.2** for detailed information about sample preparation) and using HPLC-MS analysis.

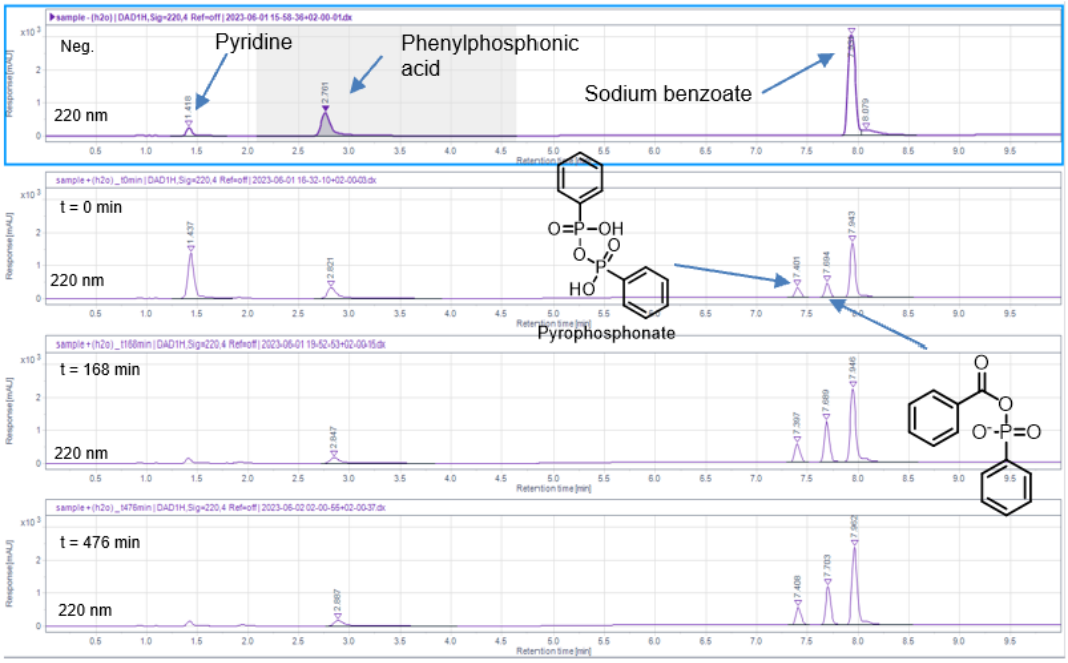

Figure 39 : Chromatogram of the reaction cycle used for the establishment of HPLC analytical method. (220 nm)

To increase sample throughput and reduce the run time an isocratic HPLC-UV (Table 8) method was also established. Different HPLC runs were conducted with different isocratic H_2O/ACN percentages and the best one was found to be 86% H_2O and 20% ACN with 12% TFA. As for the gradient HPLC method all the reagents are eluting at the beginning of the run and the $PhAcPO_3$ is eluting near to the end of the run (5.5 min). For all other runs this method, with a run time of 6 minutes, was used.

5.1.3 Catalyst evaluation for acylphosphonate anhydride hydrolysis

An investigation was conducted of multiple catalysts to determine which one is best suited for $PhAcPO_3$ hydrolysis. $PhAcPO_3$ was synthesized and isolated. The relative amount of $PhAcPO_3$ was quantified via NMR (chapter **4.3.8** for detailed information) and an external calibration was conducted using HPLC-UV system. Synthesis, isolation, and calibration of $PhAcPO_3$ and preparation of the catalyst screening samples was conducted according to the protocol in chapter **4.3.5.**

Table 10 : Structure and hydrolysis percentage of the acylphosphonate anhydride after 38 h with pKa values of each catalyst (Solution of 25 mM was prepared for $PhAcPO_3$ and 100 mM (4 equiv.) of each catalyst that was tested was added to the solution, all the experiments were done at pH 6.5 and with 500 mM of MOPS buffer in water).

Name	Structure	pKa[26]	The hydrolysis percentage [%] of the anhydride after 38h (see chapter **4.3** for detailed information about sample preparation)
No catalyst	-	-	0.2
Pyridine		5.23	31.4
4-methoxypyridine	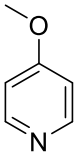	6.58	48.5
Imidazole		6.8	50.4
DMAP	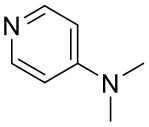	9.7	6.51
Purine	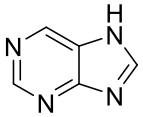	8.93	0.7
1-Ethyl Imidazole	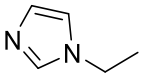	7.08	50.2
Pyrazine		0.37	11.4

The catalysts chosen for the hydrolysis evaluation were selected based on literature references.[27] The pKa of each compound is shown in **Table 10**. The differences among the respective hydrolysis agents can be explained by their pKa. On the one hand, the pKa of a nucleophile is in most cases positively correlated with nucleophilicity. On the other hand, the protonation state of the respective catalyst has to be considered as well. The reaction was conducted at a pH of 6.5. When the pKa of a compound exceeds the pH value, it implies that for 50% of the compound the acidic moiety remains protonated.

Imidazoles, 4-methoxypyridine and Py exhibited the highest hydrolysis percentage. This observation can be attributed to the distinct chemical groups present in these catalyst compounds, which can influence their performance as hydrolysis catalysts. For example, the presence of M+ group, such as the methoxy group in 4-methoxypyridine, enhances the hydrolysis process.

For this reason, Imidazoles and 4-Methoxypyrydine were investigated further because they showed a high percentage hydrolysis.

5.1.4 Optimization of NESS acylphosphonate reference system

After obtaining preliminary results, the influence of various system parameters was investigated. Acylation of $PhPO_3$ was carried by utilizing a combination of sodium benzoate and a secondary carbodiimide activation agent as illustrated in **Figure 40.** This process involved activating benzoic acid with EDC, leading to the formation of PyAc intermediate and ultimately yielding the product, which could subsequently undergo hydrolysis. EDC activation[28] was investigated for the reaction cycles at different pH values. The choice of sodium benzoate was made due to its structural similarity to the stator moiety of the desired motor compound.

As observed earlier with 4-methoxypyridine, imidazole and ethyl imidazole, all three catalysts exhibited an enhanced hydrolysis rated for $PhAcPO_3$. The initial expectation that imidazoles would enhance hydrolysis (reference) was confirmed by the results. To further optimize the reference system, additional experiments were conducted, focusing on evaluation the effectiveness of 4-methoxypyridinde and imidazole as catalysts and preventing pyrophosphonate formation. Pyrophosphate is a stable side product resulting from activation of phosphonate rather than carbon (kinetic trap).[29] To further broaden the understanding of the system, different solvent mixtures were tested: water only, water/DMF (7:3) and water/DMF (1:1).

The stator of the motor compound contains a phenyl residue with a phosphonate group in ortho position which can be acylated. Therefore, sodium benzoate represents a suitable reference compound for further investigations. Carbodiimides are arguably the most popular reagents for carboxylic acid activation and are used in carboxylic anhydride and ester-based reaction cycles frequently.[30] The selection of EDC over acetic anhydride allows us to evaluate the feasibility of using indirect fuels in this context.

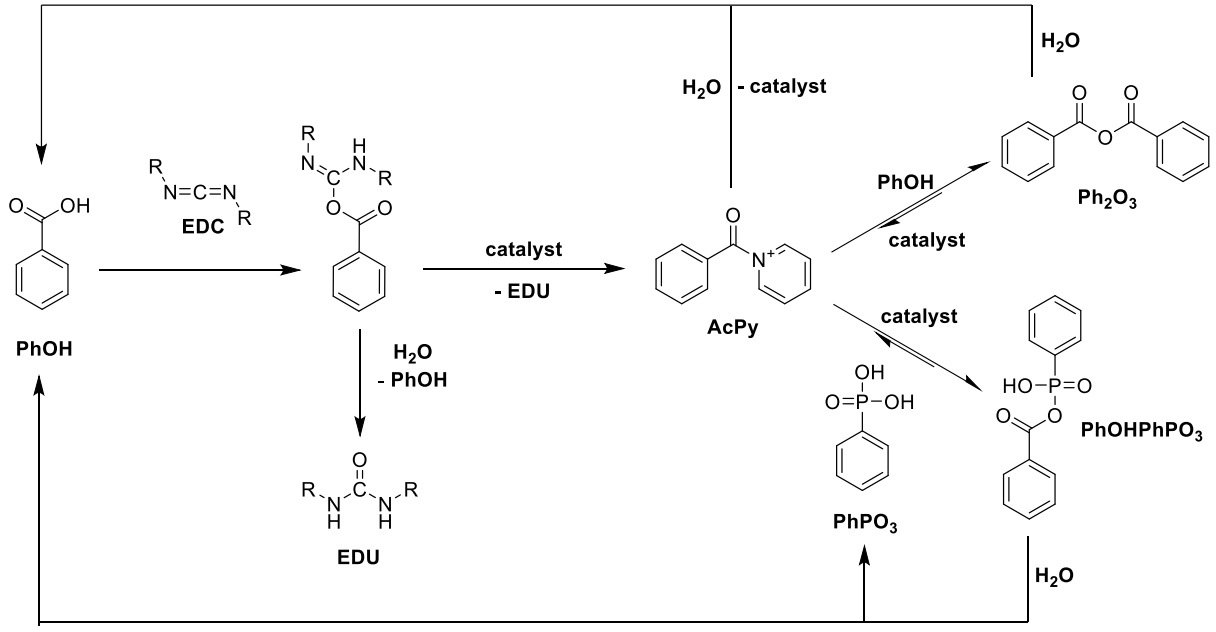

Figure 40 : Reaction cycle of indirect acylation using EDC as a secondary activation reagent, 25 mM of $PhPO_3$, 4 equiv. sodium benzoate, 4 equiv. of catalyst, 3 equiv. of EDC, pH 6.5, 500 mM of MOPS buffer in water.

The results depicted in **Table 11** show how the different parameters studied affected the pyrophosphonate formation during the reaction. Notably, 4-methoxypyridine exhibited the most

effective inhibition of pyrophosphonate formation. pH levels did not appear to significantly impact pyrophosphonate formation. Different solvent mixtures were tested to evaluate their effect on the solubility of benzoic anhydride, a byproduct formed during the reaction. Optimal conditions were determined to be 4-methoxypyridine as the catalyst and water as a solvent. Under these conditions, no pyrophosphonate formation was observed, and there was no precipitation of benzoic anhydride.

Table 11 : Influence of varying parameters on pyrophosphonate formation in the system. (Protocols of how they were prepared in chapter **4.2**)

Run n°	Catalyst used	pH	Pyrophosphonate formation	Solvent used
1	Pyridine	7.5	Observed	H_2O
2	Pyridine	6.5	Observed	H_2O
3	4-methoxypyridine	7.5	Not observed	H_2O
4	4-methoxypyridine and 1-Ethyl Imidazole (1:1)	6.5	Observed	H_2O/DMF(7:3)
5	4-methoxypyridine and 1-Ethyl Imidazole (1:1)	6.5	Observed	H_2O/DMF(1:1)
6	4-methoxypyridine and 1-Ethyl Imidazole (1:1)	7.5	Observed	H_2O
7	4-methoxypyridine and 1-Ethyl Imidazole	6.5	Observed	H_2O
8	4-methoxypyridne	6.5	Not observed	H_2O

5.1.5 Optimization study

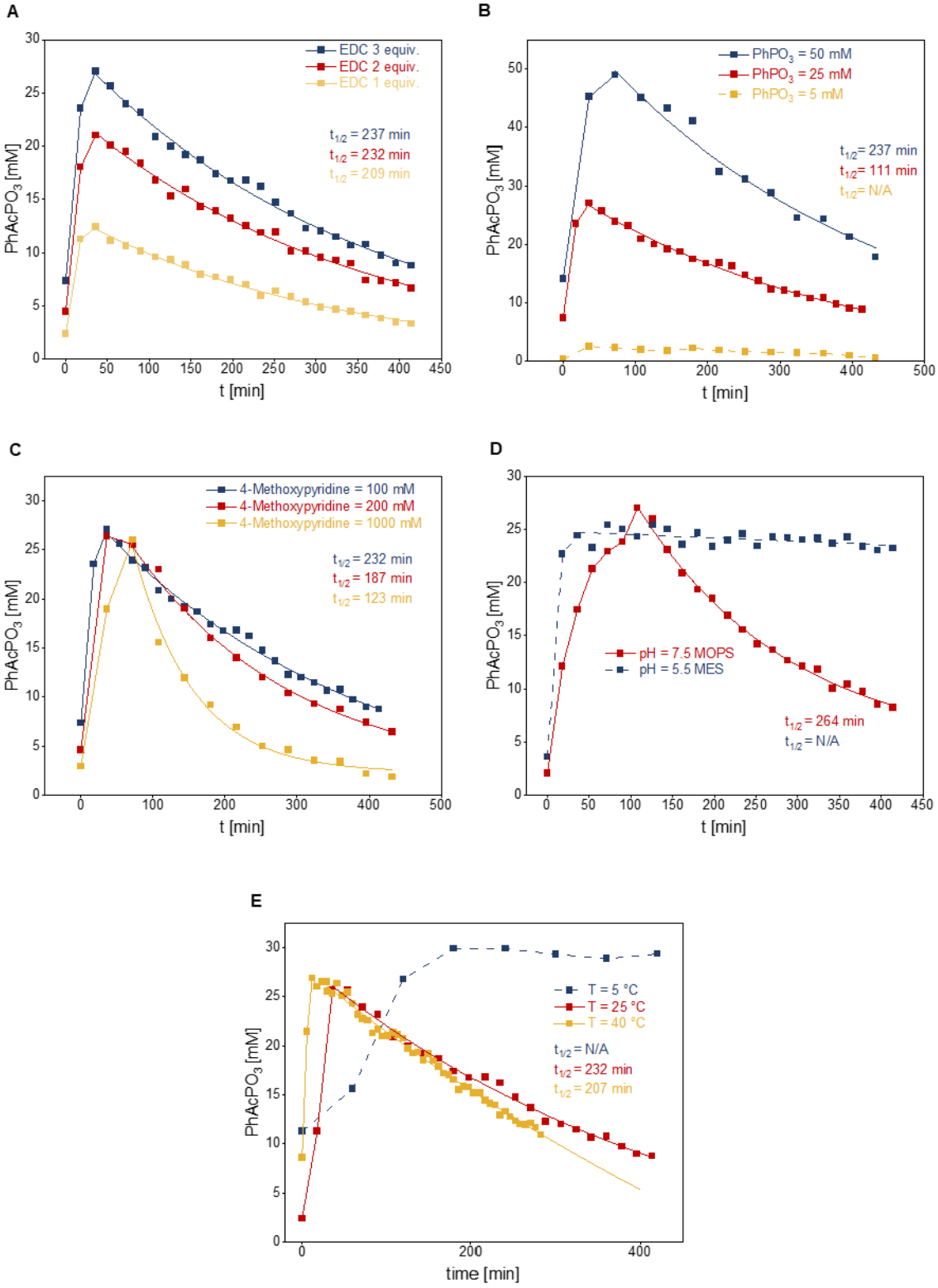

Figure 41 : Exponential fits used to model the parameters for the hydrolysis of the $PhAcPO_3$ reference system with the half-life of each parameter that was tested. A) Variation of EDC equiv. on the hydrolysis rate of $PhAcPO_3$. B) Starting concentration of the PhPO3 C) Concentration of the catalyst, 4-methoxypyrydine D) Different pH values E) Temperature variation. reference concentrations of all the compounds: 25 mM of $PhPO_3$, 4 equiv. sodium

benzoate, 4 equiv. of catalyst, 3 equiv. of EDC, pH 6.5, 500 mM of MOPS buffer in water. See chapter **4.2** for detailed information about the sample's preparation.

With the aim of optimizing and establishing a robust reference system that could be used for studying kinetics, a comprehensive parameter screening was conducted.

On **Figure 41A**, it is important to note that a high concentration of EDC, which is the activation agent of the reaction forms more of the product. An explanation for the higher yield of the product could be that the pyridinium intermediates can also hydrolyze, so adding more than 1 equiv. of EDC is going to compensate hydrolysis. 3 equiv. of EDC seem to be the best choice for the reaction cycle. It can be observed on the exponential fit that once the EDC is consumed the hydrolysis reactions prevail.

On **Figure 41B**, the concentration of $PhPO_3$ was tested, it was observed that higher concentrations of the acid result in a longer hydrolysis time, while lower concentrations exhibited faster hydrolysis. At higher concentrations, there is a higher probability of collision between reactant molecules, resulting in a slower overall hydrolysis rate. At lower acid concentrations, less reactants lead to more rapid kinetics, resulting in a shorter hydrolysis rate.

On **Figure 41C**, the concentration of the catalyst, 4-methoxypyrydine was studied. As anticipated, the concentration of 4-methoxypyrydine has a central role in the hydrolysis of the product. This can be attributed to the observation that the catalyst plays an important role in the reaction cycle because of the pyridinium reactive intermediate.[27] With only the catalyst the hydrolysis rate of the product can be regulated precisely.

On **Figure 41D** the impact of the pH can be seen, at pH 5.5 the product is formed, since it is known that the EDC optimal range is between 2-4.[31] But the hydrolysis doesn't seem to proceed at all. An explanation for this is that the pKa value of the 4-methoxypyrydine is 6.58, this means that at pH 5.5 the 4-methoxyrydine is mostly present in the protonated form in the solutions, making it less effective as a nucleophile and slowing down the hydrolysis of the product.

The temperature and its impact on the reaction cycle was studied too, on **Figure 41E**, as expected higher temperature leads to a faster formation and hydrolysis rate of the product. This behavior aligns with the fundamental principle of chemical kinetics described by Arrhenius theory.[32] His theory says that higher temperature enhances the kinetic energy of molecules, thereby increasing chances of successful collisions between the compounds and as a result promoting faster reaction rates.

In conclusion, it is important to note that the system established is robust across a broad range of parameters making it suitable for in-depth investigation of a phosphonate-based motor compound and its kinetics.

5.2 Synthesis of phosph(on)ate based rotary motors

In pursuit of the research objectives of this thesis, it was time to start the synthesis of the phosph(on)ate based rotary motor.

Initially, the Ulmann coupling based strategy was explored,[33] this strategy involved the utilization of 2-Bromophenol and L-Proline as starting materials. Despite experimenting with various conditions documented in the literature, challenges were encountered in adapting them for the synthesis of the phosph(on)ate based rotary motor.

Subsequently, a tethering approach was tried, beginning with the coupling of 2-Bromophenol and L-Proline, and then trying to do an intramolecular Ulmann coupling.

The third strategy that was tested was to start the coupling of 1-Fluoro-2-nitrobenzene with the L-Proline using a nucleophilic aromatic substitution, then reduce the nitro group to amine group and lastly with Sandmeyer reaction [34] to attach a phosphonate group. Neither this approach was met with success.

In the sections that follow, the design of the motor compound and the reasons for choosing this compound will be given.

5.2.1 Design of rotary motors

The design of the motor compound in this thesis draws inspiration from recent publication[18] on the first autonomous chemically fueled rotary motor. However, the design of the motor compound for this thesis introduces some unique elements: the stator will incorporate a phosph(on)ate group with a second substitutent in the *ortho* position (ex: H, Me, Et, Cl, Br), along with a chiral center on the proline rotor moiety serving as a crucial mechanistic probe as depicted in **Figure 42.**

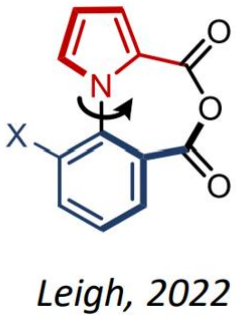

Figure 42 : First example of autonomous chemically fueled rotary motor reported by Leigh and coworkers (2022).[18]

In analogy to previous motor designs the two reactive groups, one on the stator and one on the rotor, must not be able to rotate past one another without chemical activation.[18]

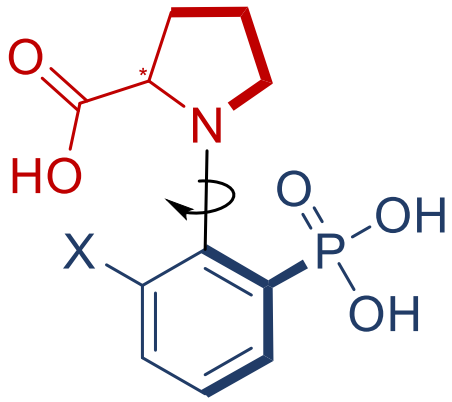

Figure 43 : Autonomous chemically fueled rotary motor, the goal of the synthesis.

The chemomechanical cycle is illustrated in **Figure 44**, it shows four fundamental states connected by two equilibria and two practically irreversible reactions. The first line (**A** and **B**) shows a motor in the chemically activated state, as an acylphosphonate, in this state the two groups can rotate and pass one another. This is not possible in the deactivated states (**C** and **D**). Installing a moderate bulky group (X, **Figure 43**) in the stator will slow down rotation enough that HPLC and NMR can be used as analytical tools.

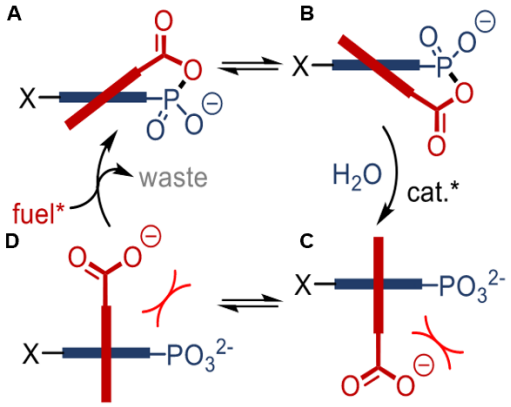

Figure 44 : Chemomechanical cycle of the motor compound, red is the rotor part, blue is the stator part.

5.2.2 Atropisomer synthesis via Ullmann coupling

Multiple reports were found in literature [35,36,33,37] about successful aryl halide-amine coupling. General procedure for the Ulmann coupling reaction can be found in chapter **4.8.**

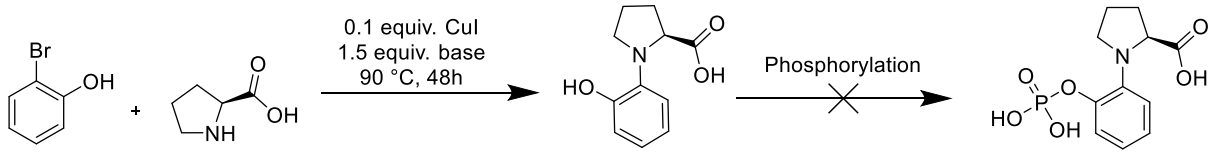

Figure 45 : Synthesis route using Ulmann coupling reaction.

To reproduce the results as in the literature an Ulman coupling reaction was done using bromobenzene that was coupled with L-Proline. Nearly quantitative conversion was obtained as shown in **Figure 47**. HPLC method for following the reactions that is shown on **Table 12** in chemicals and reagent chapter was used.

Same conditions were tried with the coupling of **1** and **2.**

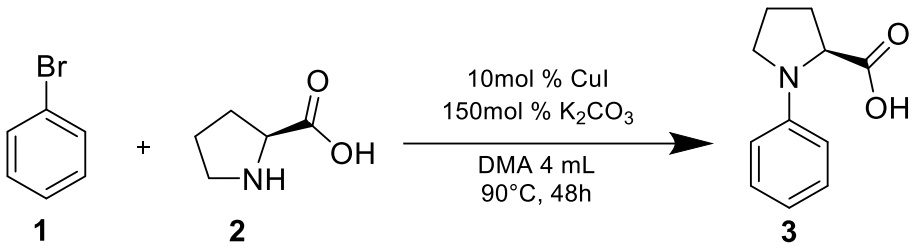

Figure 46 : Reaction scheme of the Ulmann coupling that was tried to see if the results are reproducible as mentioned in literature.

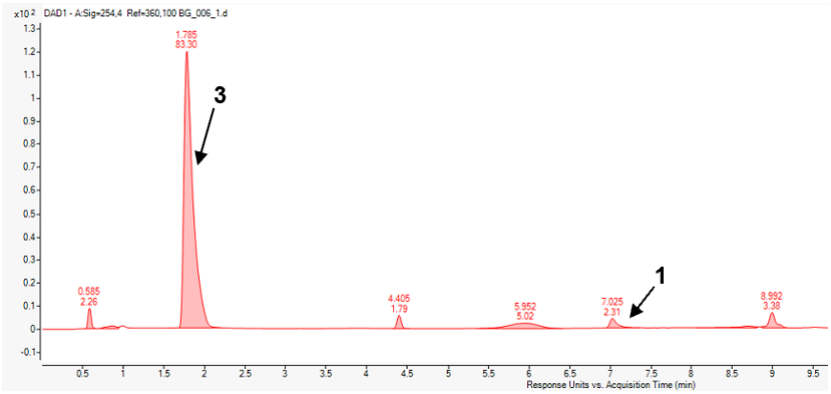

Figure 47 : Chromatogram of the proof-of-concept reaction, quantitative conversion can be observed for **3.**

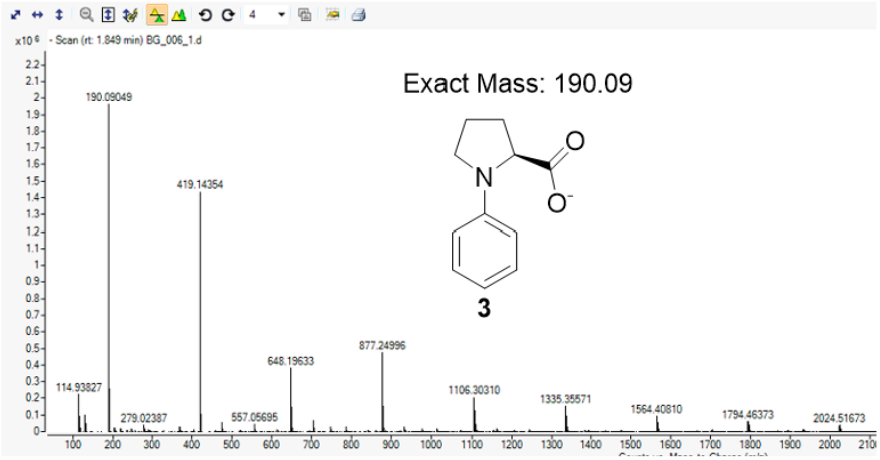

Figure 48 : MS of the proof-of-concept reaction that confirms that there is indeed quantitative yield for **3.**

5.2.2.1 Parameter screening of Ullmann coupling reactions.

All the screening parameters that were done didn't give any product with a high yield that could be isolated. The reactions conditions were based on 2 papers.[33,36] But overall, some traces of product **6**, were observed using DMSO as solvent as shown in **Figure 49.**

Table 12 : Parameters screening for Ulmann coupling reaction, all reactions were performed with 1mmol of **4,** 1.2 equiv **5**, base 2.5 equiv., reaction time 48h, temperature 90°C, 1mL of solvent, under N_2 atmosphere. Detailed procedure can be found in chapter **4.8**.

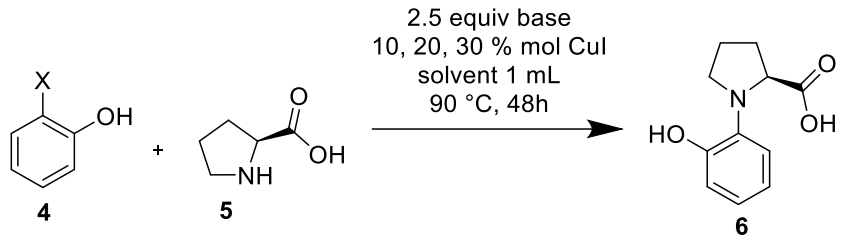

Entry	X (**1**)	CuX	CuX [mol%]	Base	Temp. [°C]	Solvent	Yield (**3**) [%]
1	Br	CuI	10	K_2CO_3	90	DMA	-
2	Br	CuI	20	K_2CO_3	90	DMA	-
3	Br	CuI	30	K_2CO_3	90	DMA	-
4	Br	CuI	10	K_2CO_3	90	DMF	-
5	Br	CuI	10	K_2CO_3	90	ACN/H_2O	-
6	Br	CuI	10	K_2CO_3	90	DMF/H_2O	-
7	Br	CuI	10	K_2CO_3	90	Dioxane	-
8	Br	CuI	10	K_2CO_3	90	DMSO	Traces
9	Br	CuI	10	Na_3PO_4	90	DMSO	Traces
10	Br	CuI	10	K_2CO_3	90	DMSO	Traces
11	Br	CuI	10	Cs_2CO_3	90	DMSO	-
12	Br	CuI	10	KOtBu	90	DMSO	-
13	Br	$Cu(Ac)_2$	10	K_2CO_3	90	DMSO	-
14	Br	CuI	10	K_2CO_3	100	DMSO	Traces
15	Br	CuI	10	K_2CO_3	130	DMSO	Traces
16	Br	CuI	10	K_2CO_3	150	DMSO	-
17	Br	Cu_2O	10	K_2CO_3	90	DMSO	-
18	I	CuI	10	K_2CO_3	90	DMSO	-
19	I	CuI	10	K_2CO_3	90	DMF/H_2O	-

Parameters were adjusted based on the plausible mechanism of the Ulman coupling reaction as discussed in literature.[35,36,33,37] The first step is the chelation of the amino acid with the Cu(I) making it more reactive towards oxidative addition with the 2-Bromophenol. Subsequently promoting coupling reaction. In the final step the product is obtained vie reductive elimination and the copper intermediate is regenerated.

The temperature didn't seem to have a major influence on the coupling. Different temperatures were tried but the results weren't conclusive. DMSO seems to work as solvent with traces observed of the product. The initial experiments with potassium carbonate as base didn't give the desired compound, it was thought that the reaction didn't proceed because of the protonation state of the arylhalide compound, therefore weaker bases were tried in orded to not deprotonate it but didn't improve the overall yield. Therefore, different bases were tried, but didn't improve the overall yield. [35,36,33,37]

2-Bromophenol was substituted with 2-Iodophenol. Since the iode atom is more reactive than brome, it was thought that it would enhance the coupling but the overall yield wasn't improved. The concentration of CuI was also variated between 10 and 30 mol %, as already explained for the plausible mechanism of the coupling, increasing the CuI percentage should improve the yield due to the higher concentration the chelation with the amino acid. It was assumed that the CuI might get somehow oxidized or quenched. This parameter neither improved the yield of the desired product.

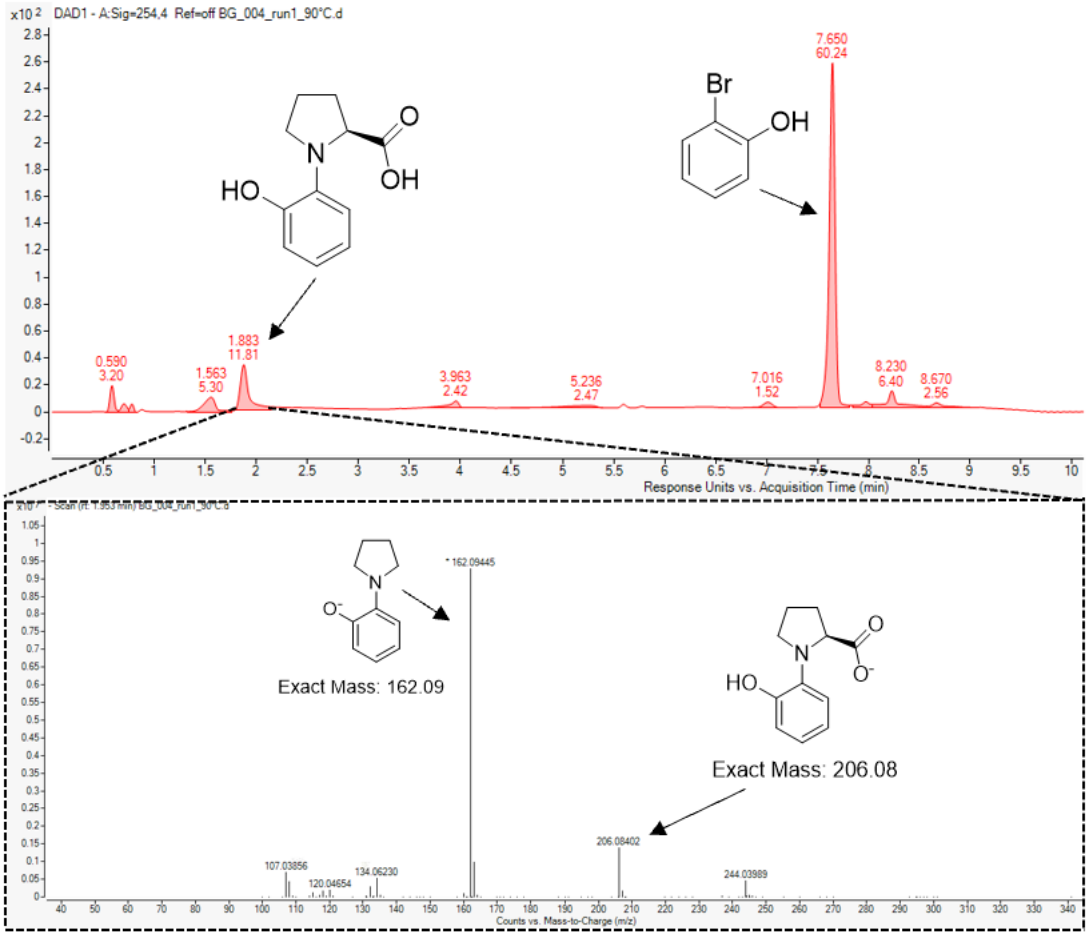

Figure 49 : Chromatogram and mass spectra of the reaction with entry n° 8 where traces of the desired product can be observed.

5.2.2.2 Microwave-mediated coupling approaches

After the failed normal Ulmann coupling approach, a microwave mediated Ulmann coupling reactions approaches was tested. Using microwave mediated Ulmann coupling might also reduce the time of reaction. [33,36]

This will allow more experiments to be done and more parameters to be tested. The parameters studied for the microwave Ulmann coupled reactions were the power of the microwave, the temperature of the reaction, the time of the reaction and the CuI equiv., those parameters were chosen regarding the results that were discussed previously, also literature [33,36] that was found on the C-N coupling with microwave.

Table 13: Microwave mediated approaches. Reaction conditions: 1 mmol of **7,** 1.2 equiv. **8**, base 2.5 equiv., 1.5mL of solvent, under N_2 atmosphere.

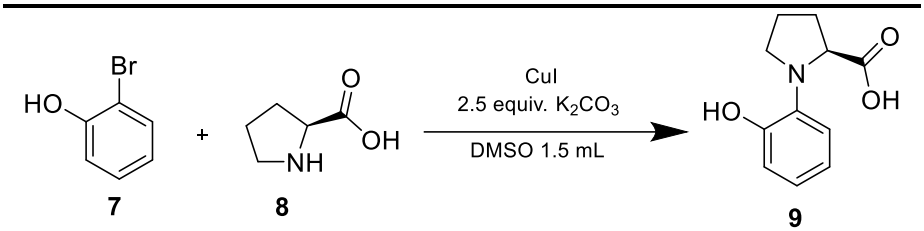

7 **8** **9**

Run n°	Temp [C°]	[W]	Time [min]	CuI equiv.	Yield
1	140	300	90	0.1	0
2	140	150	30	0.1	Traces
3	165	300	30	1	0
4	140	300	30	0.1	Traces
5	140	150	-30	1	0
6	140	150	90	0.1	Traces
7	140	300	90	1	Traces
8	140	150	90	1	0
9	165	300	30	0.1	Traces
10	165	300	90	0.1	Traces
11	165	300	90	1	0
12	165	150	90	1	0
13	140	300	30	1	0
14	165	150	30	1	0
15	165	150	90	0.1	Traces
16	165	150	30	0.1	Traces

After extraction the yields weren't conclusive, only traces were observed on some approaches (**Table 13**).

After the normal Ulmann coupling reactions and the microwave mediated Ulmann coupling approaches, the yield wasn't improved. An assumption was made that the hydroxy group on the aryl halide can possibly interfere during the coupling. Therefore, to test this observation, the hydroxy group was protected and more normal Ulmann coupling approaches were made.

5.2.2.3 Protecting group strategies

Several approaches with hydroxy group protecting strategies were tried as shown in **Table 14.**

Table 14 : All approaches using protecting groups.

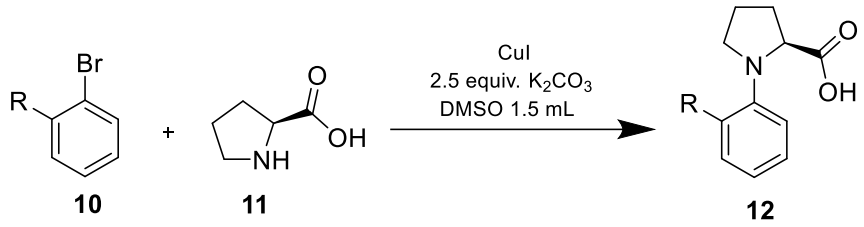

10 **11** **12**

Entry	R	Yield [%] (12)
1		3
2	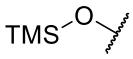	-
3	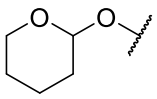	-
4	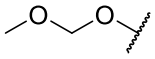	-

4 approaches were made with 4 different protecting groups. Compound **10** with entry number 1 was commercially available and purchased. All the others were synthesized and isolated. The 4 entries didn't give any trace of the product. Before proceeding with the Ulman coupling reaction, the precursors were synthesized and isolated using the 2-Bromophenol and the complete procedure can be found in synthesis and characterization chapter.

The ^{1}H-NMR spectrum of compound **12,** is shown in **Figure 50.** The chemical shifts, as well as the integrals of the signals match the expected structure. 2 regions of doublet peaks are in the aromatic region between 6.54 and 6.88 ppm, with integral value of 4. Those peaks correspond to the phenylic protons. They show coupling constants of 6.5 Hz which are in the range of ^{3}J-coupling constants. The multiplet between 4.44 and 4.47 ppm, with an integral of 1 correspond to the proton 4, the shift towards higher ppm values is due to the less shielding that is caused by the amine group and carboxylic group next to it. The singlet at 3.65 ppm and with integral of 3 corresponds to the protons (1) of the methoxy group that is used to protect the hydroxy group, the up-field shift is due to the oxygen atom. The multiplet between 3.20 and 3.26 ppm with integral value of 2 can be assigned to the protons 2, the impurity peak that is probably due to water is next to it at 3.30 ppm. Their up-field shift is due to the less shielding effect of the amino group that is next to it. The multiplet between 2.24 and 1.83 ppm, with integral of 4, corresponds to the protons 3 from amino group, their assignment to specific individual protons within the multiplet is not possible. Their shift is not as upfield as the shift from protons 2 and 4, the deshielding effect from the amino and carboxylic group don't affect them as much as protons 2 and 4. Other small impurities can be observed in the aromatic region, between 7.2 and 7.7 ppm, small quantities of the starting material probably is left, and those impurities can be assigned to them. The same assumption can be made for peaks with relatively small intensity between 1 and 1.5 ppm.

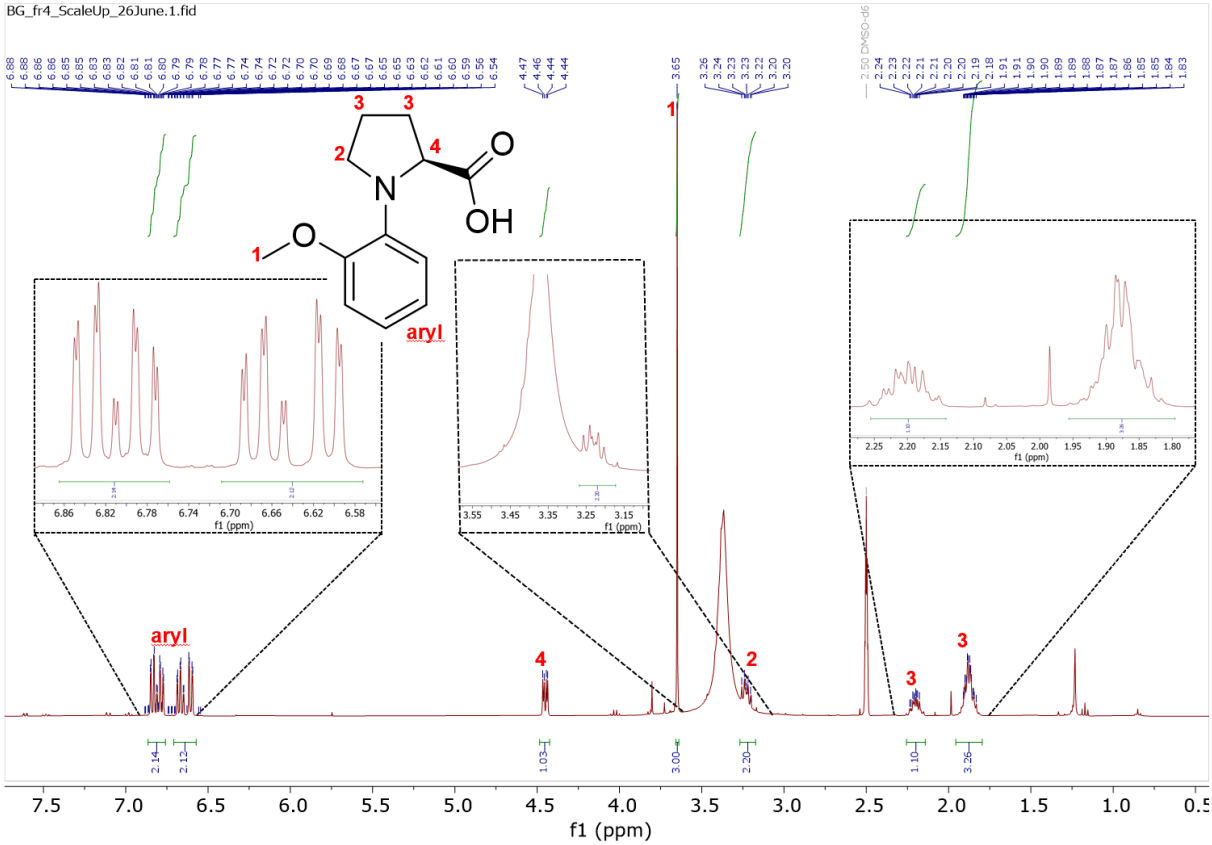

Figure 50 : ^{1}H-NMR of compound **12,** entry 1.

After isolation of **12,** entry 1, deprotecting of the methoxy group was tried. For the deprotection of the methoxy group different reactions were performed, as shown in **Table 15**.

Table 15 : Deprotection approaches summary.

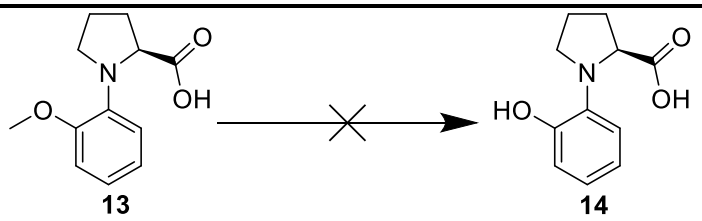

Entry	Experimental conditions	Yield [%] (**5**)
1 [38]	0.025 mmol **13,** 1.1 equiv. BBr_3, DCM 3 mL, -78°C, 0°C and r.t., 1h	-
2 [39]	0.025 mmol **13,** 5 equiv. HBr, H_2O 3mL, 115°C, 16h	-
3 [40]	0.025 mmol **13,** 9 equiv. $AlCl_3$, DCM 3mL, r.t. , 24h	-
4 [41]	0.025 mmol **13,** 4 equiv. tBuONa, DMSO 3mL, 115°C, 24h	-
5 [42]	0.025 mmol **13,** 2 equiv. ^{t}BuOK, 2 equiv. $HPPh_2$, DMF 0.5 mL, 80°C, 8h	-

Entry 1 using BBr_3 didn't give any results. Different temperatures were tried without success. Entry 2 using HBr resulted in decomposition of **13**. $AlCl_3$ wasn't successful too, different batches were tried but without any result. The same was observed for entry 4 and 5.

Due to the unsuccessful deprotection, it was decided not to pursue further exploration of the Ulmann coupling reaction and to try another approach.

5.2.3 Atropisomer synthesis via tethering approach

Following the exploration of several approaches, normal Ullmann coupling reactions and microwave mediated reactions didn't prove to give any successful results. Consequently, a new synthesis route was attempted as shown in **Figure 51.**

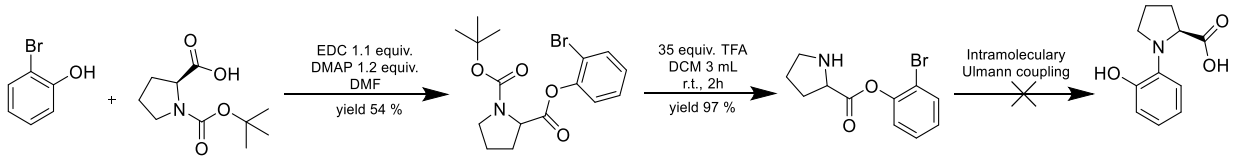

Figure 51 : Synthesis scheme of the strategy using intramolecular Ulman coupling.

The hypothesis behind this approach is that connecting proline and the bromophenol moiety via an ester and then conducting Ulmann coupling may potentially yield better results. Intramolecular Ulmann coupling may occur more easily and faster, because of the proximity of the atoms, than the previously attempted and unsuccessful intermolecular Ulmann coupling. The absence of the hydroxy group, which likely interfered during the coupling, is expected to facilitate the reaction.

5.2.3.1 Synthesis of proline aryl esters

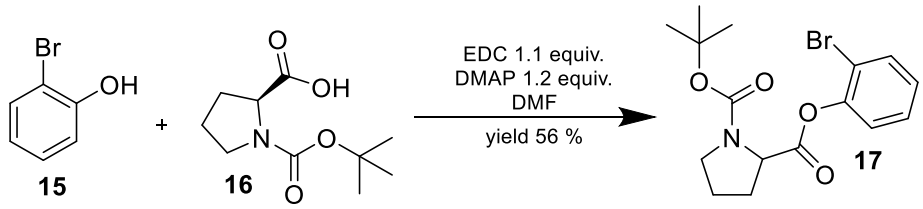

Figure 52 : Synthesis of proline aryl ester (**17**).[43]

Synthesis scheme of **17** is depicted in **Figure 52.** (Tert-butoxy carbonyl)-L-proline was added to a solution of 2-Bromophenol, then DMAP and EDC were added to the solution and the reaction mixture was stirred for 24 hours. Diethyl ether was added to the solution after 24 hours and the organic phase was separated. Washing the organic phase with water, and drying it over anhydrous $MgSO_4$, gave the product **17** in 56% yield, the obtained yield differs from the one in the literature. N-acyl urea byproducts were observed after the sample was analyzed on HPLC. The diethyl ether was evaporated on Rotavapor and compound **17** was used without further purification. Compound **17** has an axial chirality leading to the assumption that two distinct diastereomers would be synthetized and observed on an ^{1}H-NMR spectrum.

The ^{1}H-NMR spectrum of synthetized and isolated compound **17** is shown in **Figure 53**. The chemical shifts and integrals align with the expected structures of two diastereomers. The multiplet in the aromatic region from 7.62 to 7.10 ppm can be assigned to the phenylic protons. The total sum of all the integrals is around 8 which is the exact numbers of phenylic protons of the two diastereomers. Their coupling constants go in the range from 7.11 to 7.61 Hz and are in the range of ^4J-coupling constants which are from 6-10 Hz [reference]. The two multiplets at 4.60 and 4.53 ppm can be assigned to the diastereomeric proton 2, each integral from each multiplet is 1, which indeed points to the two protons from the two axial diastereomers. Their

up field chemical shift is due to the amine and carboxylic group which are next to them. The multiplets between 3.66 and 3.42 ppm with an integral of 4 can be assigned to the protons 3, the less shielding effect which is due to the amine group next to the protons 3 is causing their up-field chemical shift. The multiplets between 2.42 and 1.95 ppm and their integral of 8 can be assigned to the protons 4. The singulet at 1.48 ppm corresponds to the protons of the Boc protection group (1). No significant difference in chemical shift is expected, and the integral is anticipated to be 18 which is the sum of the two Boc groups in the two axial diastereomers. The peak next to the singulet at approximately 1.55 ppm can be assigned to the traces of water that remain in the solution.

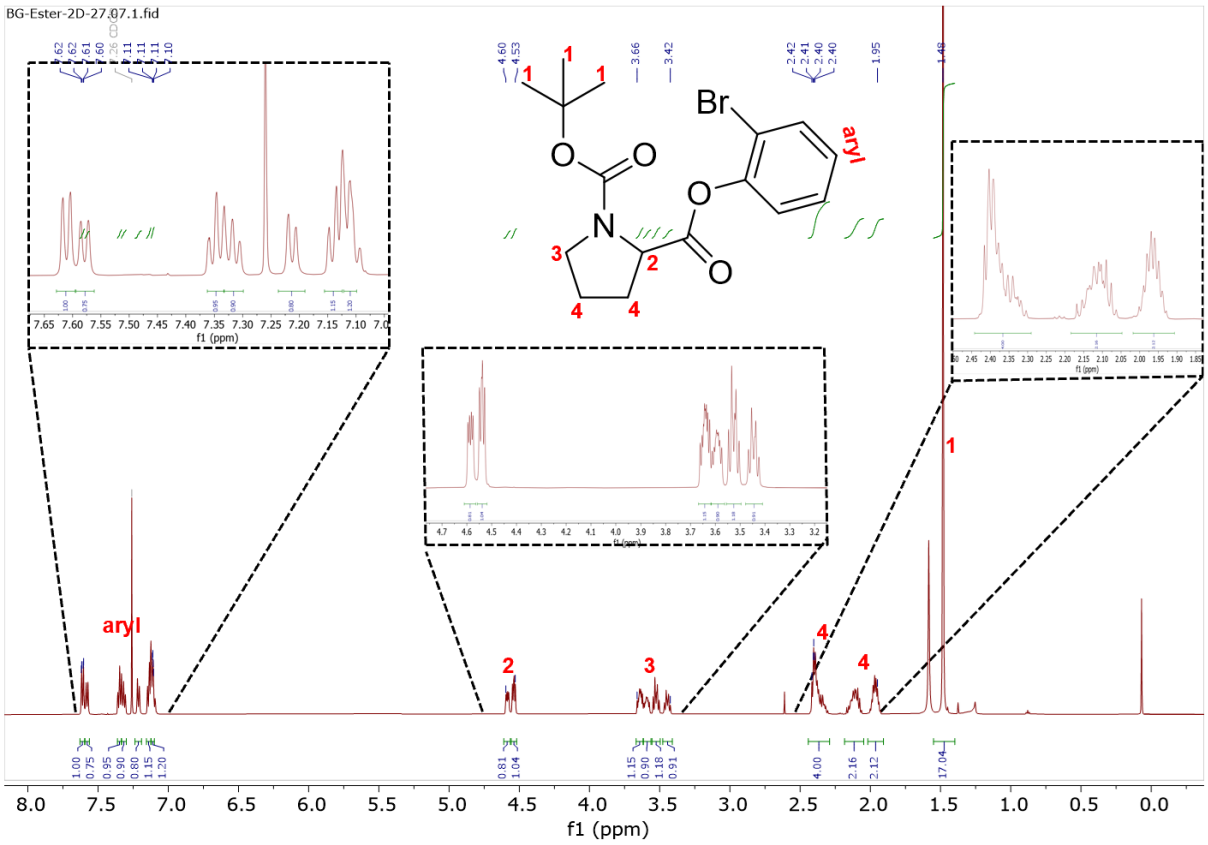

Figure 53 : ^{1}H-NMR of **17.**

The next step is deprotecting the Boc group in **17** and proceeding with the intramolecular Ulmann coupling. The deprotecting approaches that were tried are shown in **Table 16**.

Table 16 : Deprotection approaches for **17**.

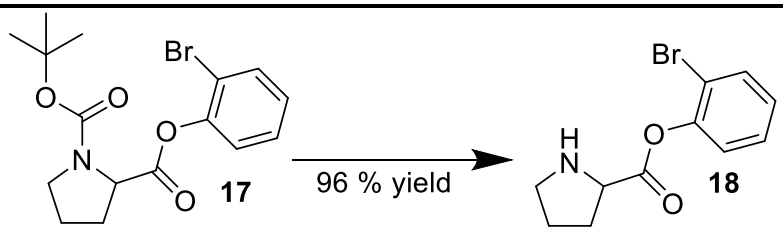

Entry	Experimental conditions	Yield [%] (**4**)
1 [44]	0.025 mmol **17,** 5M HCl in 3 mL H_2O/Dioxane (1:1), r.t., 12h	-
2 [44]	0.025 mmol **17,** 5M NaOH in 3 mL H_2O/THF, H_2O 3mL (3:1), r.t. 12h	-

3 [45]	0.025 mmol **17,** TFA 35 equiv. DCM 3mL, r.t. , 2h	97

For the deprotection of Boc group of compound **17,** three approaches were tried, the one with 35 equiv. of TFA worked quantitively with 96% yield. **17** was dissolved with DCM and then 35 equiv. of TFA was added, the solution was stirred at r.t. for 2 hours. Compound **4** was used without further purification for the intramolecular Ullman coupling.

The ^{1}H-NMR spectrum of synthetized and isolated compound **18** is shown in **Figure 54**. The chemical shifts and integrals align with the expected structure of the deprotected compound. The spectrum closely resembles that of compound **18,** with the notable absence of the singulet of the -Boc protecting group. No double peaks are observable, the reason is that **17** contains only one stereocenter**,** which is proton 1. The mixture likely consists of two enantiomers. Since enantiomers do not exhibit different physical properties, they can't be seen on the spectrum.

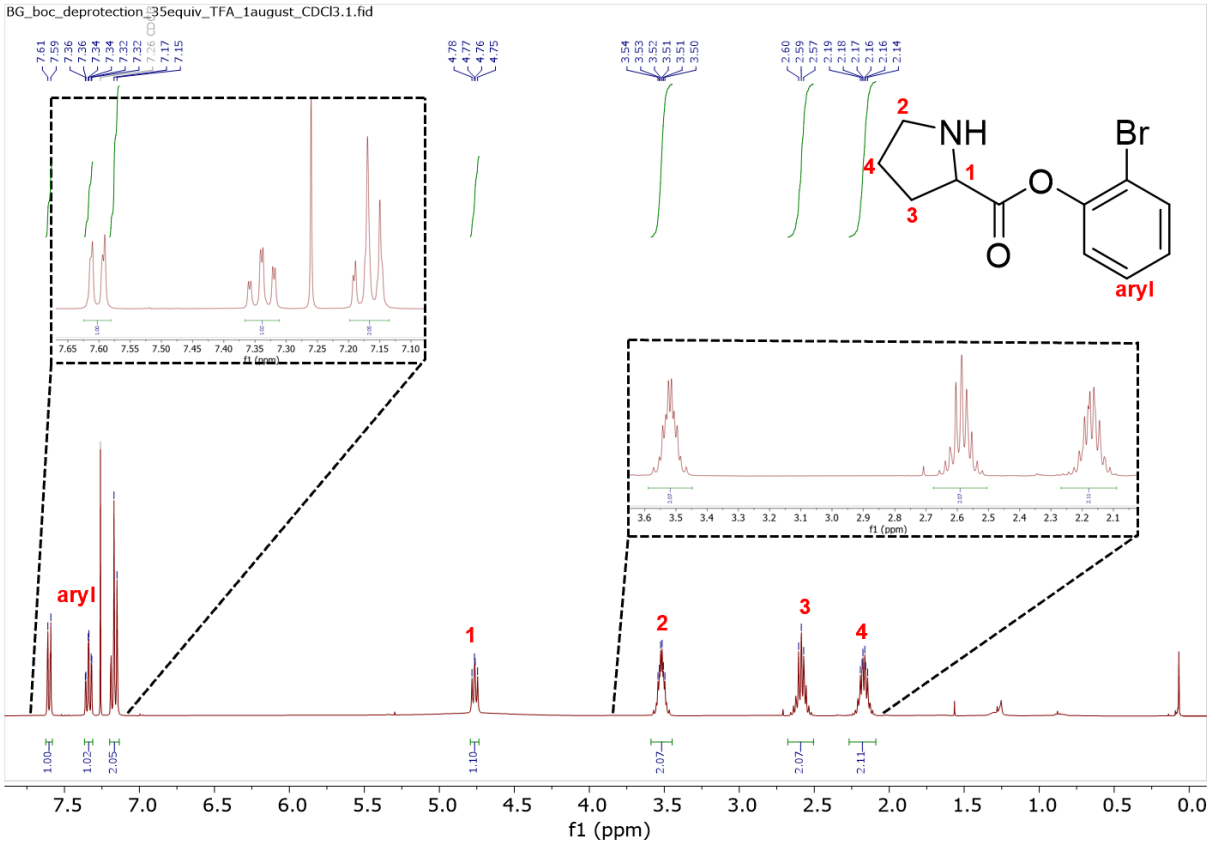

Figure 54 : ^{1}H-NMR of **18.**

5.2.3.2 Intramolecular Ullman coupling

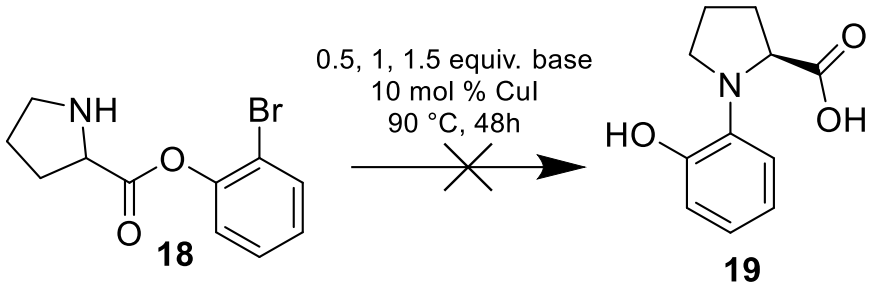

Figure 55 : Synthesis of **19**.

A summary of the different conditions attempted is put together in **Table 17.**

Table 17 : Conditions that were tried for the intramolecular Ulmann coupling.

Entry	Experimental conditions	Yield [%] (**5**)
1 [33]	0.18 mmol **20**, 2.5 equiv. K_2CO_3, 10% mol CuI, 3mL DMSO, 90°C, 48h	-
2 [33]	0.18 mmol **20**, 1.5 equiv. K_2CO_3, 10% mol CuI, 3mL DMSO, 90°C, 48h	-
3 [33]	0.18 mmol **20**, 0.5 equiv. K_2CO_3, 10% mol CuI, 3mL DMSO, 90°C, 48h	-
4 [33]	0.18 mmol **20**, 1.5 equiv. TEA, 10% mol CuI, 3mL DMSO, 90°C, 48h	-
5 [33]	0.18 mmol **20**, 10% mol CuI, 3mL DMSO, 90°C, 48h	-

The reactions were performed with the same conditions as for the normal Ulmann coupling. The ^{1}H-NMR and HPLC-MS showed no conversion. It can be assumed that the ester is sterically hindering the coupling and preventing the rotation. Or no coordination is possible with the copper iodide and the coupling can't proceed.

In summary the investigation Ulman coupling reactions, including normal, microwave mediated, and intramolecular coupling led to the assertion that functional groups as hydroxy, carboxylic moieties may interfere during the reaction potentially hindering successful coupling. As a result, a new synthesis route, in which the rotor compound will be attempted to be synthetized will be tried.

5.2.4 Atropisomer synthesis via nucleophilic aromatic substitution

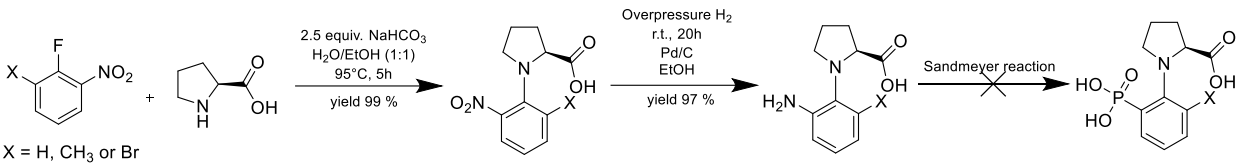

Figure 56 : New strategy for atropisomer synthesis via nucleophilic aromatic substitution.

The new synthesis route to be explored is shown in **Figure 56.** The initial step involves coupling compounds 1-fluoro-2-nitrobenzene and L-Proline, using aromatic nucleophilic substitution. Nitro groups, known for their strong electron-withdrawing effect [reference], will probably facilitate the coupling. Following the first step the nitro group will be reduced to amine group. After completion of the reduction step, the Sandmeyer reaction[reference] enables the direct conversion of the amine into a hydroxy group, followed by the insertion of phosphonate group. Or alternatively the phosphonate group can be directly inserted in *ortho* position, without first converting the amine into a hydroxy group.

5.2.4.1 Nucleophilic aromatic substitution

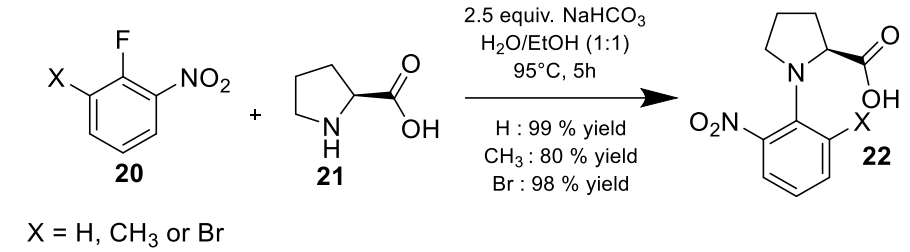

Figure 57 : Synthesis of 22, 1 equiv. of 20 and 21 was used for the reaction.

The first step using nucleophilic aromatic substitution was done according to Hee Choon Ahn and co-workers (2007).[46] **20 (X = H)** was dissolved in 30mL 1 :1 H_2O/EtOH. To the solution was added 2.5 equiv. $NaHCO_3$, followed by 1 equiv. of **21**. The resulting mixture was refluxed for 5 hours and then cooled down to r.t. After removing EtOH by evaporation, the remaining solution was acidified to pH 2-3 with 35% HCl and extracted 3 times with EtOAc. The combined organic layers were washed with brine, dried over anhydrous $MgSO_4$, and concentrated under reduced pressure. A quantitative yield of 97% was obtained. For characterization of **22**, HPLC-UV chromatogram and TOF mass spectra were recorded as depicted on **Figure 58.** With a retention time of 4.793 min is the compound **22**, the TOF mass spectra confirms it with the masses 237.09 of compound **22** and 192.10 that is the also **22** due to the high gas temperature in the ionization chamber the nitro group is cleaved. The peak at 6.867 min is **20**, which is the starting material left from the reaction. The small peak at 7.653 min is probably due to side products.

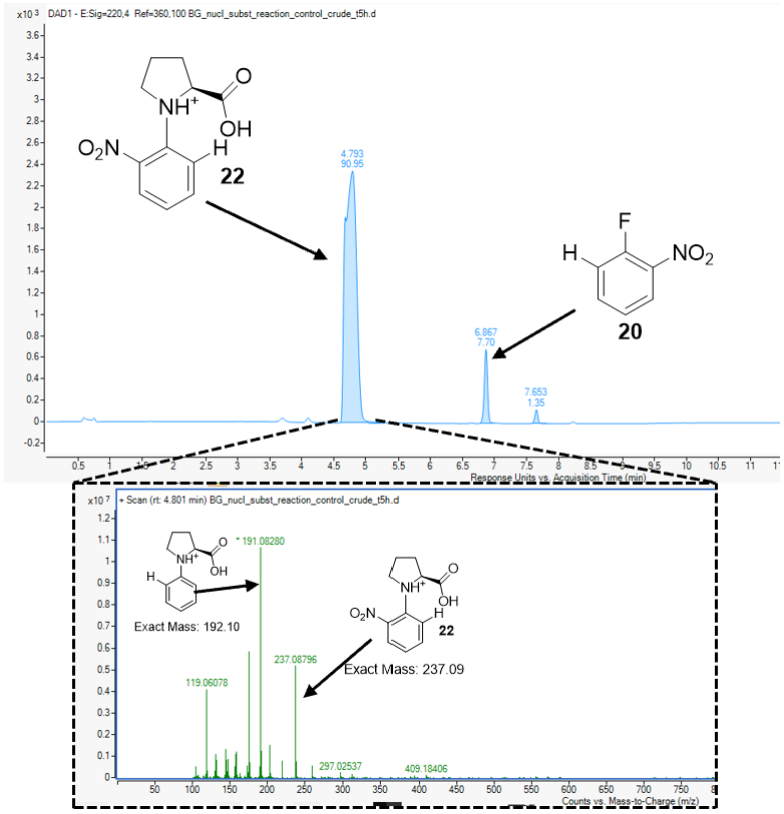

Figure 58 : HPLC-UV at 220nm and TOF mass spectra of **22** after extraction.

Once **22** was separated on a silica column, the next step was trying to reduce the nitro group in amine group.

Since the nucleophilic aromatic substitution with **20 (X = H)** worked quantitatively, it was decided to do the same reaction with a methyl stopper and bromo stopper in *ortho* position. The reaction for **X = CH_3** took longer than the one without the methyl stopper, but quantitively yield was obtained. The longer reaction time is probably due to the methyl group, that has an M+ effect on the phenyl ring.

^{1}H-NMR spectrum was recorded after extraction and purification of **22** with **CH_3** in ortho position (**Figure 59).** The integrals as well as the chemical shifts confirm the structure of **20a**. In the aromatic region, the peaks between 7.53 and 7.13 ppm, with a coupling constant range going from 7.15 to 7.53 Hz, can be attributed to the phenylic protons. The coupling constant matches the ^4J reference coupling [reference]. The doublet-doublet peaks observed between 3.96 and 3.94 ppm correspond to proton 2. The up-field chemical shift of this proton is due to its proximity to the carboxylic and amine moiety. The two multiplets between 3.55 and 3.19 ppm can be attributed to the two protons from 3. These protons are diastereotopic, so they have different chemical shifts and are not identical. The singlet at 2.40 ppm with an integral value of 3 corresponds to the CH_3 of the methoxy group in *ortho* position. The multiplets between 2.40 and 2.13 ppm, with summed integral value of 2 can be assigned to the protons 5, these protons are also diastereotopic and they are not chemically equivalent. The multiplet from 2.06 to 2.04 ppm with integral value of 2, corresponds to the protons 4.

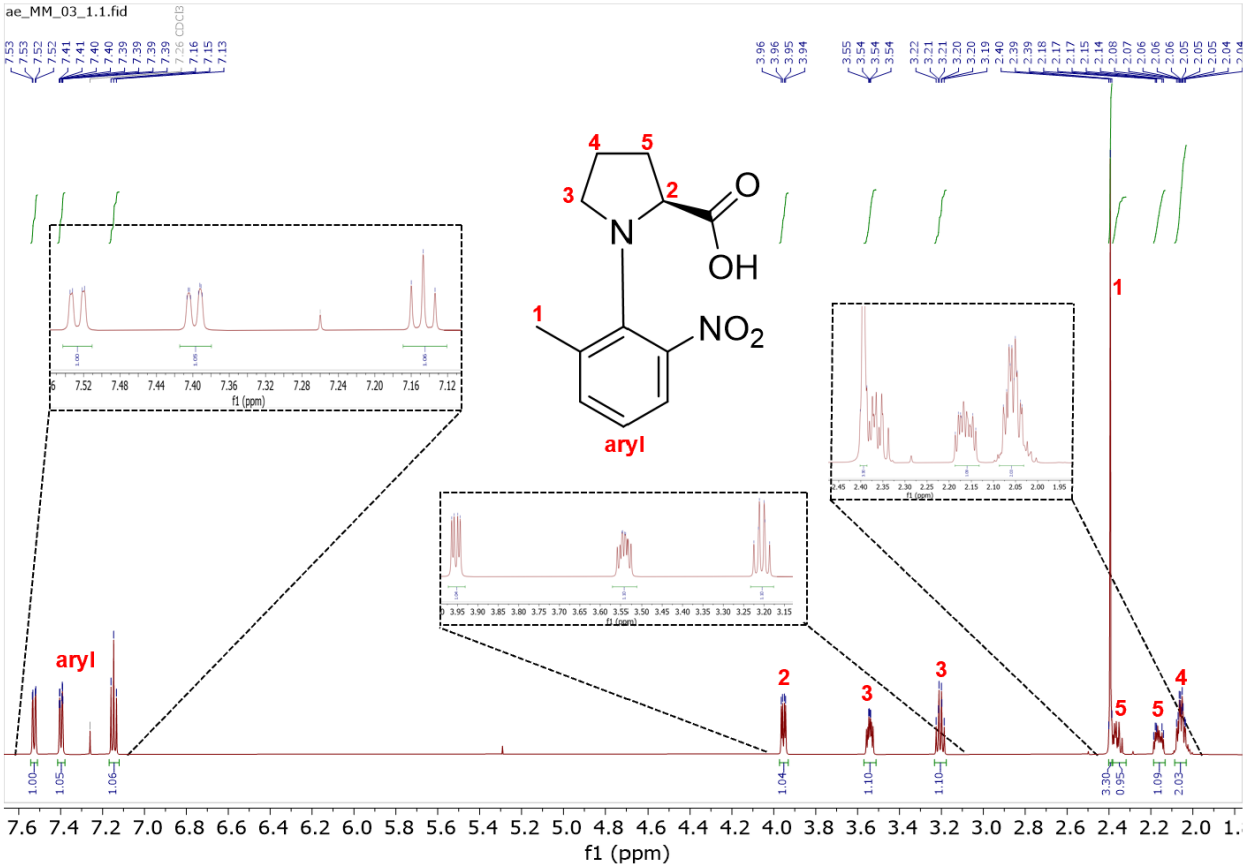

Figure 59 : ^{1}H-NMR of **22 (X = CH_3)**

5.2.4.3 Nitro group reduction

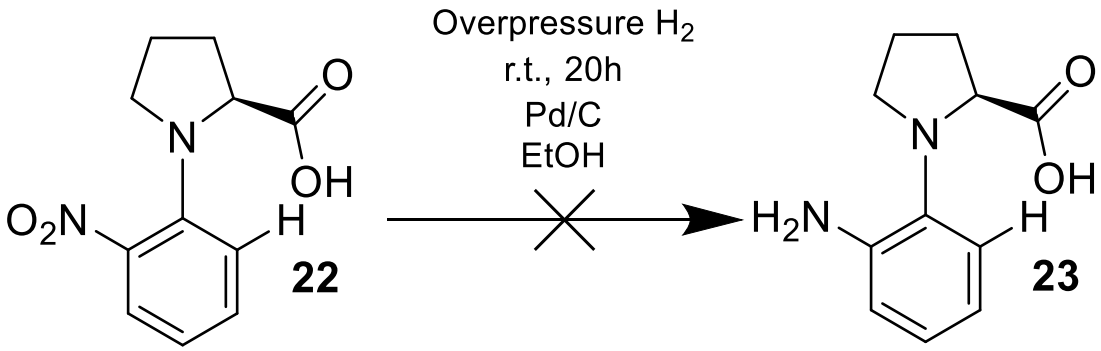

Figure 60 : Nitro group reduction to amine group reaction scheme, 10 mol% Pd/C catalyst was added to a solution of **22** in EtOH.[47]

As shown in **Figure 60,** the procedure for nitro reduction was done according to Peng Ren and co-workers (2011).[47] After stirring for 20 hours, the mixture was then filtered on celite, and the solvent evaporated. An HPLC-UV and HPLC-TOF analysis was made, chromatogram and mass spectra are depicted in **Figure 61.**

Instead of the expected amine group resulting from the reduction of the nitro group, an amide bond was formed in quantitative yield. It was then tried to hydrolyze the amide bond with multiple approaches as seen in **Table 18.**

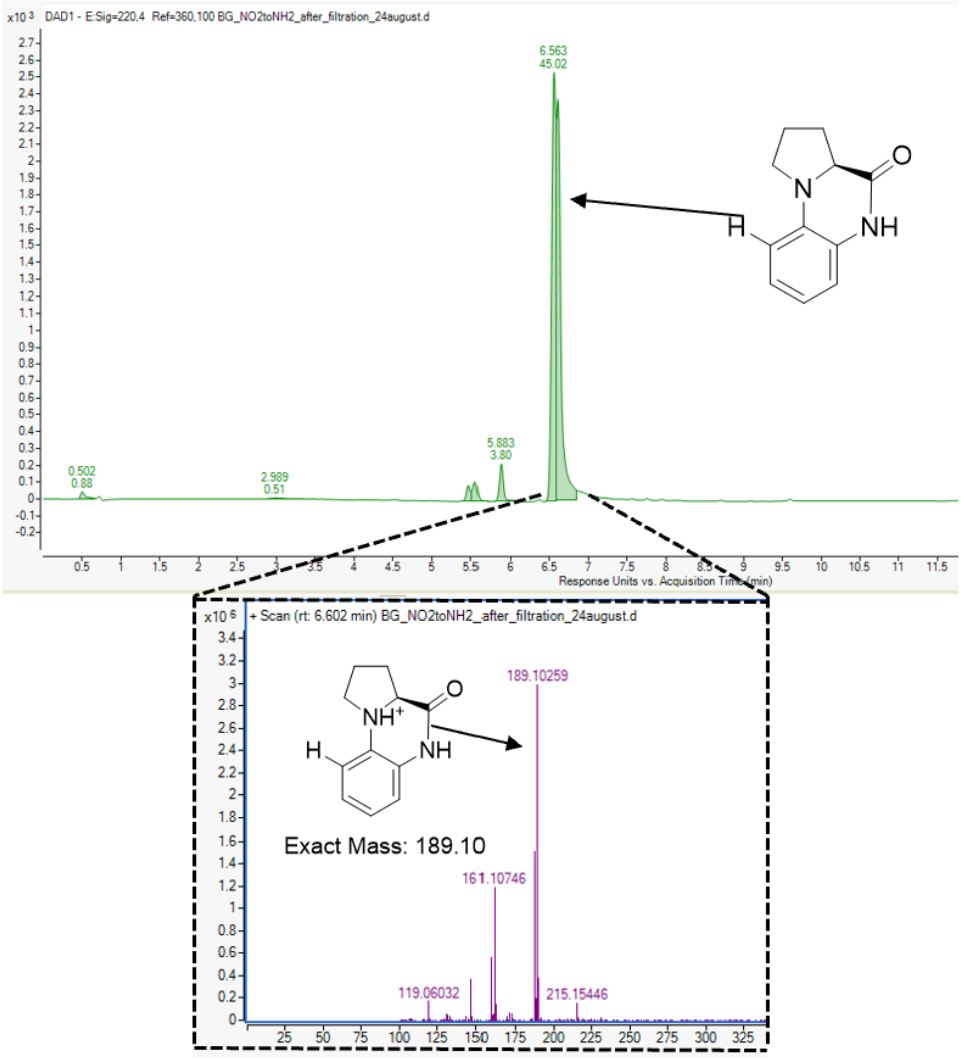

Figure 61 : HPLC-UV chromatogram and HPLC-TOF mass spectrum from reduction reaction.

Table 18 : Hydrolysis of amide bond approaches.

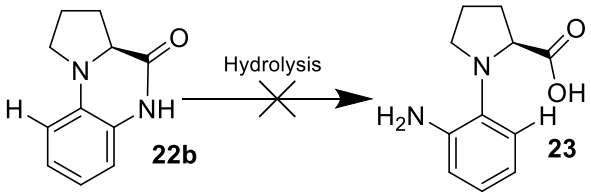

Entry	Experimental conditions	Yield [%] (**5**)
1 [48]	0.1 mmol **22b**, 0.25 M NaOH, 60°C, 24h	-
2 [48]	0.1 mmol **22b**, 0.5 M NaOH, 60°C, 24h	-
3 [48]	0.1 mmol **22b**, 1 M NaOH, 60°C, 24h	-
4 [48]	0.1 mmol **22b**, 1.5 M NaOH, 60°C, 24h	-

5 [48]	0.1 mmol **22b**, 2 M NaOH, 60°C, 24h	-
6 [49]	0.1 mmol **22b**, 2 M HCl, 60°C, 24h	-
7 [50]	0.1 mmol **22b**, 2 M H_2SO_4, 60°C, 24h	-

Basic and acidic approaches were done to try and hydrolyze the amide bond, but no conversion was observed, as a result it was decided to protect the carboxylic acid and proceed with the reduction again.

5.2.4.4 Ester protection

The carboxylic acid was protected with tert-butyl group with the reaction conditions as shown in **Figure 62**. The tert-butyl group is sterically hindering group and the assumption with choosing it as a protecting group is that due to its sterically hindering effect, it will prevent the amide bond of happening. The reduction step was done following the same reaction conditions as with the without protected carboxylic group and final yield of **24** was also quantitative with 97% yield. HPLC-UV chromatograms and HPLC-TOF mass spectrums from **23b** and **24** are shown in **Figure 63.**

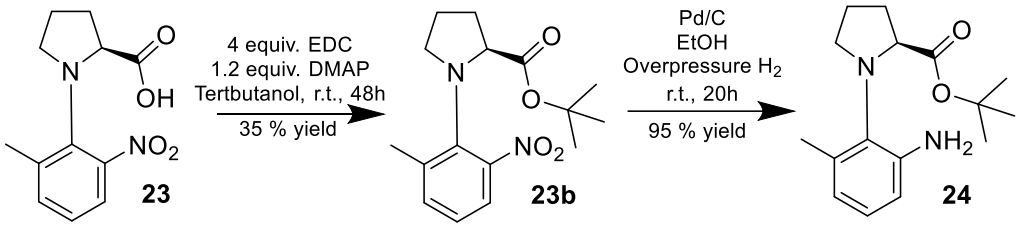

Figure 62 : Reaction scheme of carboxylic protection and the reduction of nitro group to amine group. (**23, X = CH_3**).[43]

It is important to note that in the ionization chamber due to the high temperature cleaving of the tert-butyl group can be observed. The smaller peaks on both chromatograms are probably due to impurities that are present in the solution.

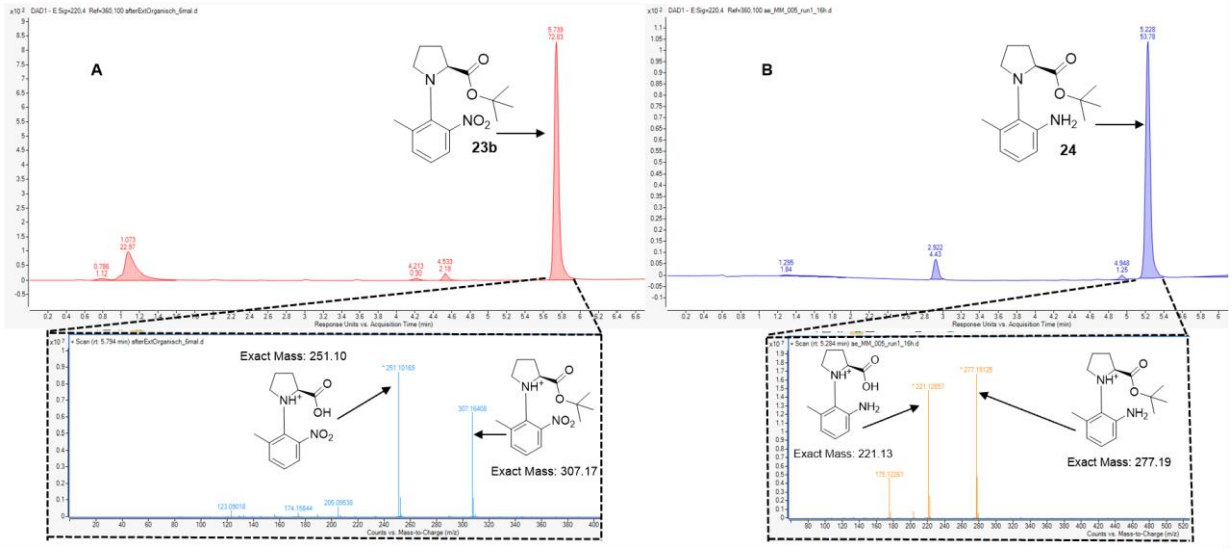

Figure 63 : **A**) HPLC-UV chromatogram at 220nm with mass spectrum of compound **23b**; **B**) HPLC-UV chromatogram at 220nm with mass spectrum of compound **24.**

23b has axial chirality and can exhibit two different diastereomers and two different enantiomers**,** but 1H-NMR of **23b** spectrum that is depicted in **Figure 64** didn't show any signs of it. This could be that a specific confirmation of the molecule is energetically favored over others to confirm this assumption DFT calculations need to be done.

^{1}H-NMR of **23b** spectrum that is depicted in **Figure 64** with the integrals and chemical shifts confirm its structure. **23** has the same structure as **23b** except for the tertbutyl group, therefore all chemical shifts and integrals match **23b**. Multiplets between 2.39 and 2.02 cannot be distinguished and assigned to specific protons, this is possibly caused by the tertbutyl group which protects the carboxylic moiety and lowers its reactivity. The singlet at 1.24 ppm with an integral value of nine can be assigned to protons 5 from the tertbutyl group.

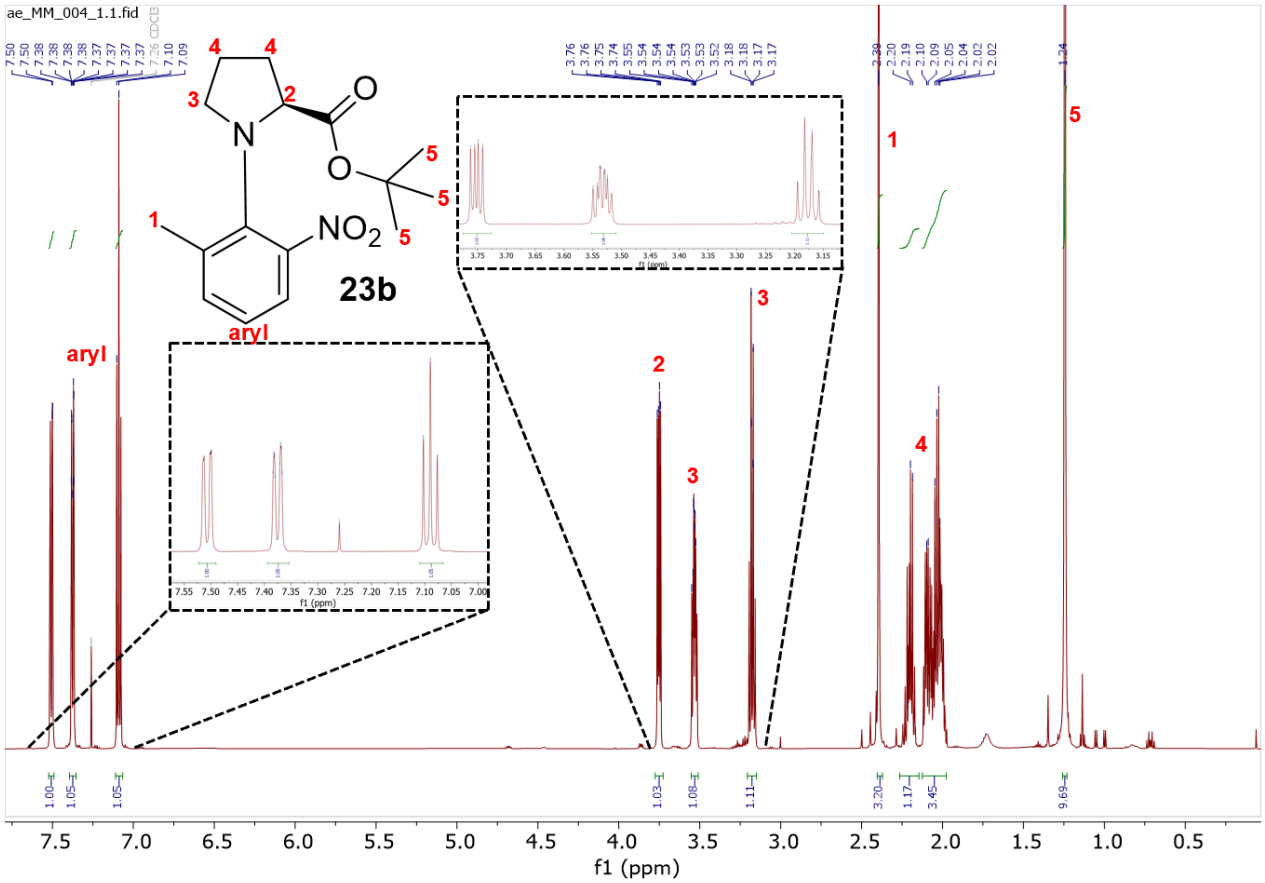

Figure 64 : 1H-NMR spectrum of **23b.**

5.2.4.5 Sandmeyer reaction

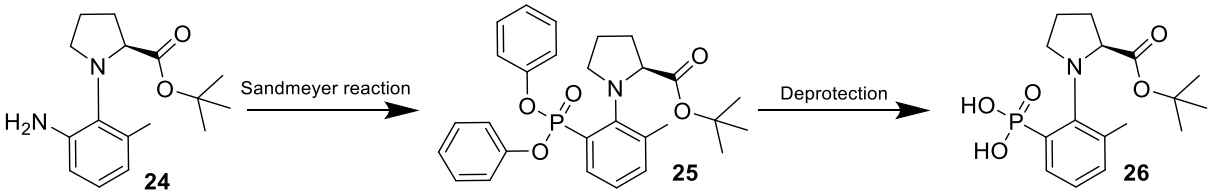

Figure 65 : Two step synthesis of **26.**

Scheme of Sandmeyer reaction is shown in **Figure 65.** For synthetizing **26** procedure from Fanyang Mo and co-workers (2018)[34] was followed. A summary of all the conditions tried are depicted in **Table 19.**

24 and TsOH*H_2O were dissolved in 4 mL of ACN, the solution was stirred at 0 °C ^{t}BuONO was then added with salicylic acid which was used for entries 4 and 7 and the reaction was stirred at 0 °C for 15 min, followed by the addition of $P(OR)_3$, the resulting mixture was stirred for 8 hours at r.t., the solution was then concentrated under reduced pressure, and the crude residue was purified on silica column. After isolation a qualitative yield of around 5-10% was achieved for entries 4 and 7. HPLC-UV chromatogram and HPLC-TOF mass spectrum is shown in **Figure 66** after purification of **25**.

Table 19 : Reaction conditions for **25**

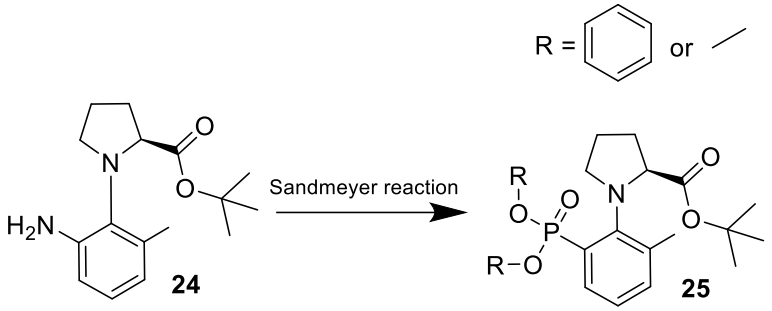

Entry	Experimental conditions	Yield [%] (**5**)
1 [34]	0.09 mmol **24**, TsOH*H_2O 1.2 equiv., ^{t}BuONO 1.5 equiv., $P(OPh)_3$ 1 equiv., 5mL ACN, 8h, 0°C to 25°C, N_2 atmosphere	Traces
2 [34]	0.09 mmol **24**, TsOH*H2O 1.2 equiv., tBuONO 1.5 equiv., $P(OPh)_3$ 3 equiv., 5mL ACN, 8h, 0°C to 25°C, N_2 atmosphere	Traces
3 [34]	0.09 mmol **24**, TsOH*H2O 1.2 equiv., tBuONO 1.5 equiv., $P(OPh)_3$ 5 equiv., 5mL ACN, 8h, 0°C to 25°C, N_2 atmosphere	Traces
4 [34]	0.09 mmol **24**, TsOH*H2O 1.2 equiv., tBuONO 1.5 equiv., $P(OPh)_3$ 3 equiv., salicylic acid 0.1 equiv., 5mL ACN, 8h, 0°C to 25°C, N_2 atmosphere	5-10
5 [34]	0.09 mmol **24**, TsOH*H2O 1.2 equiv., tBuONO 1.5 equiv., $P(OMe)_3$ 3 equiv., 5mL ACN, 8h, 0°C to 25°C, N_2 atmosphere	Traces
6 [34]	0.09 mmol **24**, TsOH*H2O 1.2 equiv., tBuONO 1.5 equiv., $P(OMe)_3$ 3 equiv., 5mL ACN, 8h, 0°C to 25°C, N_2 atmosphere	Traces
7 [34]	0.09 mmol **24**, TsOH*H2O 1.2 equiv., tBuONO 1.5 equiv., $P(OPh)_3$ 3 equiv., salicylic acid 0.1 equiv., 5mL ACN, 8h, 0°C to 25°C, N_2 atmosphere	5-10

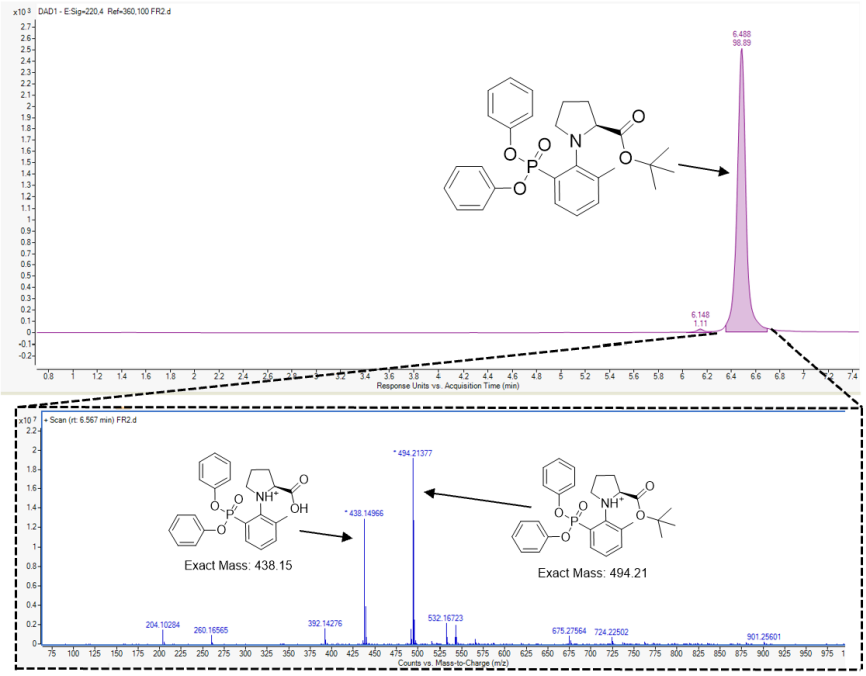

Figure 66 : HPLC-UV and HPLC-TOF of **25.**

Next step involves deprotecting the phosphonate from phenyl and methyl groups as well as removing the tert-butyl protecting group from carboxylic acid. Multiple acidic approaches with H_2SO_4 were made for deprotecting **25** but they weren't successful. This lack of success is probably due to the bulkiness of the phenyl group that hinders the deprotection reaction under mild deprotection conditions. Methyl protection group was used, since they are less bulky, but deprotection also wasn't successful. The Tertbutyl protecting group was cleaved without major problem. Strong deprotection conditions weren't tried because during previous deprotection attempts while conducting the Ulmann coupling, product decomposition was observed.

5.2.4.6 Phosphorylation

Since the deprotection didn't occur, it was decided to directly try to insert the phosphonate group to the amine group and create a phosphoramidate as shown in **Figure 67.**

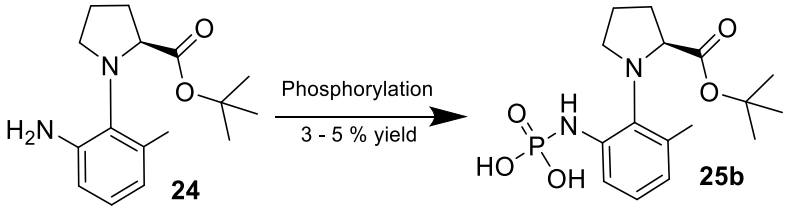

Figure 67 : Synthesis of **25b.**

0.9 mmol of **24** were dissolved in 2.5 mL THF in a flask, then 15 equiv. TEA and 3 equiv. $POCl_3$ were dissolved in 2.5 mL THF in another flask, and then the latter was added dropwise at 0 °C to the THF solution containing **24**, then the mixture was stirred for 15 minutes at r.t., and the reaction was added dropwise to a previously prepared 15 mL solution of ACN/H_2O (1:1). The mixture was then purified on a C18 column. The qualitative yield was around 3 - 5% and characterization was performed only using HPLC-UV, ^{1}H and ^{13}C NMR characterization

couldn’t be done because of the instability of the product at room temperature**.** However, the compound exhibited limited stability and underwent rapid hydrolysis making it unsuitable for kinetics studies shown in **Figure 68.**

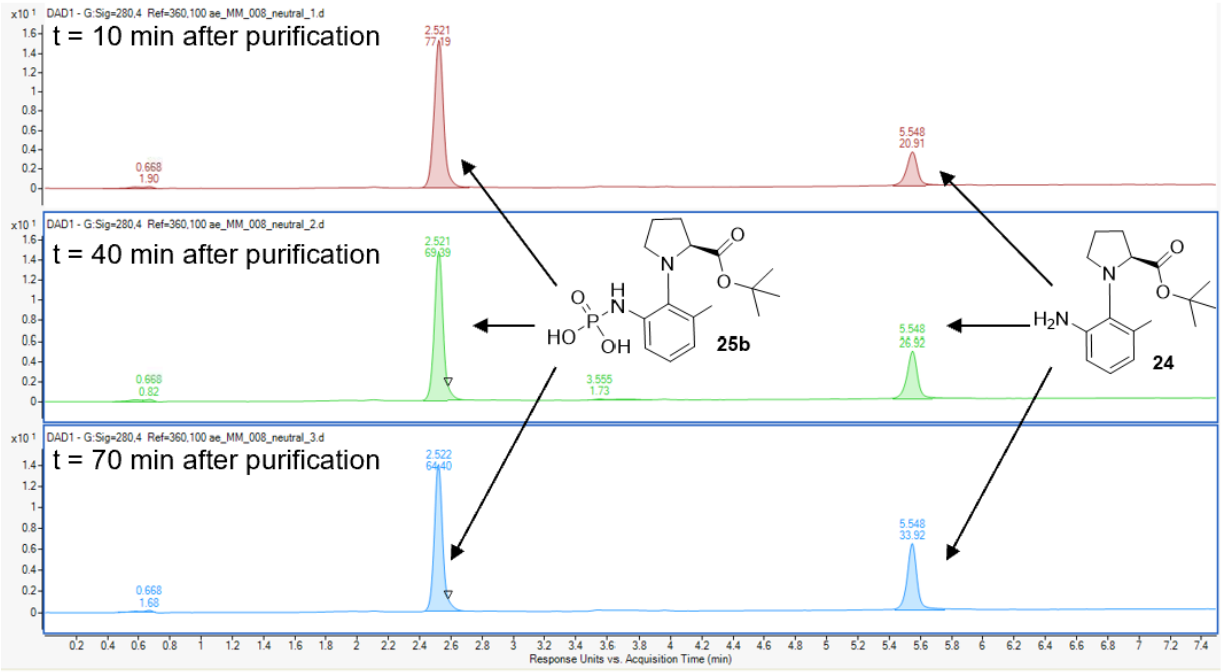

Figure 68 : HPLC-UV chromatogram over the span of 1 hour at 280nm showing the hydrolysis of **25b.**

6. Conclusion and outlook

The goal of this project was to investigate the potential of acylphosphonates as a platform for establishing NESS and to synthetize a phosphonate motor compound suitable for kinetic studies within the reaction network. A summary of the achievements is depicted in **Figure 69.**

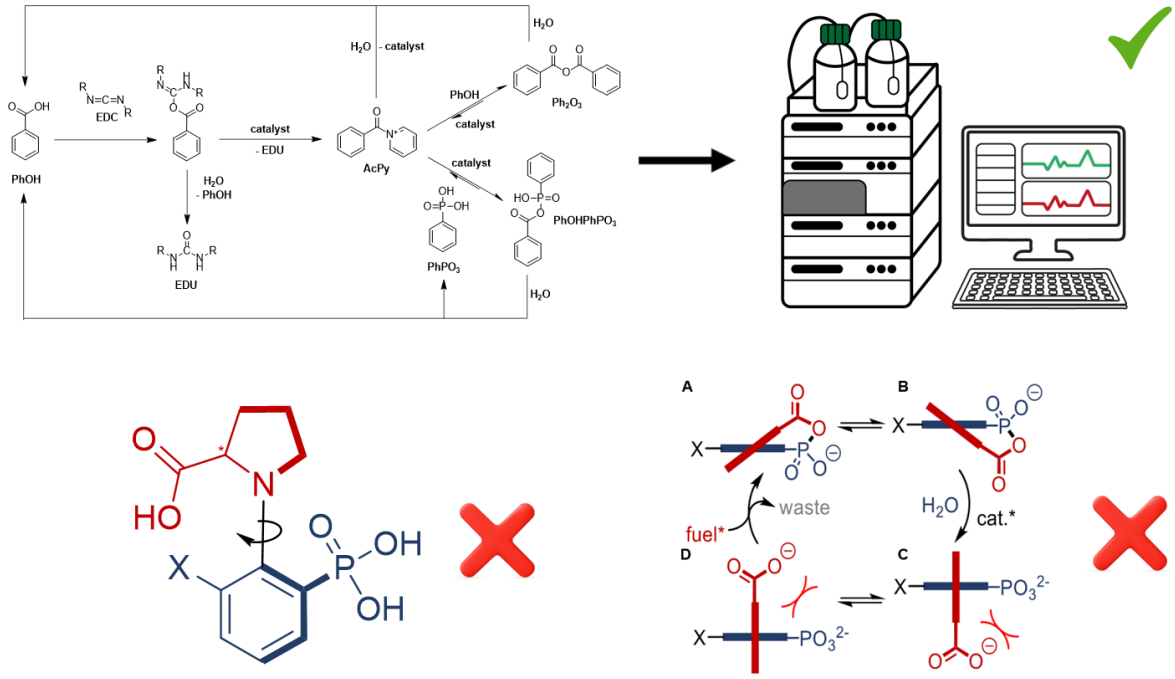

Figure 69 : Overview and summary of the bachelor thesis.

The first objective of the thesis was to establish a reference NESS system using acylphosphonate species that could be applied to study the kinetics of phosphonate-based motor compounds. Developing the necessary analytical methods was an integral part of this objective. Acylphosphonates, structurally similar to acylphosphates that had been previously employed in a NESS system[22,51] were the focus of this objective and it was successfully achieved.

The second objective was to synthesize a phosphonate based motor compound. Multiple approaches were thoroughly investigated thoroughly, including Ulmann coupling using both oil bath heating and microwave-mediated methods. Furthermore, intramolecular Ulmann coupling was explored through a tethering approach.

The last and most promising approach involved an aromatic nucleophilic substitution with Sandmeyer reaction for the insertion of the phosphonate group in *ortho* position of the stator component of the motor compound. The synthesis of the phosphonate based motor compound remained incomplete, which, in turn, hindered the investigation of its kinetics using the established acylphosphonate based NESS system.

An other different approach for the last step of the phosphonate motor compound would be to use bromo compounds and try the Hirao coupling instead of the Sandmeyer reaction.

An outlook for future research in synthetizing the motor compound involves a more thorough exploration of the Sandmeyer reaction for inserting the phosphonate group.

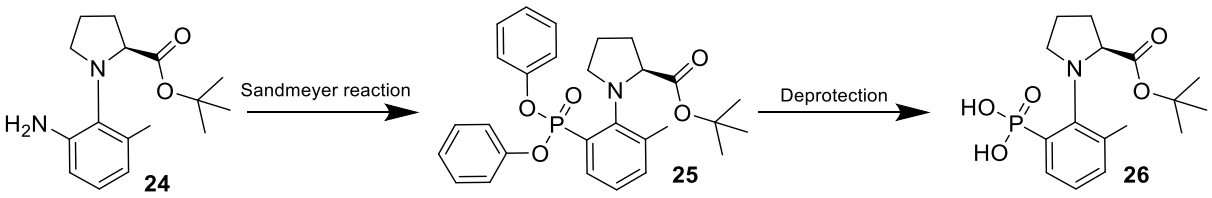

Figure 70 : Sandmeyer reaction scheme last synthesis step for the phosphonate based motor compound.

7. Acknowledgements

I would like to acknowledge and extend my heartfelt thanks to all the professors and staff at HESSO Valais-Wallis for their unwavering support, patience, and guidance throughout the three years of the bachelor's degree.

Special thanks go to Professor Max von Delius for not only accepting me into his research group but also for providing me with an invaluable opportunity to work and conduct research under the best possible conditions.

I am deeply grateful to my supervisor, Andreas Englert, who has consistently been there for me, offering his valuable time, advice, unwavering assistance, and meticulous corrections throughout the project. His guidance has been a cornerstone in the successful completion of this work.

I would also like to acknowledge and express my gratitude to the members of the research group for their contributions and support.

Many thanks to Professor Andreas Peer for his guidance and support, which greatly contributed to the success of my project.

A profound thank you is due to my family for their unceasing support and unwavering presence. Their encouragement and love have been my constant source of strength and motivation.

8. References

(1) Sweeney, H. L.; Holzbaur, E. L. F. Motor Proteins. *Cold Spring Harb. Perspect. Biol.* **2018**, *10* (5), a021931.

(2) Alberts, B.; Johnson, A.; Lewis, J.; Raff, M.; Roberts, K.; Walter, P. Molecular Motors. In *Molecular Biology of the Cell. 4th edition*; Garland Science, 2002.

(3) Roberts, A. J.; Kon, T.; Knight, P. J.; Sutoh, K.; Burgess, S. A. Functions and Mechanics of Dynein Motor Proteins. *Nat. Rev. Mol. Cell Biol.* **2013**, *14* (11), 713–726.

(4) Aprahamian, I.; Goldup, S. M. Non-Equilibrium Steady States in Catalysis, Molecular Motors, and Supramolecular Materials: Why Networks and Language Matter. *J. Am. Chem. Soc.* **2023**, *145* (26), 14169–14183.

(5) Mattia, E.; Otto, S. Supramolecular Systems Chemistry. *Nat. Nanotechnol.* **2015**, *10* (2), 111–119.

(6) Amano, S.; Esposito, M.; Kreidt, E.; Leigh, D. A.; Penocchio, E.; Roberts, B. M. W. Using Catalysis to Drive Chemistry Away from Equilibrium: Relating Kinetic Asymmetry, Power Strokes, and the Curtin–Hammett Principle in Brownian Ratchets. *J. Am. Chem. Soc.* **2022**, *144* (44), 20153–20164.

(7) Astumian, R. D. Kinetic Asymmetry Allows Macromolecular Catalysts to Drive an Information Ratchet. *Nat. Commun.* **2019**, *10* (1), 3837.

(8) Oster, G. Brownian Ratchets: Darwin's Motors. *Nature* **2002**, *417* (6884), 25–25.

(9) Erbas-Cakmak, S.; Leigh, D. A.; McTernan, C. T.; Nussbaumer, A. L. Artificial Molecular Machines. *Chem. Rev.* **2015**, *115* (18), 10081–10206.

(10) Brownian Motion, Molecular Motors and Ratchets. *Phys. Stat. Mech. Its Appl.* **2004**, *336* (1–2), 112–122.

(11) Van Noorden, R.; Castelvecchi, D. World's Tiniest Machines Win Chemistry Nobel. *Nature* **2016**, *538* (7624), 152–153.

(12) Mondal, A.; Toyoda, R.; Costil, R.; Feringa, B. L. Chemically Driven Rotatory Molecular Machines. *Angew. Chem. Int. Ed.* **2022**, *61* (40), e202206631.

(13) Koumura, N.; Zijlstra, R. W. J.; van Delden, R. A.; Harada, N.; Feringa, B. L. Light-Driven Monodirectional Molecular Rotor. *Nature* **1999**, *401* (6749), 152–155.

(14) Collins, B. S. L.; Kistemaker, J. C. M.; Otten, E.; Feringa, B. L. A Chemically Powered Unidirectional Rotary Molecular Motor Based on a Palladium Redox Cycle. *Nat. Chem.* **2016**, *8* (9), 860–866.

(15) Kelly, T. R.; Cai, X.; Damkaci, F.; Panicker, S. B.; Tu, B.; Bushell, S. M.; Cornella, I.; Piggott, M. J.; Salives, R.; Cavero, M.; Zhao, Y.; Jasmin, S. Progress toward a Rationally

Designed, Chemically Powered Rotary Molecular Motor. *J. Am. Chem. Soc.* **2007**, *129* (2), 376–386.

(16) Zhang, Y.; Chang, Z.; Zhao, H.; Crespi, S.; Feringa, B. L.; Zhao, D. A Chemically Driven Rotary Molecular Motor Based on Reversible Lactone Formation with Perfect Unidirectionality. *Chem* **2020**, *6* (9), 2420–2429.

(17) Erbas-Cakmak, S.; Fielden, S. D. P.; Karaca, U.; Leigh, D. A.; McTernan, C. T.; Tetlow, D. J.; Wilson, M. R. Rotary and Linear Molecular Motors Driven by Pulses of a Chemical Fuel. *Science* **2017**, *358* (6361), 340–343.

(18) Borsley, S.; Kreidt, E.; Leigh, D. A.; Roberts, B. M. W. Autonomous Fuelled Directional Rotation about a Covalent Single Bond. *Nature* **2022**, *604* (7904), 80–85.

(19) Gao, X.; Deng, H.; Tang, G.; Liu, Y.; Xu, P.; Zhao, Y. Intermolecular Phosphoryl Transfer of N-Phosphoryl Amino Acids. *Eur. J. Org. Chem.* **2011**, *2011* (17), 3220–3228.

(20) Lacey, J. C.; Senaratne, N.; Mullins, D. W. Hydrolytic Properties of Phenylalanyl- and N-Acetylphenylalanyl Adenylate Anhydrides. *Orig. Life Evol. Biosph.* **1984**, *15* (1), 45–54.

(21) *THE 17 GOALS | Sustainable Development*. https://sdgs.un.org/goals (accessed 2023-10-11).

(22) Englert, A.; Majer, F.; Schiessl, J.; Kuehne, A.; Delius, M. von. Acylphosphates as Versatile Transient Species in Reaction Networks and Optical Catalyst Screenings. ChemRxiv July 5, 2023.

(23) Ludlow, R. F.; Otto, S. Systems Chemistry. *Chem. Soc. Rev.* **2007**, *37* (1), 101–108.

(24) Harsági, N.; Keglevich, G. The Hydrolysis of Phosphinates and Phosphonates: A Review. *Molecules* **2021**, *26* (10), 2840.

(25) Moazzen, K.; Rossegger, E.; Alabiso, W.; Shaukat, U.; Schlögl, S. Role of Organic Phosphates and Phosphonates in Catalyzing Dynamic Exchange Reactions in Thiol-Click Vitrimers. *Macromol. Chem. Phys.* **2021**, *222* (12), 2100072.

(26) Sha, S.-C.; Zhang, J.; Carroll, P. J.; Walsh, P. J. Raising the pKa Limit of “Soft” Nucleophiles in Palladium-Catalyzed Allylic Substitutions: Application of Diarylmethane Pronucleophiles. *J. Am. Chem. Soc.* **2013**, *135* (46), 17602–17609.

(27) van der Helm, M. P.; Wang, C.-L.; Fan, B.; Macchione, M.; Mendes, E.; Eelkema, R. Organocatalytic Control over a Fuel-Driven Transient-Esterification Network**. *Angew. Chem. Int. Ed.* **2020**, *59* (46), 20604–20611.

(28) Schwarz, P. S.; Tena-Solsona, M.; Dai, K.; Boekhoven, J. Carbodiimide-Fueled Catalytic Reaction Cycles to Regulate Supramolecular Processes. *Chem. Commun.* **2022**, *58* (9), 1284–1297.

(29) Wimmer, J. L. E.; Kleinermanns, K.; Martin, W. F. Pyrophosphate and Irreversibility in Evolution, or Why PPi Is Not an Energy Currency and Why Nature Chose Triphosphates. *Front. Microbiol.* **2021**, *12*.

(30) Chen, X.; Stasi, M.; Rodon-Fores, J.; Großmann, P. F.; Bergmann, A. M.; Dai, K.; Tena-Solsona, M.; Rieger, B.; Boekhoven, J. A Carbodiimide-Fueled Reaction Cycle That Forms Transient 5(4H)-Oxazolones. *J. Am. Chem. Soc.* **2023**, *145* (12), 6880–6887.

(31) Vashist, S. K. Comparison of 1-Ethyl-3-(3-Dimethylaminopropyl) Carbodiimide Based Strategies to Crosslink Antibodies on Amine-Functionalized Platforms for Immunodiagnostic Applications. *Diagnostics* **2012**, *2* (3), 23–33.

(32) Arrhenius, S. Über die Dissociationswärme und den Einfluss der Temperatur auf den Dissociationsgrad der Elektrolyte. *Z. Für Phys. Chem.* **1889**, *4U* (1), 96–116.

(33) Narendar, N.; Velmathi, S. Copper-Catalyzed C–N Coupling Reactions of Aryl Halides with α-Amino Acids under Focused Microwave Irradiation. *Tetrahedron Lett.* **2009**, *50* (36), 5159–5161.

(34) Mo, F.; Qiu, D.; Zhang, Y.; Wang, J. Renaissance of Sandmeyer-Type Reactions: Conversion of Aromatic C–N Bonds into C–X Bonds (X = B, Sn, P, or CF3). *Acc. Chem. Res.* **2018**, *51* (2), 496–506.

(35) Ma, D.; Cai, Q. Copper/Amino Acid Catalyzed Cross-Couplings of Aryl and Vinyl Halides with Nucleophiles. *Acc. Chem. Res.* **2008**, *41* (11), 1450–1460.

(36) Sharma, K. K.; Mandloi, M.; Rai, N.; Jain, R. Copper-Catalyzed N-(Hetero)Arylation of Amino Acids in Water. *RSC Adv.* **2016**, *6* (99), 96762–96767.

(37) Zhang, H.; Cai, Q.; Ma, D. Amino Acid Promoted CuI-Catalyzed C−N Bond Formation between Aryl Halides and Amines or N-Containing Heterocycles. *J. Org. Chem.* **2005**, *70* (13), 5164–5173.

(38) Cheng, C.; Pan, L.; Chen, Y.; Song, H.; Qin, Y.; Li, R. Total Synthesis of (±)-Marinopyrrole A and Its Library as Potential Antibiotic and Anticancer Agents. *J. Comb. Chem.* **2010**, *12* (4), 541–547.

(39) Kamei, K.; Maeda, N.; Nomura, K.; Shibata, M.; Katsuragi-Ogino, R.; Koyama, M.; Nakajima, M.; Inoue, T.; Ohno, T.; Tatsuoka, T. Synthesis, SAR Studies, and Evaluation of 1,4-Benzoxazepine Derivatives as Selective 5-HT1A Receptor Agonists with Neuroprotective Effect: Discovery of Piclozotan. *Bioorg. Med. Chem.* **2006**, *14* (6), 1978–1992.

(40) Kanakis, A. A.; Sarli, V. Total Synthesis of (±)-Marinopyrrole A via Copper-Mediated N-Arylation. *Org. Lett.* **2010**, *12* (21), 4872–4875.

(41) Dilek, Ö.; Tezeren, M. A.; Tilki, T.; Ertürk, E. Chiral 2-(2-Hydroxyaryl)Alcohols (HAROLs) with a 1,4-Diol Scaffold as a New Family of Ligands and Organocatalysts. *Tetrahedron* **2018**, *74* (2), 268–286.

(42) Schwalm, C. S.; de Castro, I. B. D.; Ferrari, J.; de Oliveira, F. L.; Aparicio, R.; Correia, C. R. D. Synthesis of Pentabromopseudilin and Other Arylpyrrole Derivatives via Heck Arylations. *Tetrahedron Lett.* **2012**, *53* (13), 1660–1663.

(43) Menzio, J.; Tagliapietra, S.; Barge, A.; Serito, B.; Calegari, E.; Binello, A.; Cravotto, G. The Challenge of O-Phenylphenol Detection in Coffee: How “OPP-Conjugates” Hide Their Presence in Green and Roasted Samples. *Food Chem.* **2023**, *404*, 134597.

(44) Lo, V. K.-Y.; Wong, M.-K.; Che, C.-M. Gold-Catalyzed Highly Enantioselective Synthesis of Axially Chiral Allenes. *Org. Lett.* **2008**, *10* (3), 517–519.

(45) Baldwin, J. E.; Field, R. A.; Lawrence, C. C.; Merritt, K. D.; Schofield, C. J. Proline 4-Hydroxylase: Stereochemical Course of the Reaction. *Tetrahedron Lett.* **1993**, *34* (46), 7489–7492.

(46) Ahn, H. C.; Choi, K. N-(2-Nitrophenyl)Proline: An Intramolecular Hydrogen Bond Forming Reagent for the Determination of the Absolute Configuration of Primary Amines. *Org. Lett.* **2007**, *9* (19), 3853–3855.

(47) Ren, P.; Vechorkin, O.; Csok, Z.; Salihu, I.; Scopelliti, R.; Hu, X. Pd, Pt, and Ru Complexes of a Pincer Bis(Amino)Amide Ligand. *Dalton Trans.* **2011**, *40* (35), 8906–8911.

(48) Gurjar, J.; Fokin, V. V. Sulfuryl Fluoride Mediated Synthesis of Amides and Amidines from Ketoximes via Beckmann Rearrangement. *Chem. – Eur. J.* **2020**, *26* (46), 10402–10405.

(49) Darwish, H. W.; Hassan, S. A.; Salem, M. Y.; El-Zeany, B. A. Advanced Stability Indicating Chemometric Methods for Quantitation of Amlodipine and Atorvastatin in Their Quinary Mixture with Acidic Degradation Products. *Spectrochim. Acta. A. Mol. Biomol. Spectrosc.* **2016**, *154*, 58–66.

(50) Konno, S.; Shiraiwa, M.; Yamanaka, H. Studies on Quinoline and Isoquinoline Derivatives. VIII. Hydration and Hydrogenation of Ethynyl Substituents Attached to the Pyridine Moiety of Quinoline and Isoquinoline Rings. *Chem. Pharm. Bull. (Tokyo)* **1981**, *29* (12), 3554–3560.

(51) Englert, A.; Vogel, J. F.; Bergner, T.; Loske, J.; von Delius, M. A Ribonucleotide ↔ Phosphoramidate Reaction Network Optimized by Computer-Aided Design. *J. Am. Chem. Soc.* **2022**, *144* (33), 15266–15274.

9. List of figures/tables

9.1 List of figures

9.2 List of tables

10. Appendices

10.1 HPLC-UV Chromatogram and reaction scheme – Indirect acylation of acylphosphonates, optimization of the reaction cycle.

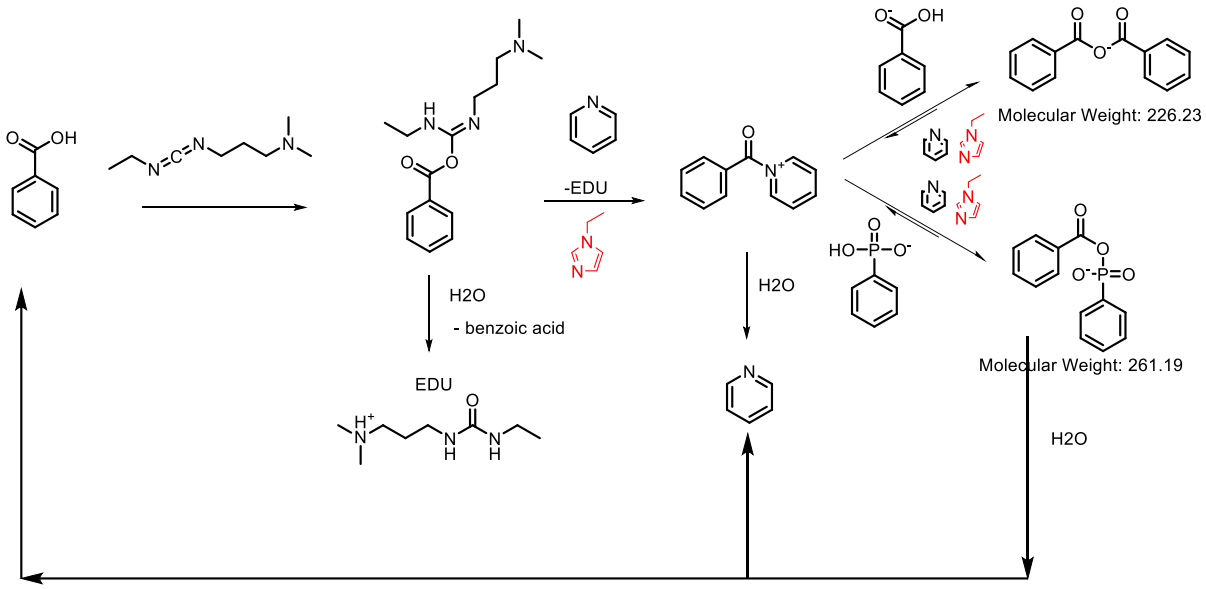

Figure 71 : Reaction cycle scheme of the indirect acylation of acylphosphonates using carbodiimides of the optimization used for HPLC-UV method.

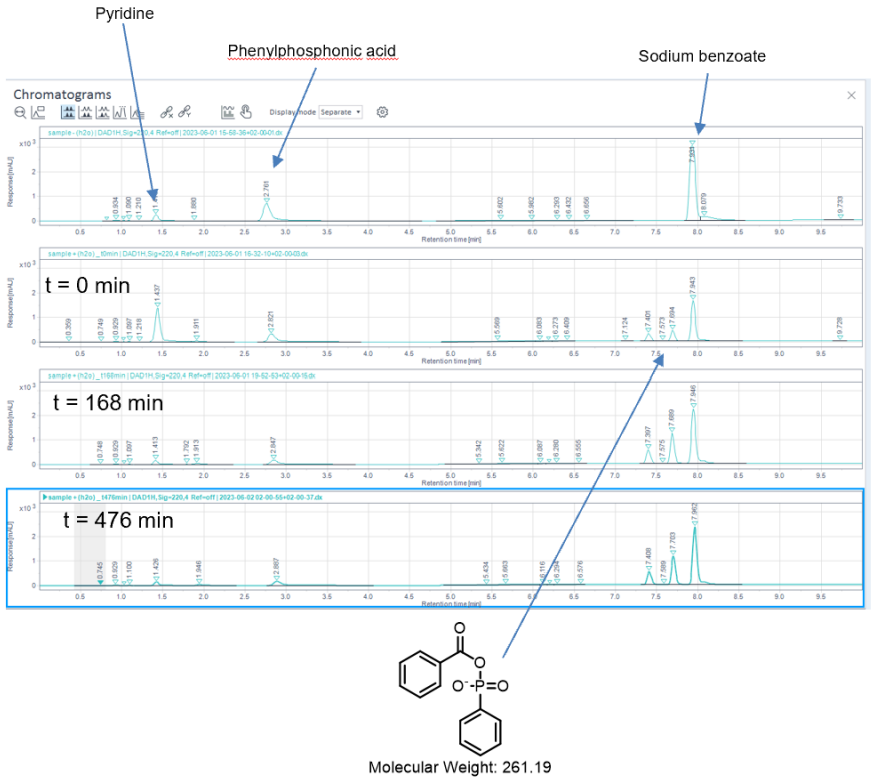

Figure 72 : HPLC-UV chromatogram from the indirect acylation of acylphosphonates.

10.2 HPLC-UV Chromatogram and reaction scheme – Direct acylation of acylphosphonates, optimization of the reaction cycle.

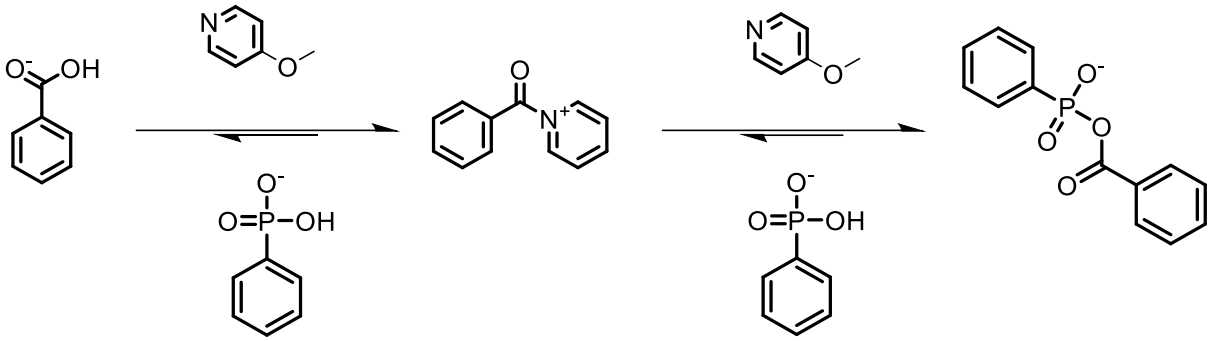

Figure 73 : Reaction cycle scheme of the direct acylation of acylphosphonates.

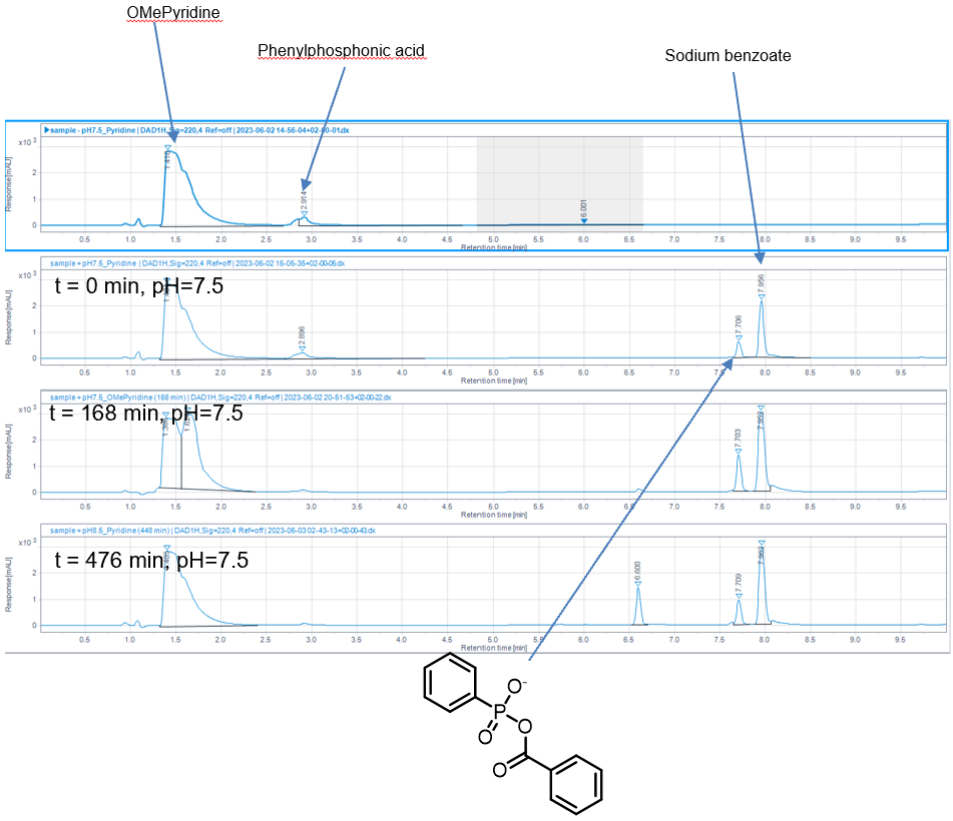

Figure 74 : HPLC-UV chromatogram from the direct acylation of acylphosphonates.

10.3 Büchi separation chromatogram of the $PhOHPhPO_3$

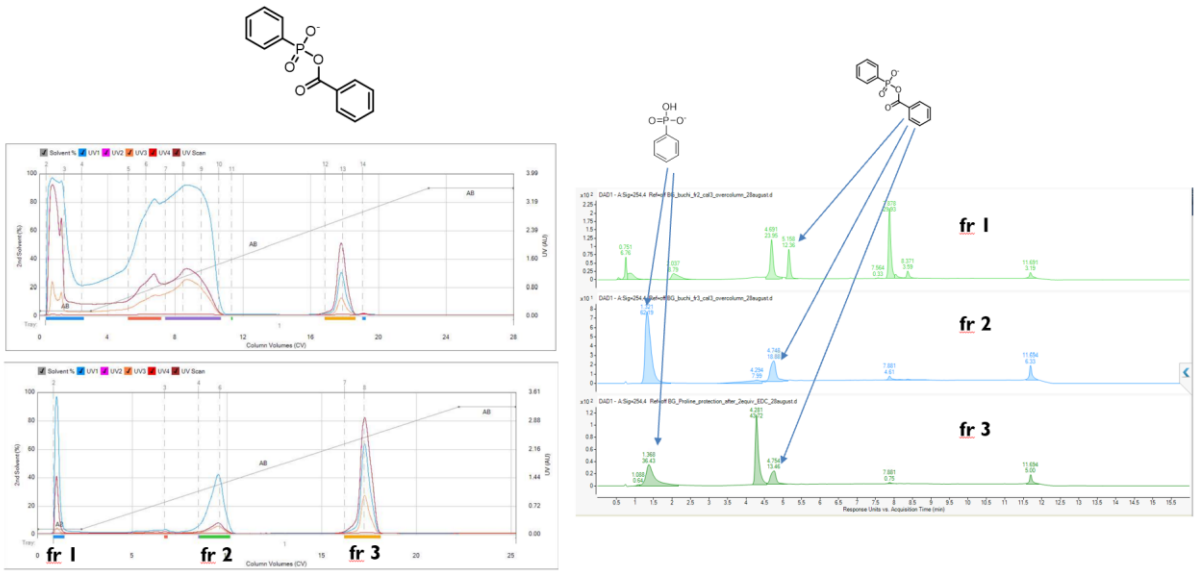

Figure 75 : Separation chromatograms of the $PhOHPhPO_3$.

10.4 HPLC-UV chromatogram of the parameters screening

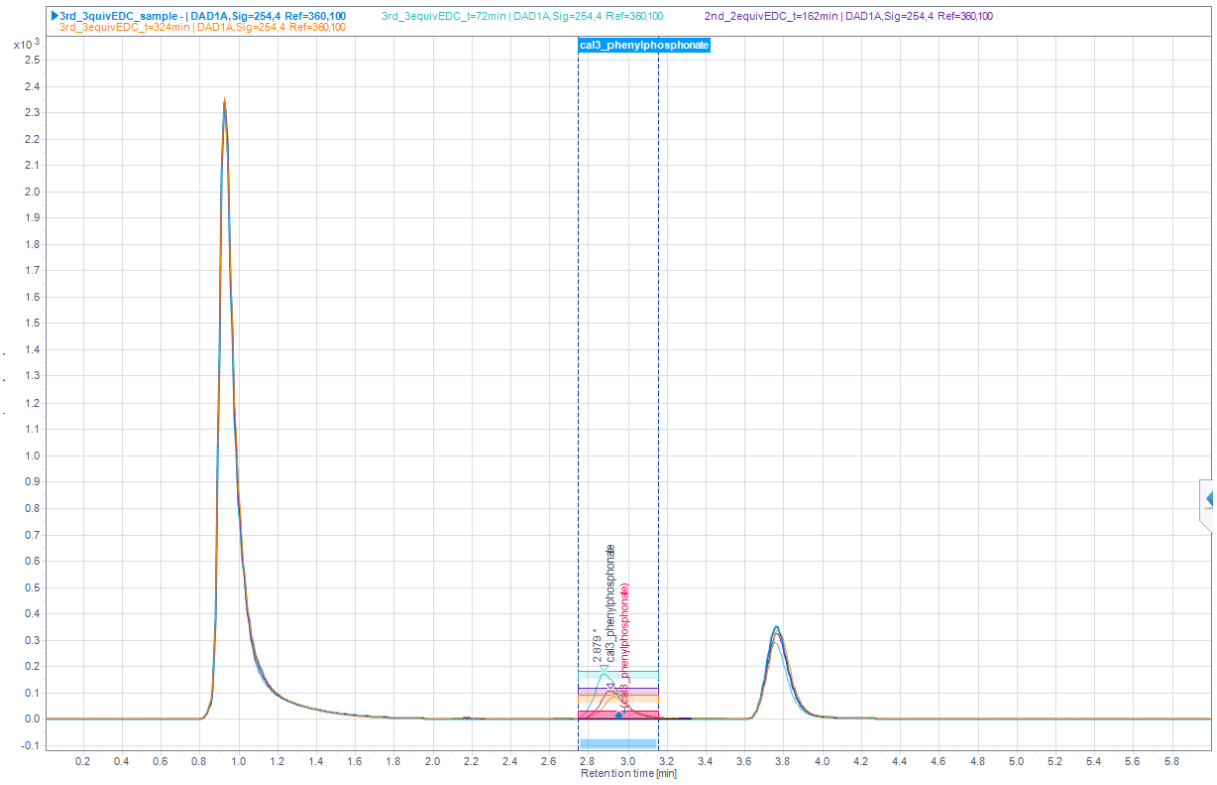

Figure 76 : HPLC-UV of 3 equiv. EDC, parameters screening (@254 nm).

10.5 HPLC-UV chromatogram of catalyst screening for hydrolysis

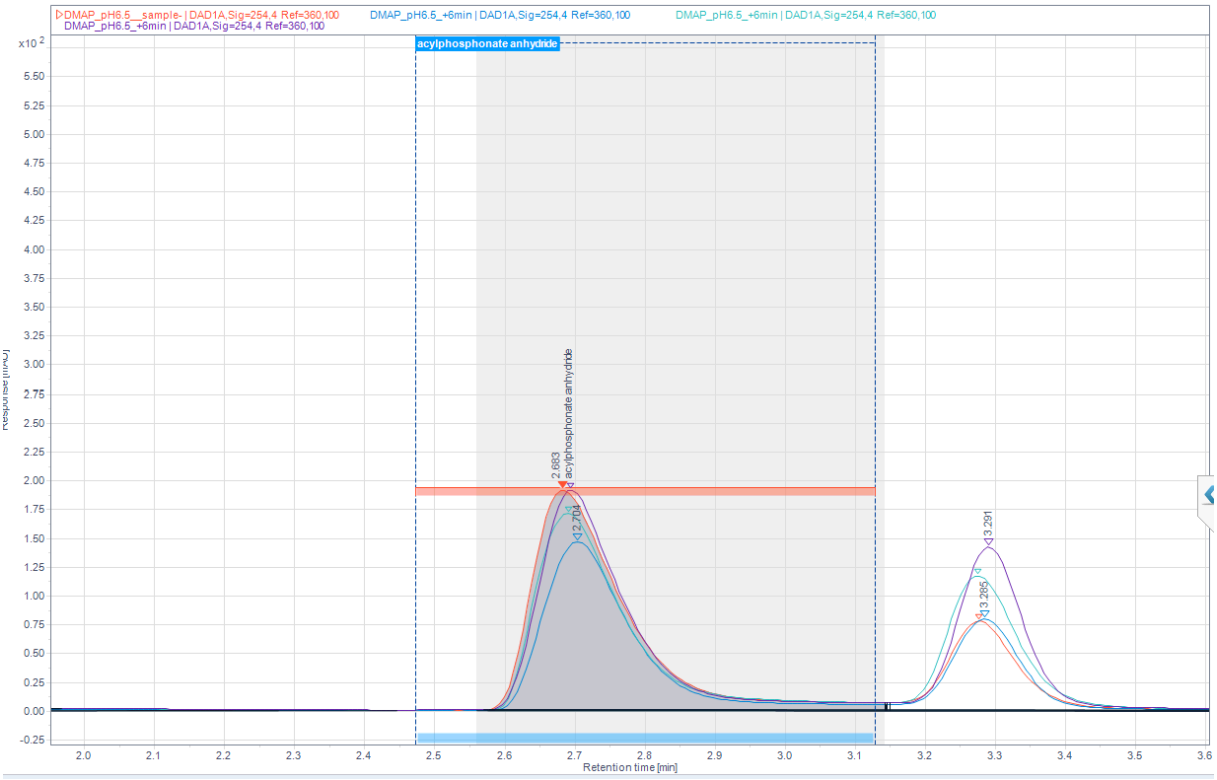

Figure 77 : HPLC-UV chromatogram of DMAP screening for acylphosphonate hydrolysis.

10.6 Calibration curve, R^2 from the calibration of $PhOHPhPO_3$ solution

Concentration [mM]	Area [-]	Average area [-]
0	0	0
1	97.61	103.18
	101.76	
	110.17	
5	363.55	385.38
	382.28	
	410.30	
10	704.64	725.51
	739.25	
	732.63	
25	1663.87	1719.79
	1743.53	
	1751.97	
50	3352.69	3454.01
	3484.47	
	3524.86	
75	5315.03	5292.69
	5313.29	
	5249.75	

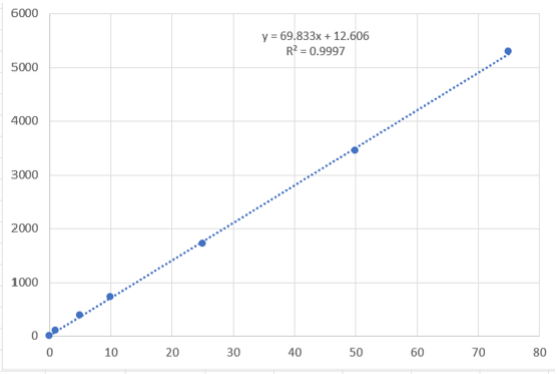

Figure 78 : Calibration curve of the $PhOHPhPO_3$ with the concentrations.